AFRL-VS-HA-TR-98-0070

MODELING OF CELESTIAL ULTRAVIOLET SOURCES

Richard C. Henry
Jayant Murthy

Johns Hopkins University
Henry A. Rowland Department of Physics & Astronomy
Baltimore, MD 21218

26 June 1998

Final Report
12 March 1993-26 June 1998

AIR FORCE RESEARCH LABORATORY
Space Vehicles Directorate
29 Randolph Road
AIR FORCE MATERIEL COMMAND
HANSCOM AFB, MA 01731-3010

" This technical report has been reviewed and is approved for publication."

RUSSELL SHIPMAN
Contract Manager
Background Characterization

STEPHAN D. PRICE
Branch Chief
Background Characterization

DAVID HARDY
Division Director
Battlespace Environment

This report has been reviewed by the ESC Public Affairs Office (PA) and is releasable to the National Technical Information Service (NTIS).

Qualified requestors may obtain additional copies from the Defense Technical Information Center (DTIC). All others should apply to the National Technical Information Service (NTIS).

If your address has changed, if you wish to be removed from the mailing list, of if the addressee is no longer employed by your organization, please notify PL/IM, 29 Randolph Road, Hanscom AFB, MA. 01731-3010. this will assist us in maintaining a current mailing list.

Do not return copies of this report unless contractual obligations or notices on a specific document require that it be returned.

REPORT DOCUMENTATION PAGE

Form Approved
OMB No. 0704-0188

1. AGENCY USE ONLY *(leave blank)*	2. REPORT DATE	3. REPORT TYPE AND DATES COVERED
	26 June 1998	Final (12 March 1993 – 26 June 1998)

4. TITLE AND SUBTITLE
Modeling of Celestial Ultraviolet Sources

5. FUNDING NUMBERS
PE 63215C
PR S321 TA GG WU AB

Contract F19628-93-K-0004

6. AUTHOR(S)
Richard C. Henry
Jayant Murthy

7. PERFORMING ORGANIZATION NAME(S) AND ADDRESS(ES)
Johns Hopkins University
Henry A. Rowland Department of Physics & Astronomy
Baltimore, MD 21218

8. PERFORMING ORGANIZATION REPORT NUMBER
98-07-01

9. SPONSORING/MONITORING AGENCY NAME(S) AND ADDRESS(ES)
Air Force Research Laboratory
29 Randolph Road
Hanscom AFB, MA 01731-3010

CONTRACT MANAGER: Russell Shipman/VSBC

10. SPONSORING/MONITORING AGENCY REPORT NUMBER
AFRL-VS-HA-TR-98-0070

11. SUPPLEMENTARY NOTES

12a. DISTRIBUTION/AVAILABILITY STATEMENT
Approved for public release;
Distribution unlimited

12b. DISTRIBUTION CODE

13. ABSTRACT ***(Maximum 200 words)***

We have constructed models of the diffuse ultraviolet background radiation (zodiacal light; direct starlight; and starlight scattered from interstellar dust) for comparison with observations that were carried out with the UVISI instruments aboard the MSX spacecraft. We have written and implemented software for the reduction of the data from the four ultraviolet and visible imagers, and the five imaging spectrometers, collectively called UVISI, aboard the MSX spacecraft. We have examined the ultraviolet celestial backgrounds data that were produced during a partial survey of the sky, and we provide examples of the data, a guide to the software, and a map and listing of the sky survey, showing what portions of the sky survey were completed. We also provide a discussion of the science goals of the sky survey in the ultraviolet.

14. SUBJECT TERMS
Ultraviolet; MSX; UVISI; models; spectroscopy; diffuse ultraviolet background radiation

15. NUMBER OF PAGES
100

16. PRICE CODE

17. SECURITY CLASSIFICATION OF REPORT	18. SECURITY CLASSIFICATION OF THIS PAGE	19. SECURITY CLASSIFICATION OF ABSTRACT	20. LIMITATION OF ABSTRACT
Unclassified	Unclassified	Unclassified	SAR

Contents

1. INTRODUCTION

This Final Report, "Modeling of Celestial Ultraviolet Sources," describes work done in support of the MSX mission that has been carried out over the period 1993 – 1998 by the Johns Hopkins University.

The work has resulted in many products, all of which are either presented here, or referenced if publicly available elsewhere. The major work centered on two tasks, modeling of celestial ultraviolet light, and preparation and implementation of software for dealing with the UVISI data from the MSX mission. The latter task flowed out of the modeling effort, because comparison with actual data, hoped for from the MSX mission, was a vital tool for validation of the UV models. In that connection, we prepared a proposal to the National Aeronautics and Space Administration (NASA) for continuing support of the MSX UVISI sky survey. Relevant extracts from that proposal form parts of this report, as it contains a great deal of the technical description of the work under this contract.

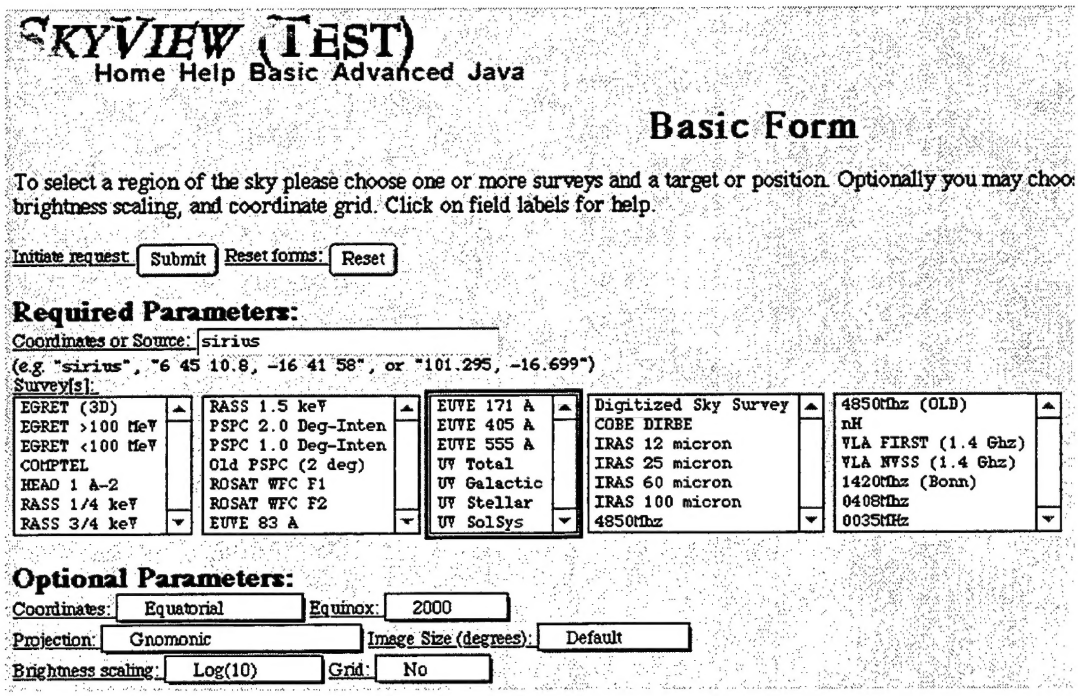

Figure 1. At the site http://skys2.gsfc.nasa.gov/test/cgi-bin/skvbasic.pl is found the result of our modeling effort carried out under this contract. In this figure, we have highlighted in gray the ultraviolet models that we created. In Figure 2, below, we show the result of selecting UV Total and Aitoff-Hammer (all-sky) coordinates.

It is unfortunate that NASA was not able to support the request for continued operation of the UVISI instruments. While the performance of the instruments for the purposes of providing data for comparison with the modeling effort was not as good as had been hoped for when we began this work, this still represented a significant opportunity to perform a useful sky

survey that would have at least partially validated the models. As it stands, NASA has selected GALEX to perform an all-sky survey for point sources, and has no approved mission to study the diffuse UV background (for which this contract provided the models.)

2. MODELING SUMMARY

The modeling effort was carried out over a five year period by the Principal Investigator and Co-Investigator, assisted by Drs. Julian Daniels and Marsha Allen, as well as by graduate students. We detail the modeling in the following pages, but we start by calling attention to the fact that the models have been made publicly available by the SkyView NASA site: see Figures 1 and 2:

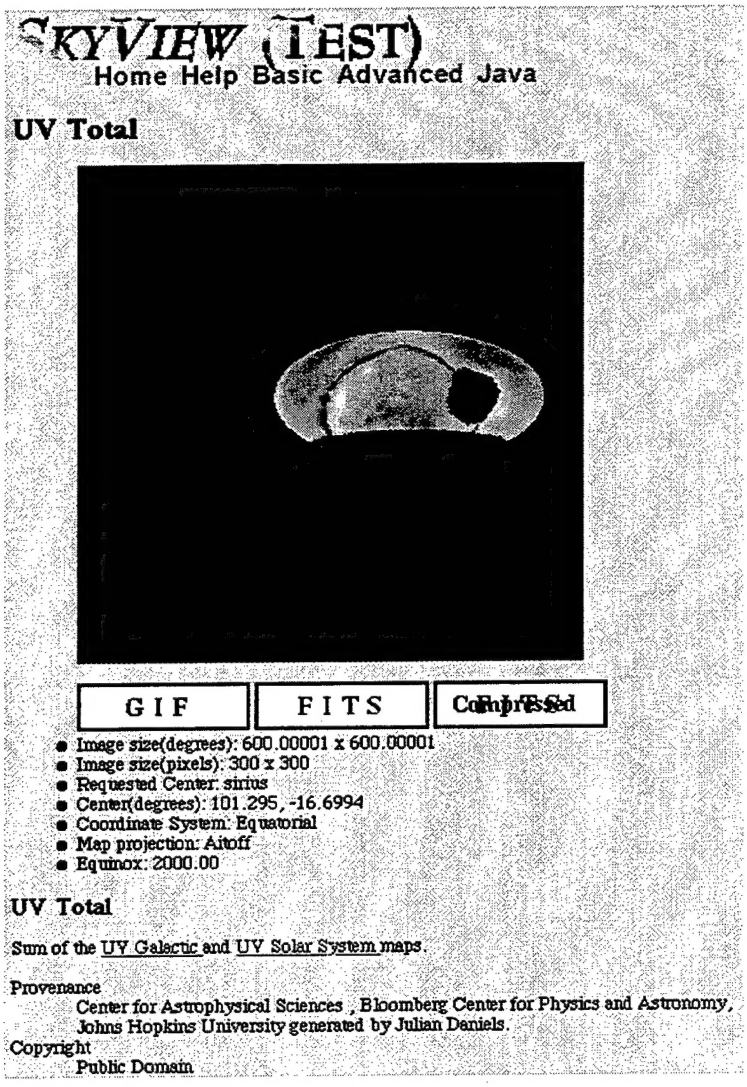

Figure 2. The result of submitting a SkyView request for a Hammer-Aitoff projection of the sky with "Total UV." The scientific basis for part of the modeling effort is given by Murthy and Henry ([5] 1995), which credits Air Force support.

2.1 Model of the Ultraviolet Zodiacal Light

The model for the ultraviolet zodiacal light is given by:

$$I_z = I_z (r, p, e, \lambda, \beta) \quad (1)$$

where I_z is the intensity of the zodiacal light and is a function of the heliocentric distance, *r*; the position of the observer relative to the dust symmetry plane, *p*; the epoch of observation, *e*; the wavelength, λ; and the viewing direction, β, usually defined by helio-ecliptic coordinates (helio-ecliptic longitude and helioecliptic latitude).

With respect to *r*, the observation can be terrestrial (ground based, or satellite) or interplanetary (e.g. deep space probes). The dependence of intensity, I, on heliocentric distance for an observer at *r* AU, ($0.3 \leq r \leq 1.0$) as measured by the Helios probe is ([16] Leinert 1980):

$$I_r = r^{-2.3} \times I_{(1\ AU)} \quad (2)$$

Concerning *p*, annual variations of 10% - 20% at the poles (peak to peak) originate in the slight inclination of the zodiacal cloud's symmetry plane in relation to the ecliptic ([21] Levasseur, 1994): the symmetry plane differs in the inner and outer solar system; at $r > 1$ AU it is close to the invariant plane.

$$\text{For } r < 1 \text{ AU, } i = 3.0^\circ \pm 0.3^\circ \text{ and } \Omega = 87^\circ \pm 4.0^\circ \quad (3a)$$

$$\text{For } r \geq 1 \text{ AU, } i = 1.5^\circ \pm 0.4^\circ \text{ and } \Omega = 96^\circ \pm 15^\circ \quad (3b)$$

where I = inclination to the ecliptic and Ω = ecliptic longitude of the ascending node.

Regarding *e*, short-time enhancements of brightness in peculiar directions have been ascribed to optical detection of meteor streams ([19, 20] Levasseur and Blamont, 1975, 1976; [18] Levasseur, 1976; [2, 3] Baggaley, 1977a, b) and to the accretion of dust near L4-L5 libration points of the Earth-Moon system ([25] Mercer et al., 1978). Analyses do not confirm any significant correlation between ZL and solar activity, either with respect to flares ([26] Misconi, 1977) or to the whole cycle ([9] Dumont and Levasseur-Regourd, 1978).

With respect to λ, the UBV colors of Zodiacal Light are given by ([17] Leinert et al., 1982):

$$I_V/I_B = 1.14 - 5.5 \times 10^{-4}\,\varepsilon \qquad (4a)$$

and $$I_B/I_U = 1.11 - 5.0 \times 10^{-4}\,\varepsilon \qquad (4b)$$

where ε = solar elongation in degrees. An intensity ratio of 1.0 corresponds to solar color. The above expression gives a maximum range in I_U/I_V of 0.79 - 1.14.

According to Murthy et al. ([28] 1990) the ZL spectrum is close to solar, although slightly reddened, over the range 2000 Å to 3000 Å; and his review of experimental data over the period, 1972 - 1990, neglecting very spurious observations indicates the ZL spectrum to deviate from a solar color of 1 by a maximum factor of 5. In addition, Weinberg and Sparrow ([34] 1978) report that over a very large domain 2500 Å to 25000 Å, the ZL is practically solarlike.

Murthy et al. ([28] 1990) also indicate that the color of the zodiacal light (relative to the visible) is found to increase linearly with ecliptic latitude implying that the small grains responsible for the UV scattering have a much broader distribution with distance from the ecliptic plane that do the larger particles responsible for the visible scattering properties of the interplanetary cloud are relatively uniform from 2000 Å to the visible.

It results from the preceding survey of these second-rank parameters (whose effect is either weak or restricted to rather unusual conditions) that the ZL first and foremost depends on the helioecliptic coordinates of the line of sight; and has a spectrum close to solar.

Given the above analysis, the specific model for the ultraviolet zodiacal light that we have implemented is given by

$$I_z = I_z\,(\beta, \lambda) \qquad (5)$$

with the symbols as in Eq. (1). I_z as a function of helioecliptic coordinates is obtained using the data of Levasseur-Regourd and Dumont, 1980: their data is a result of observations at Tenerife Observatory during the period 1964 to 1975. The data do not include zodiacal light measurements within a 20° cone of the sun. The solar spectrum is used to represent the variation of zodiacal light with λ.

Our model is generated with a spatial resolution of 5° in helioecliptic coordinates using linear interpretation from a look-up grid. The look-up grid values are extracted directly from the

source grid (also having a spatial resolution of 5°, [22] Levasseur-Regourd and Dumont, 1980). The uncertainty in brightness is 10% in the bright regions and 20% in the faint regions. The solar spectrum in the ultraviolet wave-band is generated, with a spectral resolution of 5 Ångstroms, from Kurucz ([14] 1979) models of stellar atmospheres using a solar temperature of 5500 K. Code is generated in Fortran 77 and stored as a standard FITS file.

The models are smooth and visually uninteresting, so (unlike with the stellar and dust-scattered starlight models, which are given below) we do not illustrate them.

2.2 Model of the Diffuse Galactic Light

The model for the Diffuse Galactic Light (DGL) is given by

$$I_D = I_D \{ \; I(\alpha, \delta, \lambda, \phi), \; \tau(\alpha, \delta, \lambda, \phi), \; D_a(\alpha, \delta, \lambda, \phi), \; D_p(\alpha, \delta, \lambda, \phi) \} \qquad (6)$$

where I_D is the intensity of the DGL radiation at the earth.

$I(\alpha,\delta,\lambda,\phi)$ is the interstellar galactic radiation field in the ultraviolet as a function of galactic longitude, α, galactic latitude, δ, earth distance, ϕ, and wavelength, λ. It is dominated by emission from a relatively small number of O and B stars, with some contributions from hot A stars in the near UV. $\tau(\alpha, \delta, \lambda, \phi)$ is the dust optical depth, as a function of galactic longitude, α, galactic latitude, δ, earth distance, ϕ, and wavelength, λ. τ can be expressed in terms of n_H. The distribution of gas, and therefore the dust, is not well constrained and may vary considerably in different directions (see [6] Dickey & Lockman, 1990 or [24] McKee, 1990).

$D_a(\alpha, \delta, \lambda, \phi)$ is the galactic dust grain albedo function, which is dependent upon galactic coordinates, α and δ (dust grain size/type/distribution may not be uniform in galactic space), earth distance, ϕ and wavelength, λ.

$D_p(\alpha, \delta, \lambda, \phi)$ is the galactic dust grain phase function asymmetry factor, which is dependent (like the dust grain albedo function) upon galactic coordinates, α and δ, earth distance, ϕ and wavelength, λ.

A catalogue integration will yield a reasonable estimate of the interstellar radiation field ([13] Henry, 1977). We have used the SKYMAP star catalogue (Version 3.3, [10] Gottleib, 1978)

as our source of stars and from the information tabulated therein (the location, brightness, spectral type, and distance of each star) in conjunction with stellar atmospheric models ([14] Kurucz, 1979) to evaluate the radiation field at the stellar surface. The canonical ([32] Spitzer, 1978) galactic average value of $n_H = 1.2$ cm $^{-3}$ has been used to evaluate the interstellar extinction due to dust and hence the vector ISRF at any point in space, α, β, and ϕ.

For the dust density at α, β, and ϕ, the Bell Labs H I survey ([33] Stark et al, 1992) has been used to estimate the total HI column density N(H I) along the line-of-sight, which was then converted into a dust optical depth (τ) using the cross-sections of Draine & Lee ([7] 1984). These cross-sections implicitly assume a uniform gas-to-dust ration of N(HI)/E(B-V) = 5.8 x 10^{21} cm^{-2} ([4] Bohlin, Savage & Drake 1978). For the n_H distribution an exponential scale height of 200pc has been used. The exponential scale height of 200 pc is very close to the two component model of Lockman, Hobbs, & Shull ([23] 1986), consisting of a gaussian of scale height 135 pc and an exponential of scale height 500 pc, each containing one half of the total amount of gas.

The model assumes that the optical constants of the grains are invariant over the entire sky. Also, there is no multiple scattering and self-shielding of the dust particles.

The amount of scattering radiation off dust grains is evaluated using the well-known Henyey-Greenstein scattering function and further radiation extinction occurs between dust grains at α, β along the line-of-sight to the earth.

Our model, then, as in Eq. (6), is given by

$$I_D = I_D (I, \tau, D_a, D_p) \qquad (7)$$

with the symbols as explained above.

To perform the actual calculation of the scattered starlight from an arbitrary line of sight, we divide the line of sight into a number of cells; calculate the amount of scattered radiation from each of the cells using a Henyey-Greenstein scattering function for 1 value of the phase function, 0.1; a dust grain albedo of 0.1 and an n_H galactic scale height of 200pc, The DGL model is generated at the following wavelengths: 915 Å, 950 Å, 1100 Å, 1900 Å, 2100 Å, 2600 Å, and 3100 Å and is linearly extrapolated to cover the range 915 Å to 3100 Å with a spectral resolution of 5 Å and a spatial resolution of 2 degrees, with all code generated in IDL and stored as a standard FITS file. In the next three figures (3, 4, and 5), we illustrate the model results, which are described (see Appendix B) completely by Murthy and Henry ([29] 1995). The blank region, is a region where no 21-cm hydrogen data are available from

which to infer the column density of dust in that direction. A few artifacts are present in the model. An absolute intensity scale is provided in the figures. All these figures have the galactic center at the center of the figure, with galactic longitude increasing to the left, as it does on the sky. The North Galactic Pole is at the top of each figure, and the South Galactic Pole is at the bottom.

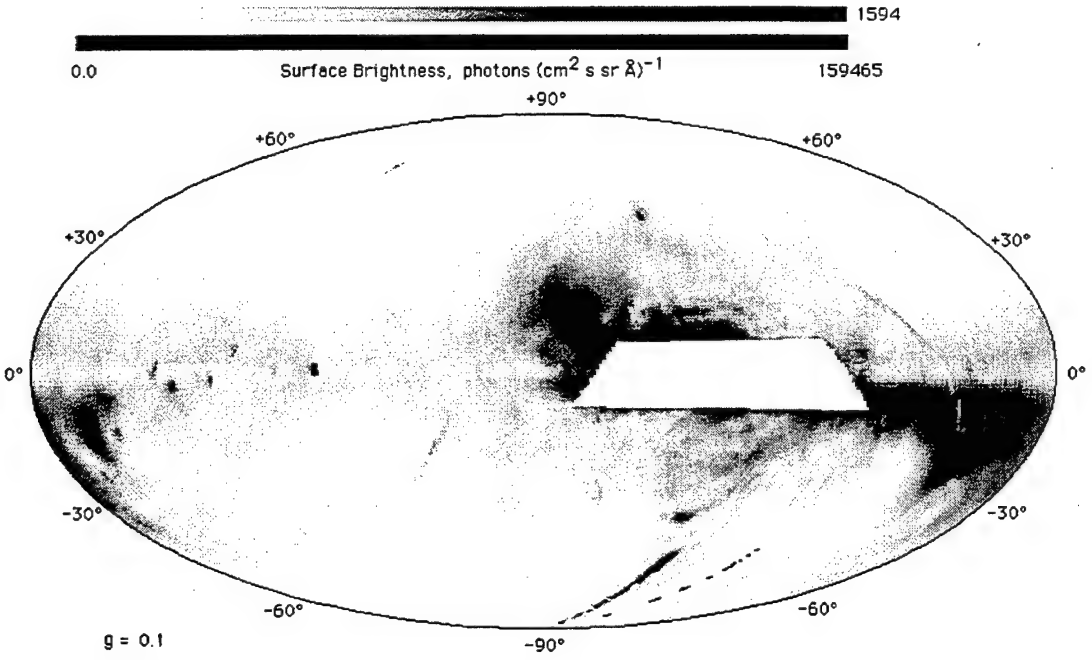

Figure 3. Starlight (1565Å) scattered from dust, if the scattering parameter $D_p = 0.1$

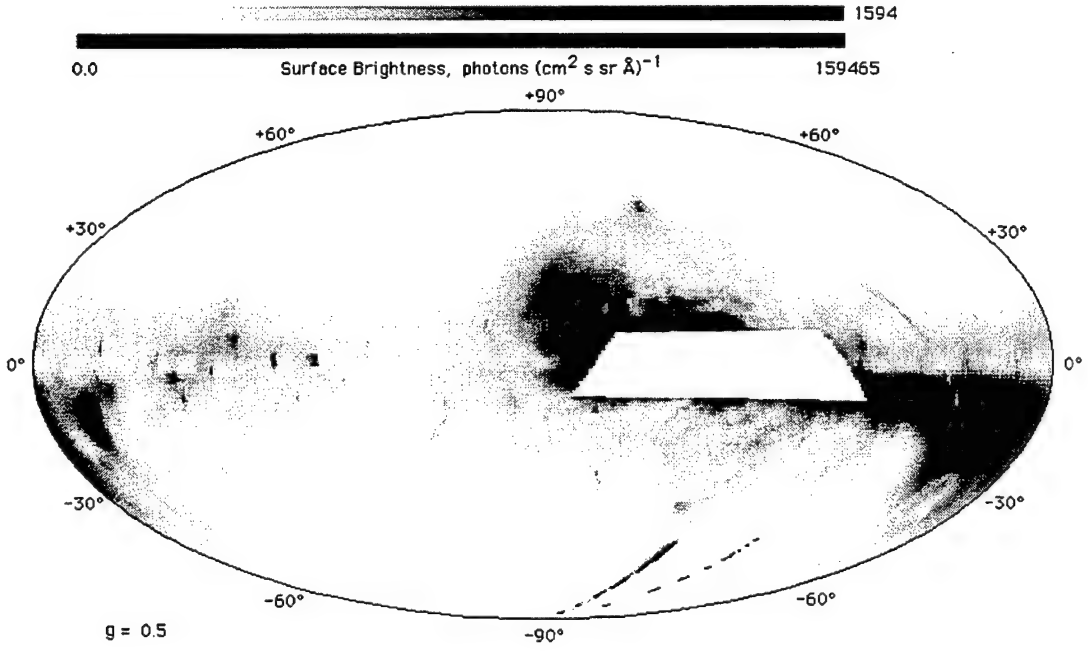

Figure 4. Dust-scattered starlight at 1565Å. The intermediate case $D_p = 0.5$

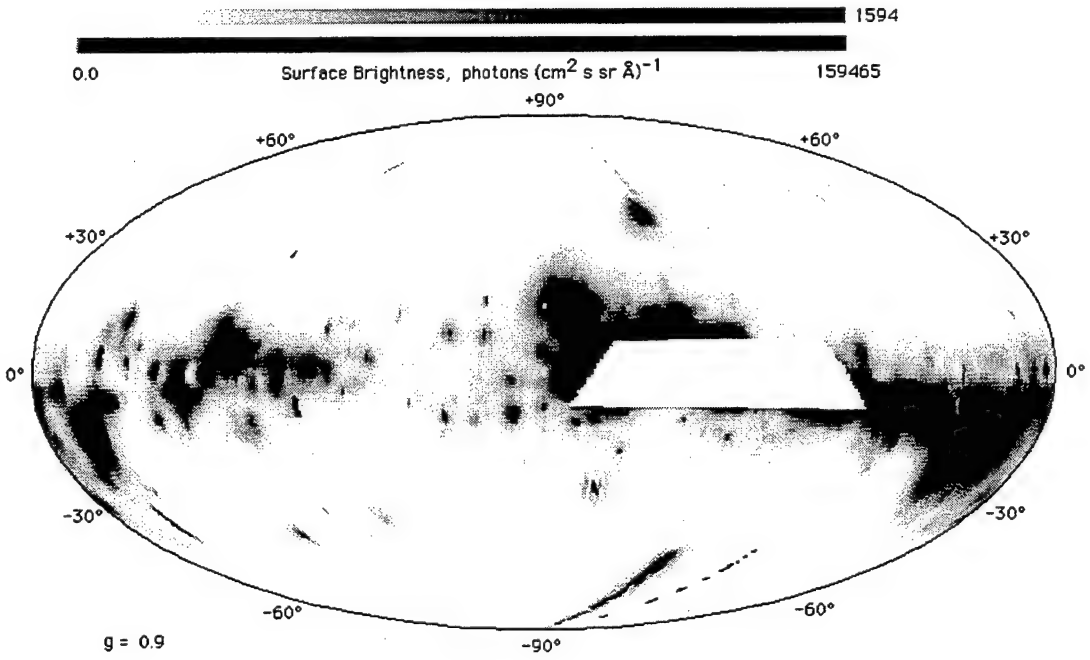

Figure 5. Starlight scattered from dust, if the scattering parameter $D_p = 0.9$ In this case, the dust-scattered starlight is concentrated around individual stars. Notice that the brightness at the North Galactic Pole is considerably reduced over the other two cases. The correct value for D_p is not known.

2.3 Ultraviolet Model of Starlight

The model for starlight is given by

$$I_S = I_S \{ I(\alpha, \delta, \lambda, \phi), \tau(\alpha, \delta, \lambda, \phi) \} \tag{8}$$

where I_S is the intensity of stellar radiation at the earth.

$I(\alpha,\delta,\lambda,\phi)$ is the intensity of the stellar surface radiation emission in the ultraviolet as a function of galactic longitude, α, galactic latitude, earth distance, ϕ , and wavelength, λ.

$\tau(\alpha, \delta, \lambda, \phi)$ is the dust optical depth, as a function of galactic longitude, α, galactic latitude, δ, earth distance, ϕ , and wavelength, λ . τ can be expressed in terms of n_H. The distribution of gas, and therefore the dust, is not well constrained and may vary considerably in different directions (see Dickey & Lockman 1990 or McKee 1990).

The SKYMAP star catalogue (Version 3.3, [10] Gottleib 1978) has been used for the source of stellar data and is as complete as possible to 9.0 mag blue (B) and visual (V). Approximately 255,000 stars are included in the catalogue. Each star includes the following date: Position (with error); spectral type (there is some error in quoted spectral class: for MK types, this is assumed to be one-tenth of the spectral class and one-third of a luminosity class; for stars with only HD (Henry Draper catalog) or SAO (Smithsonian Astrophysical Observatory) spectral types, this is taken as three-tenths of a spectral class and two-thirds of a luminosity class); distance (with error) UBV photometry (quoted error, from references within Gottleib, are typically 0.02 mag); and interstellar absorption in the ultraviolet (no error given). The intensity of the stellar surface emission [I_F in equation (9)] is derived from the location, brightness, spectral type, and distance of each star from SKYMAP in conjunction with the stellar atmospheric models of [14] Kurucz, 1979).

To evaluate the intensity of the stellar radiation flux at the earth, the following approximation is used (Murthy, 1994) for each star.

$$I_E = I_F(\lambda) \times e^{-(\sigma(\lambda)\, E\,(B-V) \times\, 0.53)} \tag{9}$$

Where I_E is the Stellar radiation flux at the earth and I_F is the stellar surface radiation flux. E(B-V) is the color excess for each star, $\sigma(\lambda)$ is the Hydrogen molecular cross-section at wavelength, λ.

Our model is then give by

$$I_S = I_S\{\, I(\alpha, \delta, \lambda, \phi),\ I_a\,(\alpha, \delta, \lambda, E)\,\} \tag{10}$$

With symbols as in Eq (8); I_a is the absorption function for each star at galactic coordinates α, β and is equivalent to the exponential component in E (9), while E is the color index for each star.
Using the specific model above, stellar radiation flux at the earth is integrated into 2 by 2 degree galactic cells over the range 900-2500 Ångstroms at 5 Å intervals. The model is linearly interpolated to 3100 Ångstroms. The code is generated in IDL and stored as a standard FITS file.

We illustrate the direct starlight model:

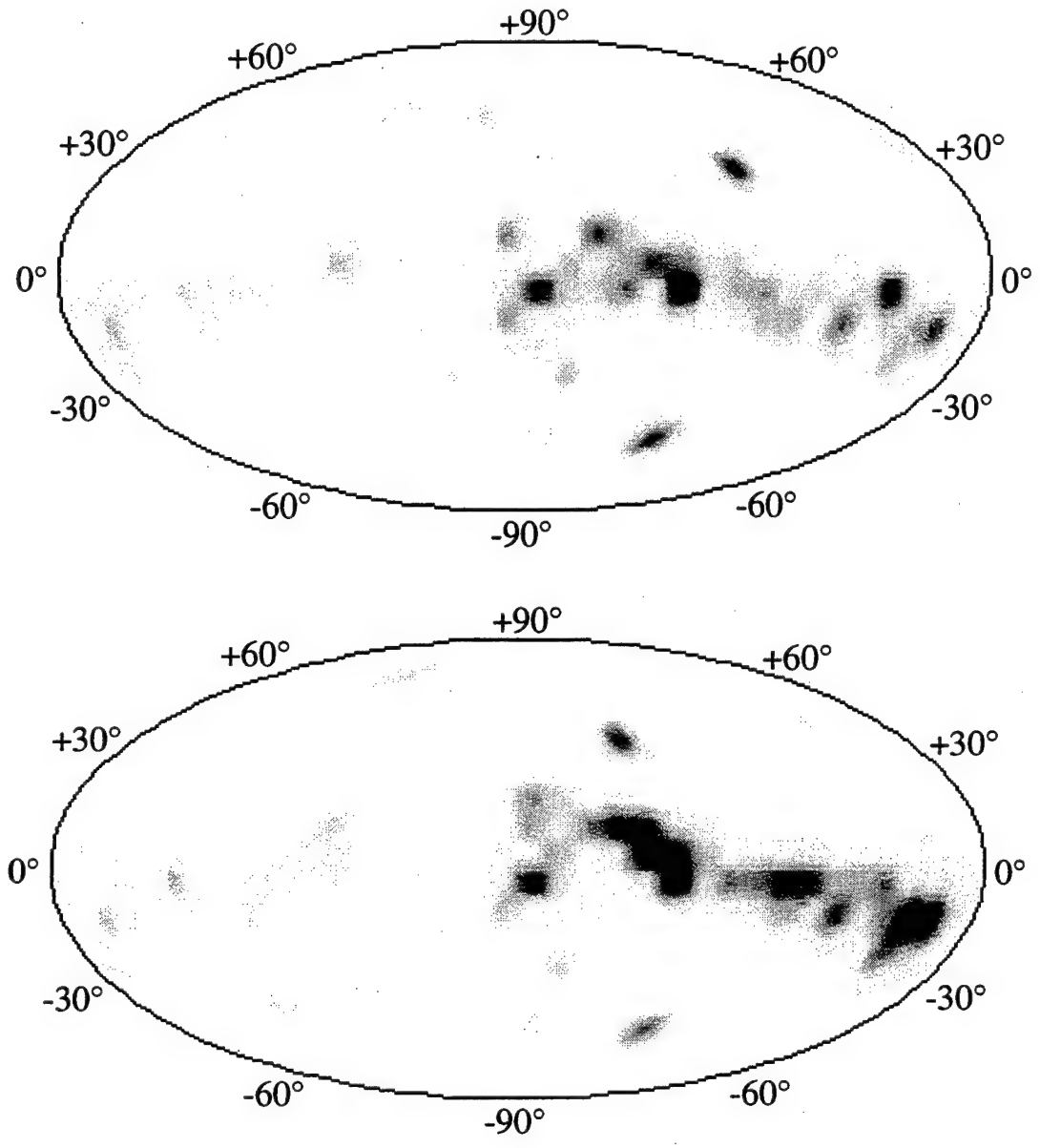

Figure 6. Comparison of our model stellar fluxes (top) with the observed TD-1 stellar fluxes (bottom). The orientation of the plots are the same as in the case of the illustrations of dust-scattered starlight (above). The wavelength is 1565A, and the scales of intensity are linear and are the same for both plots.

3. UVISI CAPABILITIES

MSX is a Ballistic Missile Defense Organization (BMDO) experiment designed to obtain observations of a wide range of natural and man-made phenomena observable from a space based platform. The satellite was launched in April of 1996 and the UVISI instruments are used to obtain astronomical ultraviolet background data. In Figure 7 we show the location of the UVISI instruments on the MSX spacecraft, and in Tables 1 and 2 we provide the

characteristics of the UVISI imagers, and in Table 3 the UVISI hyperspectral imagers (often called SPIM's). The wavelengths listed are those at which the response is 10% of peak.

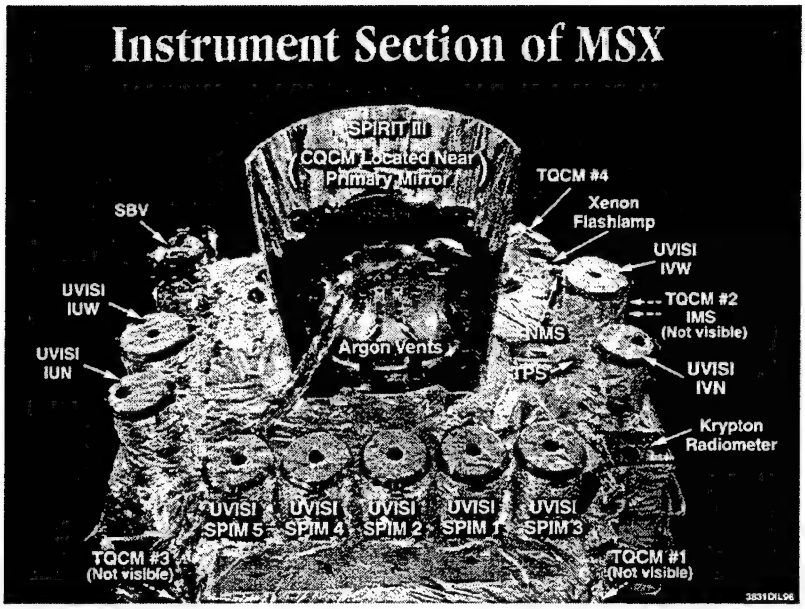

Figure 7. The location of the UVISI instruments on the MSX Spacecraft. There are four UVISI imagers: IUN, IUW, IVN, and IVW (see Table 1). In addition, there are five imaging spectrometers, or SPIM's (see Table 2).

Most ultraviolet astronomy is carried out by NASA. NASA has an impressive history of accomplishment in ultraviolet astronomy; however, it is widely acknowledged that there are two glaring gaps in the NASA (indeed, in the world) ultraviolet astronomy effort.

1.) There has been no adequate sky survey to discover and catalog faint UV point sources (although after declining to fund continued operations of UVISI, NASA selected GALEX, a point-source UV sky survey, for implementation).

2.) there has been no significant examination of the diffuse sky background in the ultraviolet (although NASA has selected HUBE, a UV diffuse-background radiation experiment, as a MIDEX Alternate mission).

It is in the area of filling these gaps that MSX capabilities are important. The NASA deficiencies were emphasized at the topical session at the IAU Symposium 179 "New Horizons from Multi-Wavelength Surveys" held at Johns Hopkins University in August 1996 (Price et al. 1997).

Table 1. The UVISI Imagers

Filter \ Imager->	IUN	IUW	IVN	IVW
1-Closed				
2-ND ($x10^{-3}$)	1930 - 2740 Å	1140 - 1430 Å	2500 - 8390 Å	3000 - 8500 Å
3-WB3	**2240 - 2710 Å**	1240 - 1370 Å	3410 - 4770 Å	5250 - 6390 Å
4-Open	**1990 - 2670 Å**	**1250 - 1540 Å**	2970 - 8340 Å	3000 - 8310 Å
5-WB2	**1900 - 2500 Å**	1150 - 1320 Å	2480 - 3190 Å	4230 - 4310 Å
6-WB1	2640 - 3030 Å (polarizing)	**1420 - 1760 Å**	4720 - 6390 Å	3800 - 9000 Å (near focus)
Photocathode	RbTe	CsI	Ext S20	Ext S20
Window	MgF_2	MgF_2	SiO_2	SiO_2
Pixel Size	19'' x 22"	2.6' x 3.2'	19" x 22"	2.6' x 3.2'
Area (cm^2)	130	25	130	25

Table 2. Sensitivity of the UVISI Imagers, as Measured On-orbit by the Proposers

Imager and filter	Magnitude limit	flux limit (ergs cm^{-2} s^{-1} $Å^{-1}$)
IUW filter 6 (1420-1760 Å)	14	7.0×10^{-13}
IUN filter 4 (1990-2670 Å)	20	1.0×10^{-16}
IUN filter 5 (1990-2500 Å)	18	1.5×10^{-15}
IUN filter 6 (2640-3030 Å)	17	1.7×10^{-14}
IVN filter 3 (3410-4770 Å)	20	
IVN filter 6 (4720-6390 Å)	18	
IVW filter 5 (4230-4310 Å)	12	

Approximate sensitivity limits, S/N=10, for an unreddened B0V star. These magnitude limits are very tentative at this time and are based on only a few stars, of uncertain spectral types. The UV imager flux limits are based on scaled TD-1 fluxes of stars identified in the UV imager fields and are much more reliable. For comparison, the HUBE claimed limit at 1500 Å is 1.5×10^{-16} ergs cm^{-2} s^{-1} $Å^{-1}$.

4. UVISI PERFORMANCE

In addition to the paper [29] in the Astrophysical Journal, presenting details of the modeling of the diffuse galactic light, we have made a variety of other presentations and publications

involving our UVISI and MSX activities in connection with the present work. We list them here:

1. M. M. Allen, J Murthy, J. Daniels, A. R. Dring, R. E. Newcomer, R. C. Henry, L. Paxton, E. Tedesco, "UV Observations of Extended Galaxies with UVISI," The Universe at Low and High Redshift, University of Maryland College Park, 2 - 4 May 1997

2. A. R. Dring, J Murthy, M. M. Allen, J. Daniels, R. E. Newcomer, R. C. Henry, L. Paxton, E. Tedesco, S. D. Price, "UVISI Observations of Orion Dust," BAAS, 29, 785, 1997

3. M. M. Allen, J Murthy, J. Daniels, A. R. Dring, R. E. Newcomer, R. C. Henry, L. Paxton, E. Tedesco, S. D. Price, "UVISI Observations of The Pleiades," BAAS, 29, 805, 1997

4. J Murthy, M. M. Allen, J. Daniels, A. R. Dring, R. E. Newcomer, R. C. Henry, L. Paxton, E. Tedesco, S. D. Price, "UVISI Observations of the Galactic Plane," BAAS, 29, 838, 1997

5. J. Daniels, J Murthy, M. M. Allen, A. R. Dring, R. E. Newcomer, R. C. Henry, L. Paxton, E. Tedesco, S. D. Price, "UVISI Observations of the Large Magellanic Cloud," BAAS, 29, 805, 1997

6. S. D. Price, M. Cohen, R. G. Walker, R. C. Henry, M. Moshir, L. J. Paxton, F. C. Witteborn, M. P. Egan, R. F. Shipman, "Astronomy on the Midcourse Space Experiment," BAAS, 28, 1341, 1997

7. R. C. Henry, J. Murthy, M. Allen, J. Daniels, A. R. Dring, L. J. Paxton, E. F. Tedesco, and S. D. Price, "UVISI Observations of the Small Magellanic Cloud," BAAS, 28, 1387, 1997

8. S. D. Price, E. F. Tedesco, M. Cohen, R. G. Walker, R. C. Henry, M. Moshir, L. J. Paxton, and F. C. Witteborn, *"Astronomy on the Midcourse Space Experiment,"* in Proceedings of IAU Symposium 179, *New Horizons from Multi-Wavelength Sky Surveys*, ed. B. J. McLean, D. A. Golombek, J. J. E. Hayes, and H. E. Payne, 115, 1997

9. R. C. Henry, J. Murthy, M. Allen, M. Corbin, and L. J. Paxton, *"Spectroscopy and Imaging of the Cosmic Diffuse UV Background Radiation,"* SPIE Conference Vol. 1764, "Ultraviolet Technology IV", ed. Robert E. Huffman, 61, 1992

Ultraviolet Sky Survey The principal result of our UVISI work is the creation of a partial survey of the ultraviolet sky. This survey was begun in two wavelenth bands with the wide-field imager, with the narrow-field imager taking a simultaneous image at the center of the

wide-field imager field of view. The sky survey was designed by Dr. Stephan D. Price and Dr. Richard C. Henry, and is shown in Figures 8 and 9:

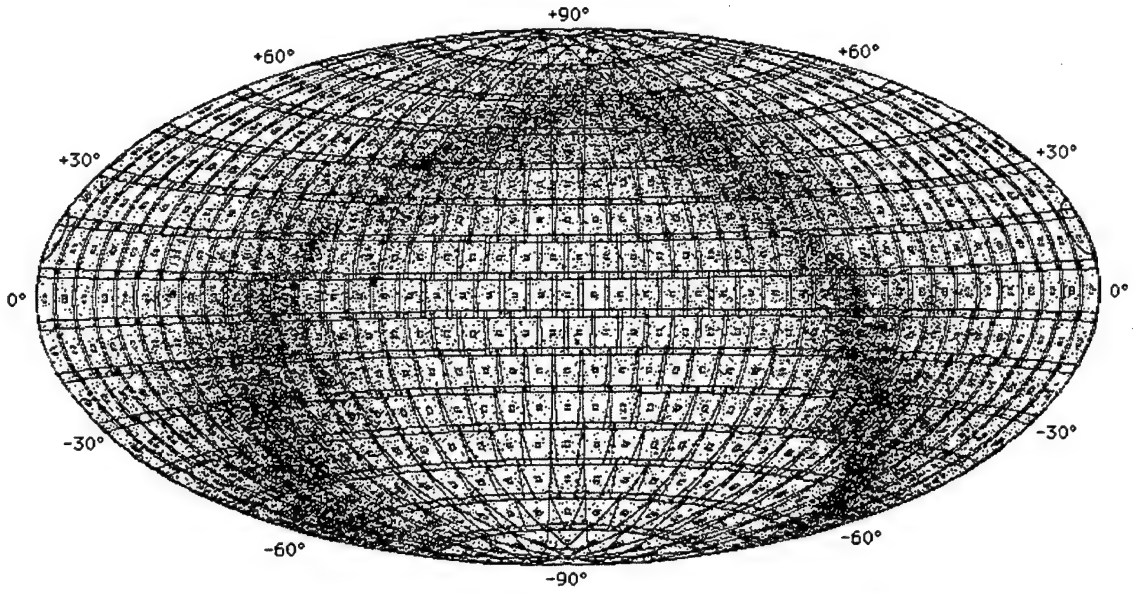

Figure 8. Ecliptic-Coordinate Map of the Sky Survey that is currently under way (detail of polar coverage: see Figure 9). Black dots are the TD-1 stars; red rectangles are the UVISI wide-field imager footprints.

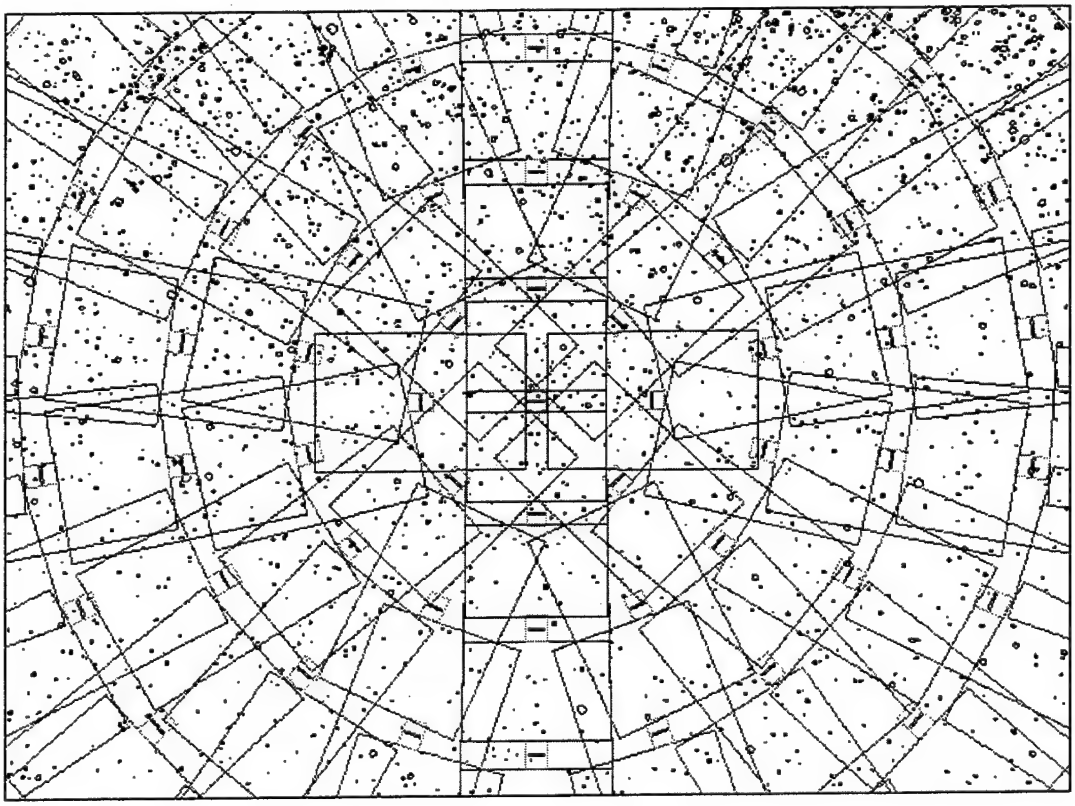

Figure 9. The Pole region, showing UVISI sky survey coverage. Green is IUN (narrow-field) fov.

A typical UVISI target is shown in detail in Figure 10:

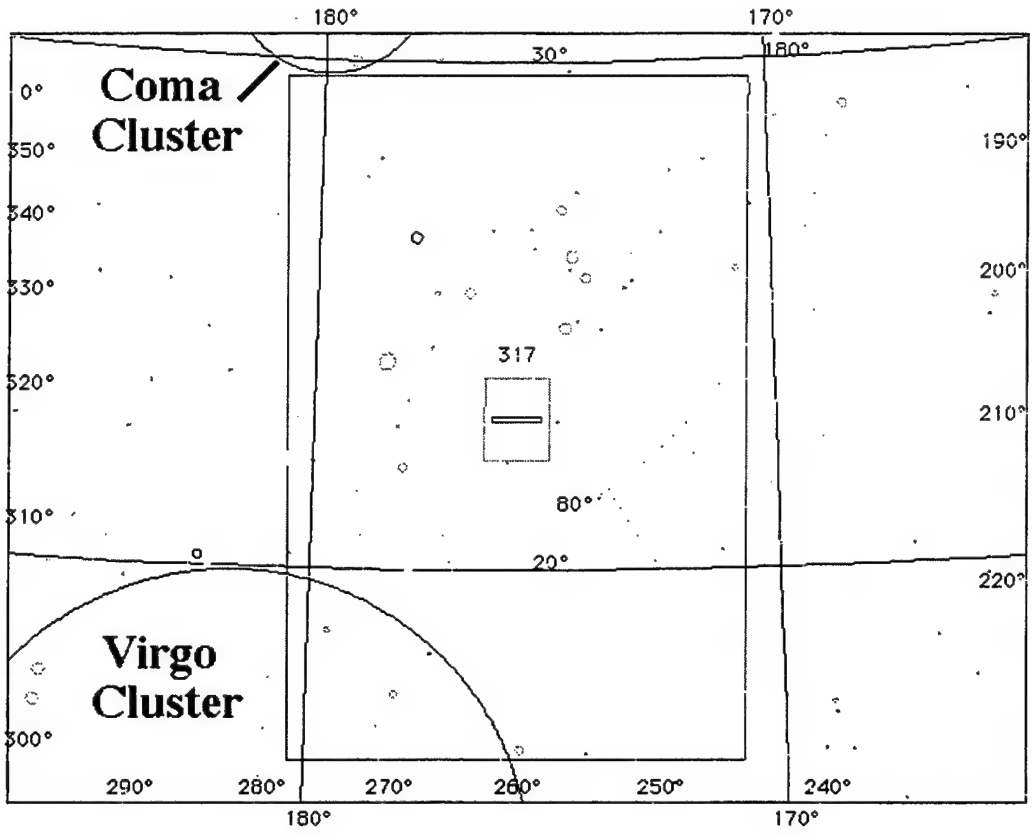

Figure 10. UVISI Target 317 from the sky survey. The large rectangle is the wide field of view. The small rectangle below the number "317" is the fmall field of view, and the thin rectangle within that is the SPIM momentary field of view: the SPIM's are scanned across the narrow field of view. This target is near the North Galactic Pole, where the Virgo and Coma clusters of galaxies happen to be located. The stars of our own galaxy are shown individually, size of plotted point indicating expected UV brightness as estimated by our model procedure. The map is in ecliptic coordinates, with galactic coordinates superimposed.

Th UVISI sky survey was only partially been carried out (Figure 11) to assess sensitivities and optimal observing parameters. The progress of this sky survey to termination could be monitored by consulting **http://msx4.pha.jhu.edu/survey.html**, and clicking on "Progress of the Survey." The plan was to survey the entire sky with IUW in two colors, 1250 - 1370 Å and 1420 - 1760 Å. The initial 1420 - 1760 Å band survey was to be carried out in a systematic fashion; approximately 30% of the sky has already been covered as can be seen from the web site. Recognizing that the 2.6' x 3.2' IUW pixels are simply too large for convenient ground or space based follow up, we planned to identify the interesting objects, such as extended complex sources detected during the 1420-1760 Å survey and target these for IUN higher sensitivity and spatial resolution measurements. Most of the 1250 - 1370 Å

survey would have been obtained during these IUN follow-up observations and during the IUN measurements obtained for other scientific objectives. Only a small number (<100) of dedicated observations would have been needed to complete the survey.

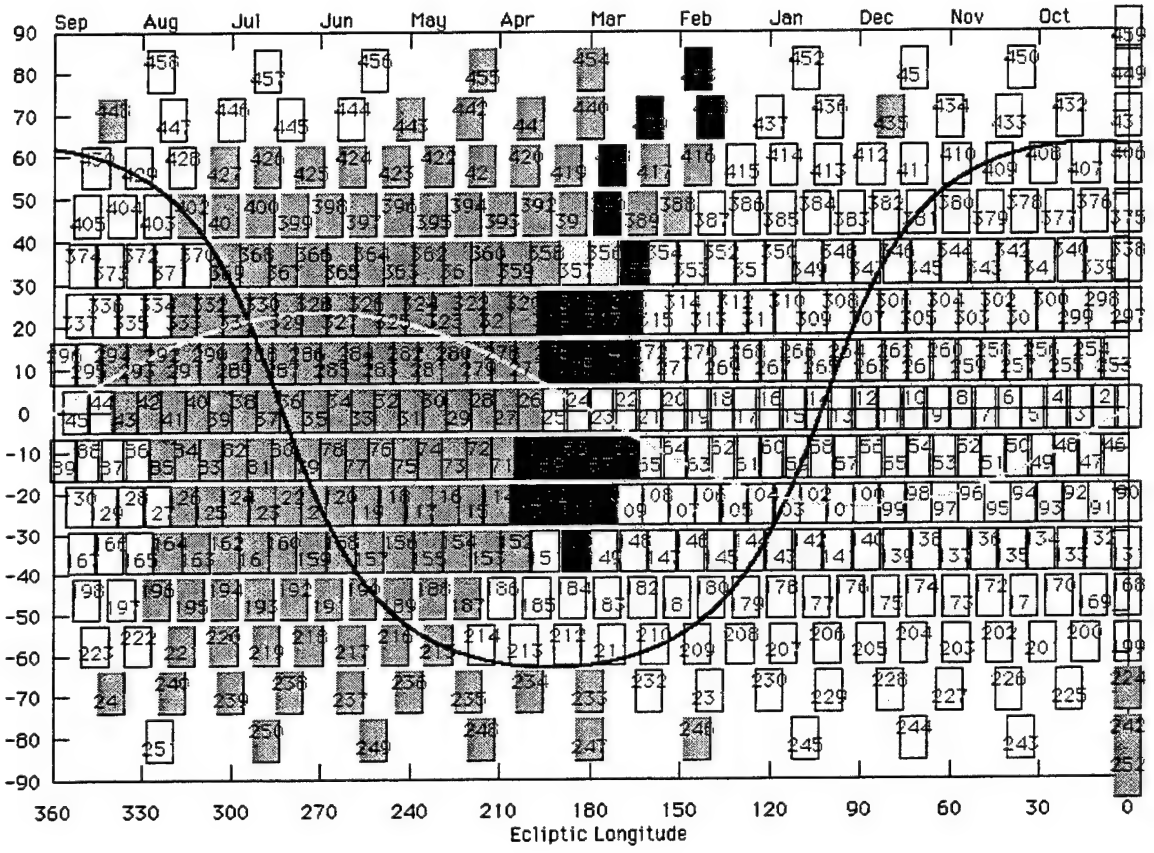

Figure 11. The UVISI sky survey as it was carried out: white targets were never observed. Black targets were observed at 1280 Å – 1380 Å; grey targets at 1450 Å – 1800 Å; targets #356 and #357 at *both* wavelengths.

Concurrent with the systematic IUW survey, the IUN imager was to carry out a survey in three bandpasses, 1990-2670 Å, 1990-2500 Å and 2240-2710 Å on a representative 2% of the sky. An additional 5% of the sky were to have been surveyed by IUN during follow-up observations and those obtained on specific fields of interest. As noted previously, the IVN also simultaneously obtains data in the optical ultraviolet spectral regions. The observations with the narrow field of view imagers may have the greatest value for astronomy, because of its much greater sensitivity and smaller pixel size (19" by 22"). The IUN pixels are small enough that interesting objects discovered can subsequently be identified and accurate positions obtained from follow-up ground based observations. The precise positions permit

the objects to be found and studied using the powerful UV instruments aboard HST and FUSE.

Admittedly, the IUN sky survey would have been necessarily incomplete, covering approximately 7% of the sky during a hoped-for two year mission. We have assured that as planned, the coverage would have been *representative*, such that the number of new sources anticipated for the entire sky at the IUN sensitivities can be statistically extrapolated from these results. The ultraviolet color information from the survey will be used to sort the objects as the spectral characteristics.

5. UVISI DATA

We can only provide a small sample, so as to exhibit the UVISI data. Many more examples may be seen by consulting the references in section 4. First, in Figure 12 we show an IUW image of the constellation Orion, one of the brightest ultraviolet regions in the sky Then, in Figure 13, we show an IUN image of the Large Magellanic Cloud. Details of the IUN observations of the *Small* Magellanic Cloud are given in [11] presentation number 7, in section 4.

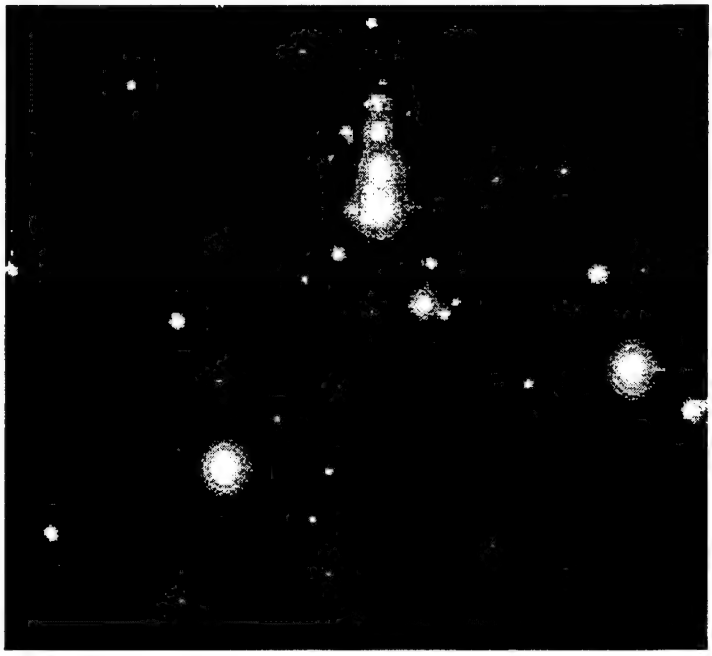

Figure 12. IUW (Wide-field UV) image of Orion in the 1420 - 1760 Å passband

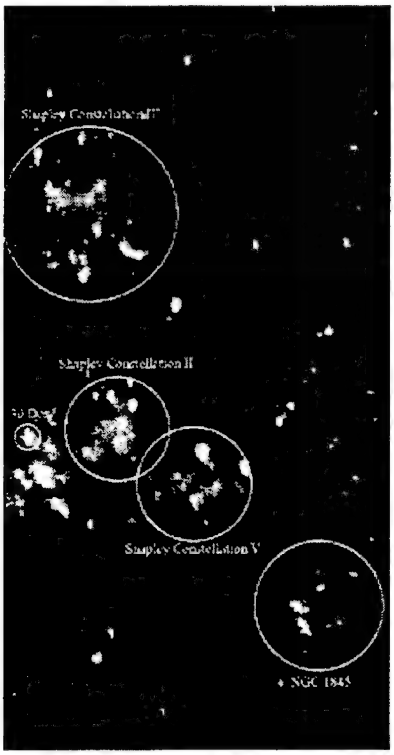

Figure 13. IUN image of the Large Magellanic Cloud.Various Shapley Constellations are visible, as well as the cluster NGC 1845

On the page 19 we present a detailed examination of a typical IUN target. In observation analysed so far, we find that approximately 1/3 of the sources found in IUN are not in SIMBAD - implying that they have never before been observed, or at least identified. Although most of these sources are too faint to observe with the SPIMs, we nevertheless obtain a measurement of the color of these objects through the several different filters of the imagers. This yields an important diagnostic on these objects and those few with unusual colors can be selected out of the vast horde of point sources (to a limiting equivalent magnitude of about 20) for follow-up studies with one of the great observatories.

In Figure 14, we show an IUW image of the Large Magellanic Cloud, including the bright 30 Doradus region and several Shapley Constellations. In Figure 15, we show a blow-up view of part of the sky survey observing plan that was shown in Figure 8. The region selected includes the Virgo Cluster of Galaxies (circle at top right in Figure), and the constellation Virgo itself.

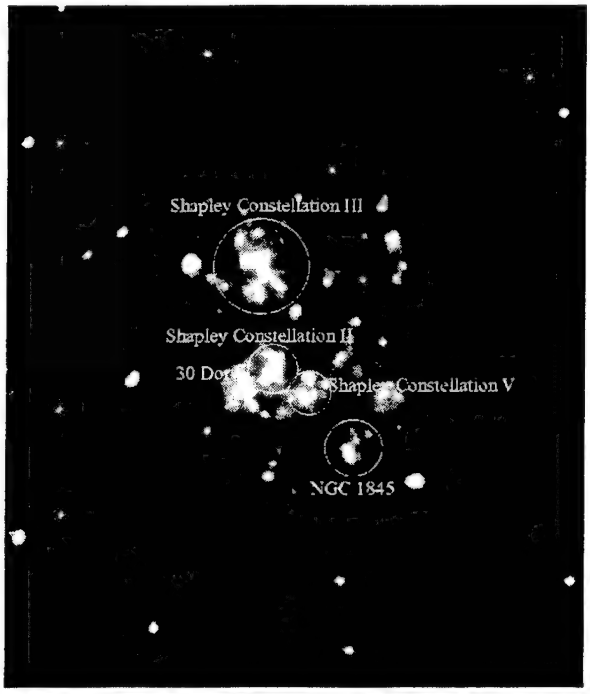

Figure 14. IUW (Wide-field UV) image of the Large Magellanic Cloud. In Figure 7 we showed the corresponding IUN (Narrow-field UV) image of the LMC.

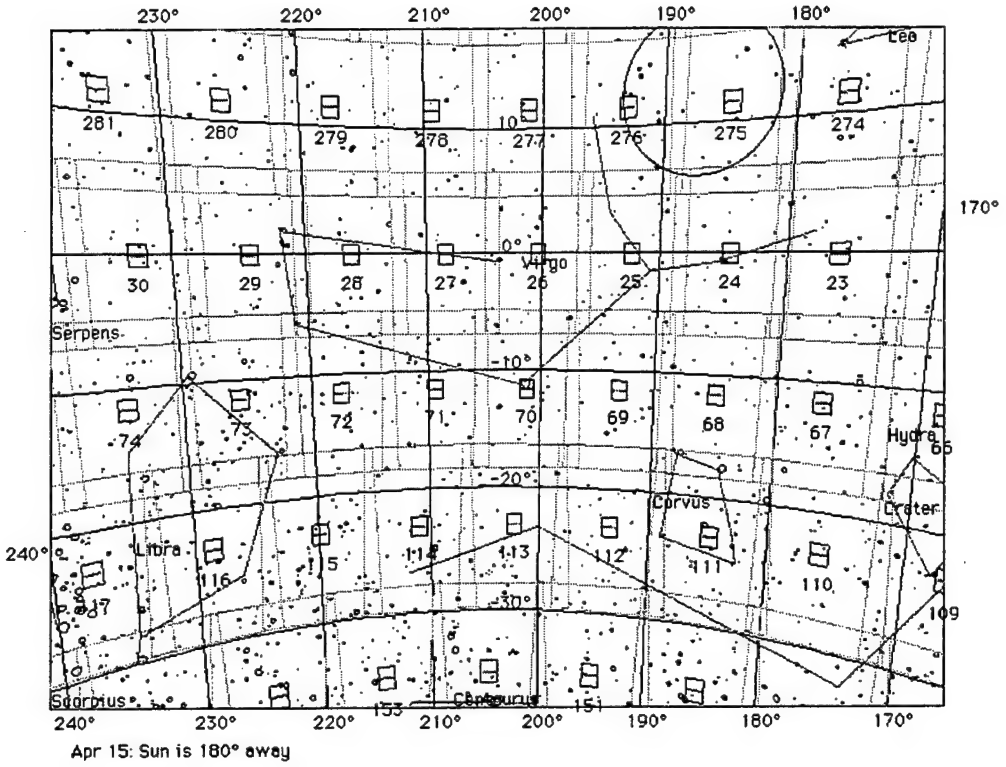

Figure 15. Planning map of the Virgo cluster (blue circle) region.

6. DATA ANALYSIS SOFTWARE

In many ways the largest single task carried out under the present contract, was the creation of a full set of software for the acquisition and reduction of the data from the UVISI complement of instruments on the MSX mission. This software complement is in place at the PLDAC and at the Applied Physics Laboratory of the Johns Hopkins University, and is in active use. The software was used for all treatment of UVISI data under the Celestial Backgrounds Experiment; Stephan D. Price Principal Investigator.

6.1 Introduction

The UVISI instruments are a complement of 4 imagers and 5 spectroscopic imagers (SPIMs) which flew aboard the MSX spacecraft in April 1996. The detectors in each of the instruments are intensified CCDs whose output appears as a series of two dimensional arrays at 0.5 second intervals (Level 1 data). The UVISI programs are designed to operate on the Level 1CA files; i.e. the data after they have been operated upon by UVISI CONVERT (Suther *et al.* 1993) and UVISI POINT. The programs described in this document form a self contained and automated set of routines designed to create a number of data products suitable for further analysis --- the Level 3 data files. The Level 3 products include image files of both high and low spatial resolution; analogous files from the SPIMs; and a list of point

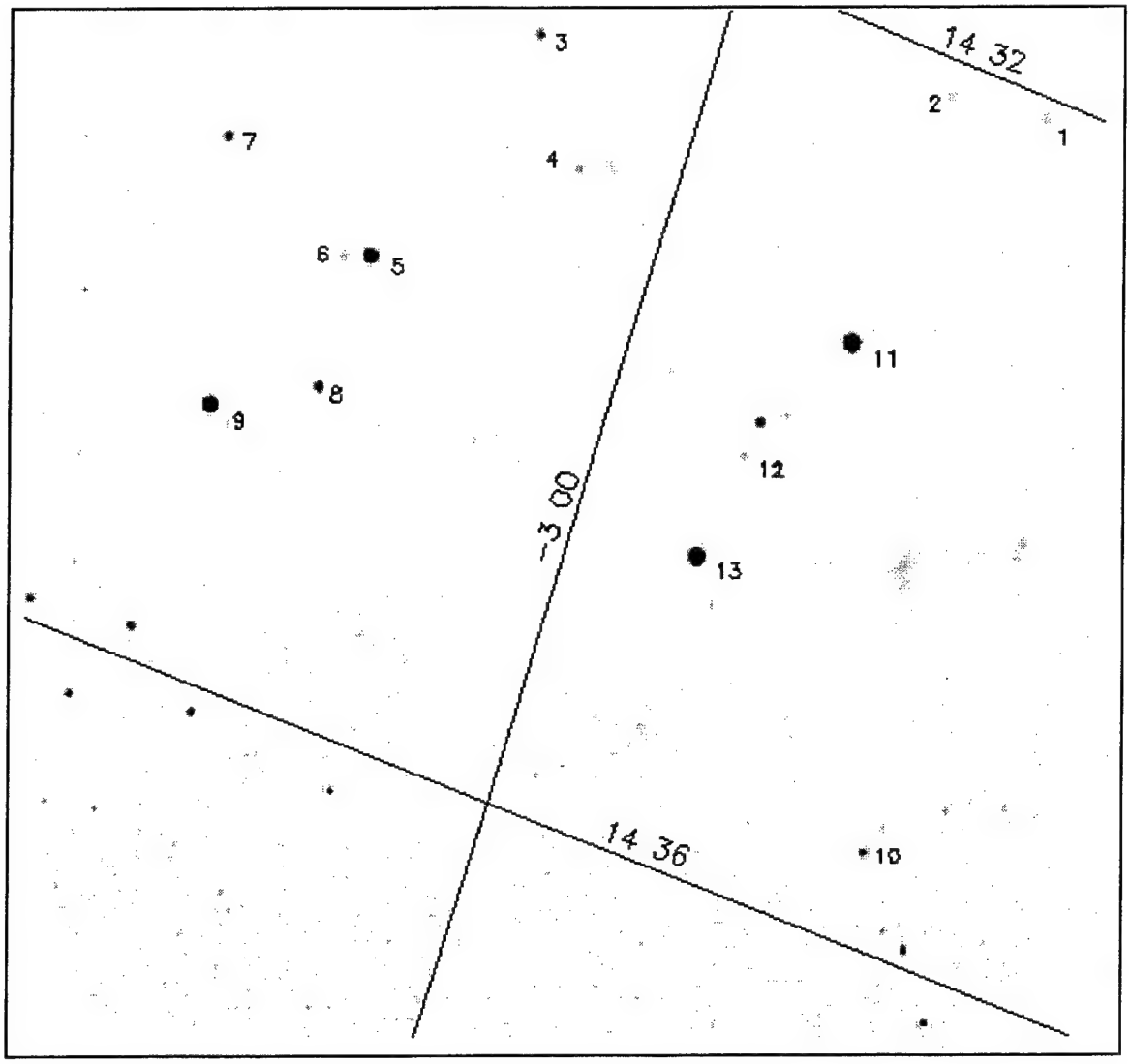

Figure 16. MSX UVISI Narrow-Field Imager, Filter position 4 (open: 1990 - 2670 Å) 233 - second exposure on a high-galactic latitude field (l = 347.2° b = 50.3°), target # 279

SIMBAD Identifications in Target 279:

1	BD-02 3857	4	CCDM J14330-0253B	7	StKM 1-1166	10	BD-02 3863
2	Z 1428.9-0305	5	AG-02 874	8	AG-02 875	11	BD-02 3859
3	CCDM J14330-0253A	6	HIC 71195	9	AG-02 876	12	Z 1431.4-0251
						13	BD-02 3862

sources with spectral information for each of the point sources but are restricted to operating on the data from a single DCE. Because of the immense volume of data, the only feasible methods of attaining the scientific and programmatic objectives of the mission are through the analysis of these Level 3 products.

6.2 Level 3 Products

The primary purpose of the Level 3 products is to render the output of the UVISI instruments into a format suitable for further analysis. As such we have identified several different products which are described below. All files are in standard FITS format.

Imagers

We create three classes of files from each imager active during a DCE. The most basic data product from the Level 3 processing of the imagers is the co-added FITS images of the entire DCE. These images consist of a uniform grid at the same spatial resolution as the original data. In the case of the raster scans typically performed in the cryo phase of the MSX mission, the data are smeared over several pixels and thus each frame must be shifted and added. In the post-cryo phase the observations were typically point-and-stare allowing the computationally simpler method of simply stacking frames.
Point sources in the Level 3 images are identified through the use of a matching algorithm (which matches the PSF) and their locations and magnitudes are written to a point source file. The Diffuse Background File (DBF) is intended for the analysis of large scale trends in the zodiacal light and the diffuse cosmic background. It is created by masking out point sources in the Level 3 images and then regridding the data into pixels of a much lower spatial resolution (nominally 0.25°).

SPIMs

The primary data product for analysis is a three-dimensional FITS file with two spatial dimensions and the third dimension being spectral.

Future Analysis

We are currently in the process of verifying the absolute calibration and performance of the UVISI instruments. We have identified a number of targets whcih are suitable for further analysis, such the Large Magellanic Cloud and M33. We are now proceeding with the analysis of those regions.

6.3 Programs

Introduction

The UVISI programs are all written in *IDL*, a widely used programming language created by Research Systems, Inc. of Boulder. *IDL* is well suited to the analysis of astronomical data both because of its excellent array techniques and because of the large number of astronomical routines publicly available. We have created a *control file* to process the UVISI data. This file is an *IDL* routine which reads an individual parameter file for each DCE and runs each of the UVISI programs in the correct order. We present one line summaries of each of the UVISI programs below with more complete documentation in the following pages. Flowcharts and program listings are in the Appendices.

1.	UVISI	Control procedure to run all others
2.	UV_INITHEADER	Initialize variables from CONVERT
3.	UV_READHEADER	Reads headers from Level 1CA files
4.	UV_READDATA	Reads data from Level 1CA files
5.	UV_IMCON	Creates Level 3 images
6.	UV_PSEXTRACT	Extracts point sources from Level 3 images
7.	UV_DBF	Creates a Diffuse Background File
8.	UV_SPIMCON	Creates spectral DBF
9.	UV_COORDS	Converts pixels to RA and Dec and vice versa
10.	UV_VALIDATE	Performs sanity checks on data

uvisi.pro

CALLING SEQUENCE: uvisi,*inp_file*

PURPOSE: Control file which runs all other UVISI programs. This is the only file the end user should ever have to access.

INPUTS: *inp_file* parameter file which specifies the location and number of SPIM and imager files

OUTPUTS: Each procedure creates appropriate data files

PROCEDURE: This procedure runs all of the Level 3 programs with the appropriate parameters. We do not expect these parameters to change frequently throughout the course of the mission and thus expect that the same procedure should be run for all

DCEs. Reads number of imager files and their names and then number of SPIM files and their names from a parameter file. A sample parameter file follows:

images	***(Directory to place output)***
DCE_01	*(Prefix before output files)*
1	*(Number of imagers)*
/disk1/uvisi/IUW.1_CA	*(Name of imager files)*
5	*(Number of SPIMs)*
/disk1/uvisi/spim1.5_CA	*(Name of SPIM files)*
/disk1/uvisi/spim2.6_CA	
/disk1/uvisi/spim5.bin	
iuw_align	
iun_align	
ivw_align	
ivn_align	
spim1_align	
spim2_align	
spim3_align	
spim4_align	
spim5_align	

NOTES: We require that UVISI CONVERT be run with the following options:
output unit type=7 (Level 1C data)
dark count correction=0

UV_IMCON.PRO

CALLING SEQUENCE: UV_IMCON,im_files,out_files,image_dir.
file_prefix=file_prefix,threshold=threshold

PURPOSE: Creates Level 3 images from Level 1CA output of UVISI CONVERT.

INPUTS: *im_files* string array containing names of imager files
image_dir optional parameter, if set files are placed in that directory else they are placed in same directory

OUTPUTS: *out_files* string array containing names of output files

KEYWORDS: *threshold* optional parameter; if set all elements below this value are passed unchanged

file_prefix Optional parameter; if set then this is placed in front of files

PROCEDURE: This program is called by the UVISI main procedure to create the Level 3 images from the Level 1CA imager files. The Level 2a files are individual CCD frames taken at 0.5 second intervals and are 244 by 256 pixels in size. All the frames are coadded to form the Level 3 image for one DCE. The Level 3 file has the same spatial resolution as the imagers but all the frames are placed into a uniform grid. If instrumental parameters are changed a new Level 3 file is created. Thus the number of output files is equal to the number of changes in the instrumental parameters. The format of the output file is such that the first plane represents the average signal in the entire DCE in that pixel while the second plane represents the exposure time per pixel. The procedure follows:

V. Information about the instruments is read from the header and variables are initialized. This program is used for all imagers.

VI. A frame is read and the observation parameters (such as scan rate) are set from the frame header.

VII. Set up grid based on frame

VIII. Noise spikes removed through comparison with the previous frame

IX. Threshold the data to get rid of the CCD read noise. The individual photon hits show up as spikes above that noise.

X. If the DCE was scanning then offset frame to account for fractional offsets from the grid otherwise simply add pixels

XI. Add into grid using weighted sum. Grid extended if need be.

XII. New frame read and process continues until the instrumental parameters change.

XIII. After completion all files converted into FITS format.

UV_INITHEADER

CALLING SEQUENCE: uv_initheader

PURPOSE: Initializes header variables to appropriate values

INPUTS: None

OUTPUTS: None

PROCEDURE All variables from header placed into COMMON blocks

PROCEDURES CALLED: None

UV_READHEADER

CALLING SEQUENCE: uv_readheader,lun

PURPOSE: Reads header variables from Level 1CA files

INPUTS: lun Logical unit number of Level 1CA file. File must have been opened prior to call.

OUTPUTS: None

PROCEDURE All variables from header placed into COMMON blocks

PROCEDURES CALLED: None

UV_READDATA

CALLING SEQUENCE: uv_readdata,lun

PURPOSE: Reads one frame from Level 1CA data and sets up coordinates.

INPUTS: lun Logical unit number of Level 1CA file. File must have been opened prior to call.

OUTPUTS: None

PROCEDURE: Frame and errors read using a binary read.

PROCEDURES CALLED:

UV_READHEADER Reads headers from Level 2A files

UV_QUAT_RA Converts quaternians to RA, Dec, Theta

UV_COORDS Calculates coordinates from headers

NOTES: Depends on definitions from UVISI CONVERT Build 2

UV_PSEXTRACT

CALLING SEQUENCE: uv_psextract,*im_files,ps_files,psthreshold=psthreshold*

PURPOSE: Extract point sources from Level 3 images (output of UV_IMCON)

INPUTS: *im_files* Names of Level 3 images from UV_IMCON

OUTPUTS: *ps_files* Names of output point source files. These files are ASCII and are converted into FITS files by UV_WRITE_PSLIST

KEYWORDS: *ps_threshold* Threshold above which pixels are checked to see if they are due to noise

PROCEDURE: This procedure is called by the main *UVISI* procedure to extract point sources from the Level 3 images. It is run directly after *UV_IMCON* and requires the FITS images from that program. A new point source file is created for each change of

instrumental parameters, such as instrument or gain. We have empirically defined a PSF for each imager and fit that PSF to the data. The output files are ASCII files

1) Get amount and direction of motion from name of image file
2) Read in first image file (FITS format)
3) Find maximum value in image
4) If it is greater than threshold then continue else skip out of program
5) Extract small region around putative point source
6) Fit local background plus point spread function to data. A chi square minimization technique is used in the fitting.
7) If the chi square is significantly less than that for the background alone we have found a point source.
8) We continue to add point sources until the chi square stops decreasing at which point we go back to step 4.
9) After running through all the image files for one DCE, we write the data out in a ASCII file.

PROCEDURES CALLED:

UV_COORDS	Converts pixel coordinates to RA and Dec and vice versa
READFITS	Read FITS format files
SXPAR	Extracts parameters from FITS header into IDL variables

UV_DBF

CALLING SEQUENCE	uv_dbf,*im_files,ps_file=ps_file,grid_space=grid_space*
PURPOSE:	Produces Diffuse Background Files from output of *UV_IMCON*
INPUTS:	im_files Names of Level 3 imager files (output of UV_IMCON) *ps_file* Names of ASCII point source files (output of *UV_PSEXTRACT*)
OUTPUTS:	None (FITS file is created)
KEYWORDS:	*grid_space* Spatial resolution for DBF grid: defaults to 0.25°

PROCEDURE: This procedure creates the Level 3 Diffuse Background Files from the Level 3 images and the point source files. These files are low spatial resolution files with point sources removed and are intended to probe the gross spatial structure of the diffuse radiation field. The procedure follows:

1) The instrument type and parameters of the observation are read from the image files (im_files). Note that there can be more than one image file per DCE.

2) The locations and brightnesses of the point sources is read from the Point Source File.

3) A grid is set up based on the spatial extent of the first file and the spacing in the DBF. If a new file is read, the dimensions of the DBF are checked and extended if necessary.

4) The point sources (from the point source file) are masked out in the image file. The size of the mask is the number of pixels over which the point source is smeared plus an extra two pixels on either side. These points are given an arbitrarily large error so that they have zero weight in a weighted sum.

5) The imager pixels are stuffed into the much larger DBF pixels using a weighted sum.

6) If there are no more files, the DBF is written out as a FITS file.

PROCEDURES CALLED:

READFITS: Reads FITS formatted files

SXPAR Reads parameters from FITS header into variables

NOTES: This procedure will only be run for the narrow field of view imagers as the wide field of view imagers have a lower spatial resolution than the default 0.25° resolution anyway. The DBF will be superseded by the appropriate Level 4 file.

UV_SPIMCON

CALLING SEQUENCE

uv_spimcon,*spim_files,ps_file,spim_descript,sp_dat,grid_space= grid_space*

PURPOSE: Creates output files from each of the five SPIMs. Also adds spectral information to each point source in SPIM slit

INPUTS: *spim_files* Names of SPIM files

ps_file Names of point source files (in standard processing we set this to nopoints so that no point source spectra are explicitly processed)

OUTPUTS:

spim_descript Array identifying SPIMs; same dimension as spim_files

sp_dat structure containing two spectra:

ps_spectrum Spectra of point sources in slit. If point source not observed by a SPIM, array filled with -1.

err_spectrum Errors associated with point sources

KEYWORDS:

grid_space Spatial resolution of output file defaults to 0.25°

PROCEDURE:

This program creates the "spectral image" files which are the Level 3 data products from the SPIMs and adds spectral information to those point sources which are observed by the SPIM slits. Point sources which have been identified by *UV_PSEXTRACT* are masked out in the SPIM frames which are then added into the low spatial resolution (0.25° default) grid. The spectra from the point sources are extracted and placed into the array *ps_spectrum*. The associated errors are calculated and placed into *err_spectrum*. The procedure follows:

1) DBF grid initialized using first frame
2) Noise removal performed by checking each pixel against neighbors: if more than 3 sigma above all then flagged as noise.
3) Check for point sources (from PS file) in SPIM entrance slit
4) If yes then produce spectrum
5) Add pixels into appropriate bins of DBF
6) Write out as FITS file

PROCEDURES CALLED:

uv_initheader Initializes UVISI header

uv_readheader Reads UVISI header

uv_fitswrite Writes out SPIM DBF

uv_quat_ra Converts quaternians into ra, dec, theta

uv_coords Converts pixels from imager frame of reference to SPIM frame and vice versa

UV_FITSWRITE

CALLING SEQUENCE uv_fitswrite,*fname,data,errs,fits_var*

PURPOSE: Write FITS files from images (output of *UV_IMCON, UV_SPIMCON, UV_DBF*)

INPUTS: *fname* Name of FITS file output

data Data array

errs Array of uncertainties

fits_var Structure containing parameters need for FITS header

OUTPUTS: None. FITS files written

PROCEDURE: Standard FITS header written using information in COMMON blocks and inputs

UV_WRITE_PSLIST

CALLING SEQUENCE: uv_write_pslist,*ps_files,spim_descript,sp_dat*

PURPOSE: Write FITS file for Point Sources

INPUTS: *ps_files* ASCII file containing point source information

spim_descript String array containing description of SPIM parameters

sp_dat Structure containing two arrays

ps_spectrum Array containing spectra for each of point sources to be written

err_spectrum Array containing uncertainties for each of point sources

OUTPUTS: None. FITS table written.

PROCEDURE: Standard FITS header written using information in COMMON blocks and inputs.

UV_COORDS

CALLING SEQUENCE:

uv_coords,*ra_start,dec_start,theta_start,ra,dec,theta,x,y,z,inv,inst*

PURPOSE: Convert coordinates from astronomical coords (RA, Dec, and Theta [the roll angle]) to an instrument based system and vice versa

INPUTS:

ra_start RA, Dec for grid start. Taken from header of first frame and are for the center of the first frame

dec_start

theta_start Roll angle for spacecraft

ra, dec, theta coordinates for frame under consideration

inv If 1 (default) hen convert from ra, dec, theta to x, y, z (where z is the rotation between frames) if (-1) goes other way

inst Instrument number: 1 - 4 being imagers, 5 - 9 being SPIMs

OUTPUTS:

x,y Position in instrument coordinates. Inverse provides RA, Dec and Theta

z rotation angle between frames

PROCEDURE A matrix representing rotation from starting frame to current frame is calculated and used to give x, y from starting frame.

UV_QUAT_RA

CALLING SEQUENCE: uv_quat_ra,*q,align,ra,dec,theta*

PURPOSE: Converts quaternions to RA, Dec, Theta

INPUTS:

q Four element quaternion matrix

align Alignment matrix

OUTPUTS:

RA, Dec RA and Dec in sensor coords

Theta Roll angle in sensor coordinates

PROCEDURE: Quaternions are converted to a rotation matrix. Misalignment sbetween different instruments correted by an alignment matrix provided as part of CONVERT. RA,Dec, and Theta extracted from rotation matrix.

6.4 Flow Charts

On pages 32 - 48, we present the flow charts that accompany and document our programs. These are:

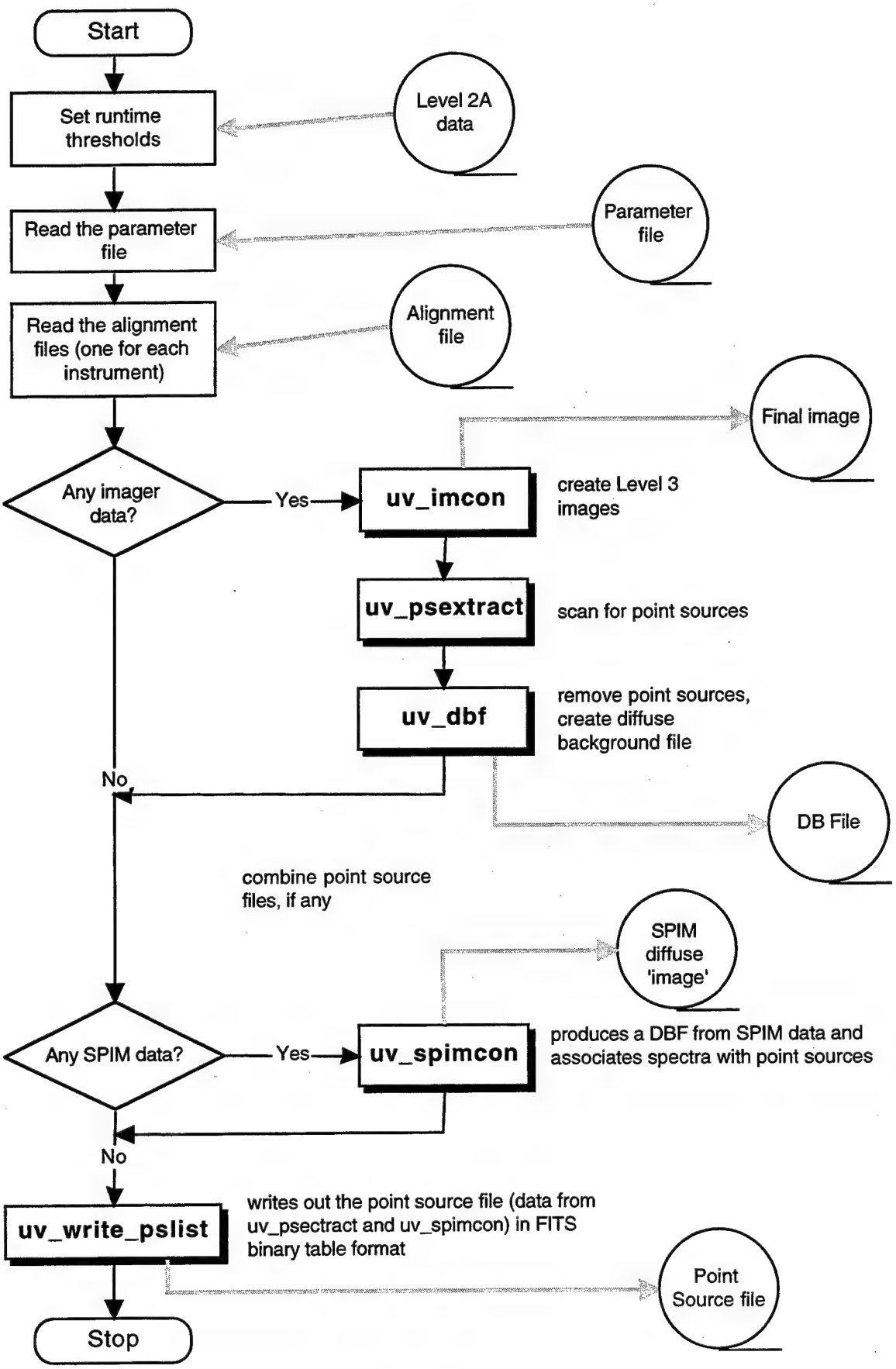
Start
Set runtime thresholds
Level 2A data
Read the parameter file
Parameter file
Read the alignment files (one for each instrument)
Alignment file
Final image
Any imager data?
Yes
uv_imcon
create Level 3 images
uv_psextract
scan for point sources
uv_dbf
remove point sources, create diffuse background file
No
DB File
combine point source files, if any
SPIM diffuse 'image'
Any SPIM data?
Yes
uv_spimcon
produces a DBF from SPIM data and associates spectra with point sources
No
uv_write_pslist
writes out the point source file (data from uv_psectract and uv_spimcon) in FITS binary table format
Point Source file
Stop

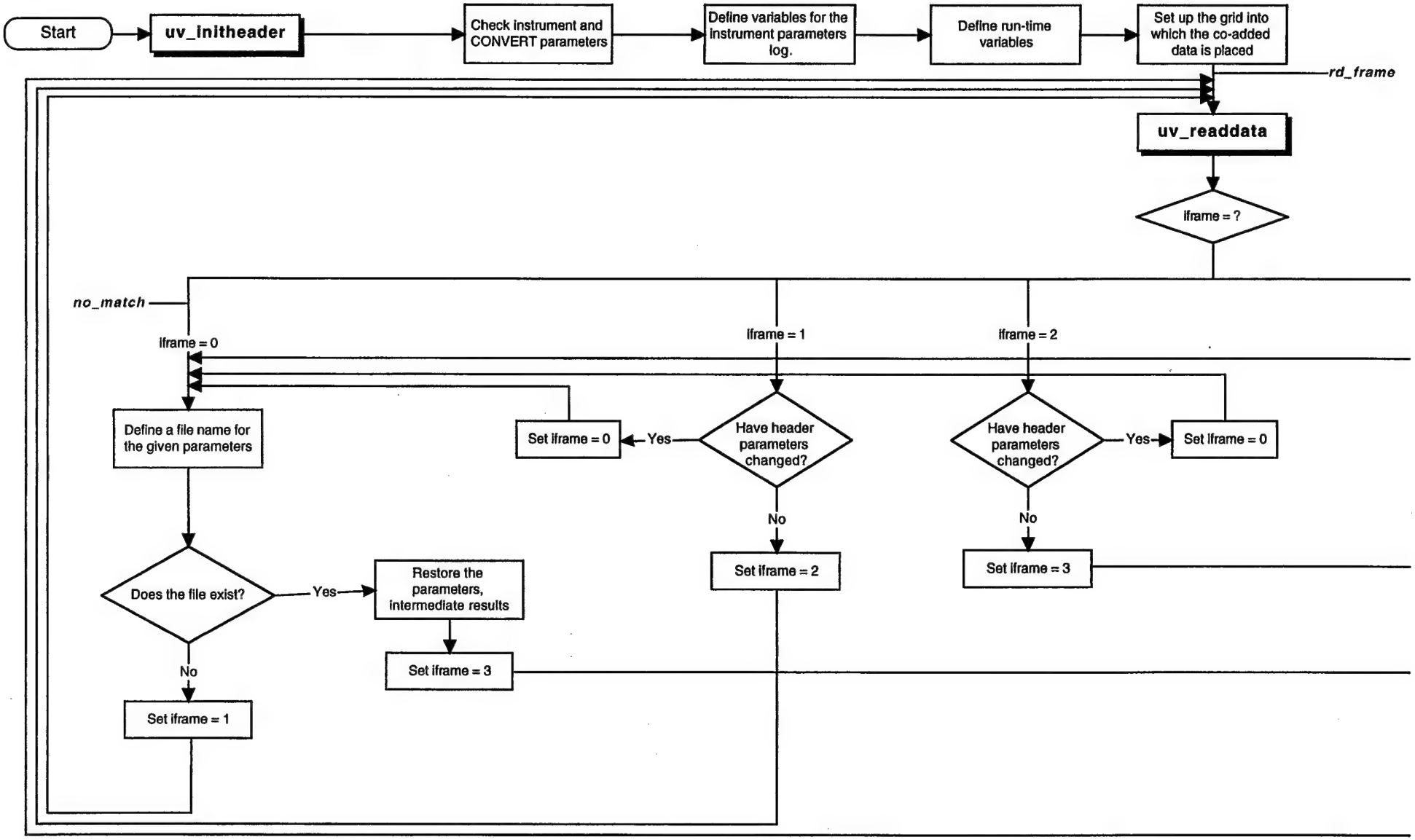
Start
uv_initheader
Check instrument and CONVERT parameters
Define variables for the instrument parameters log.
Define run-time variables
Set up the grid into which the co-added data is placed
rd_frame
uv_readdata
iframe = ?
no_match
iframe = 0
iframe = 1
iframe = 2
Define a file name for the given parameters
Set iframe = 0
Yes
Have header parameters changed?
Have header parameters changed?
Yes
Set iframe = 0
No
No
Does the file exist?
Yes
Restore the parameters, intermediate results
Set iframe = 2
Set iframe = 3
Set iframe = 3
No
Set iframe = 1

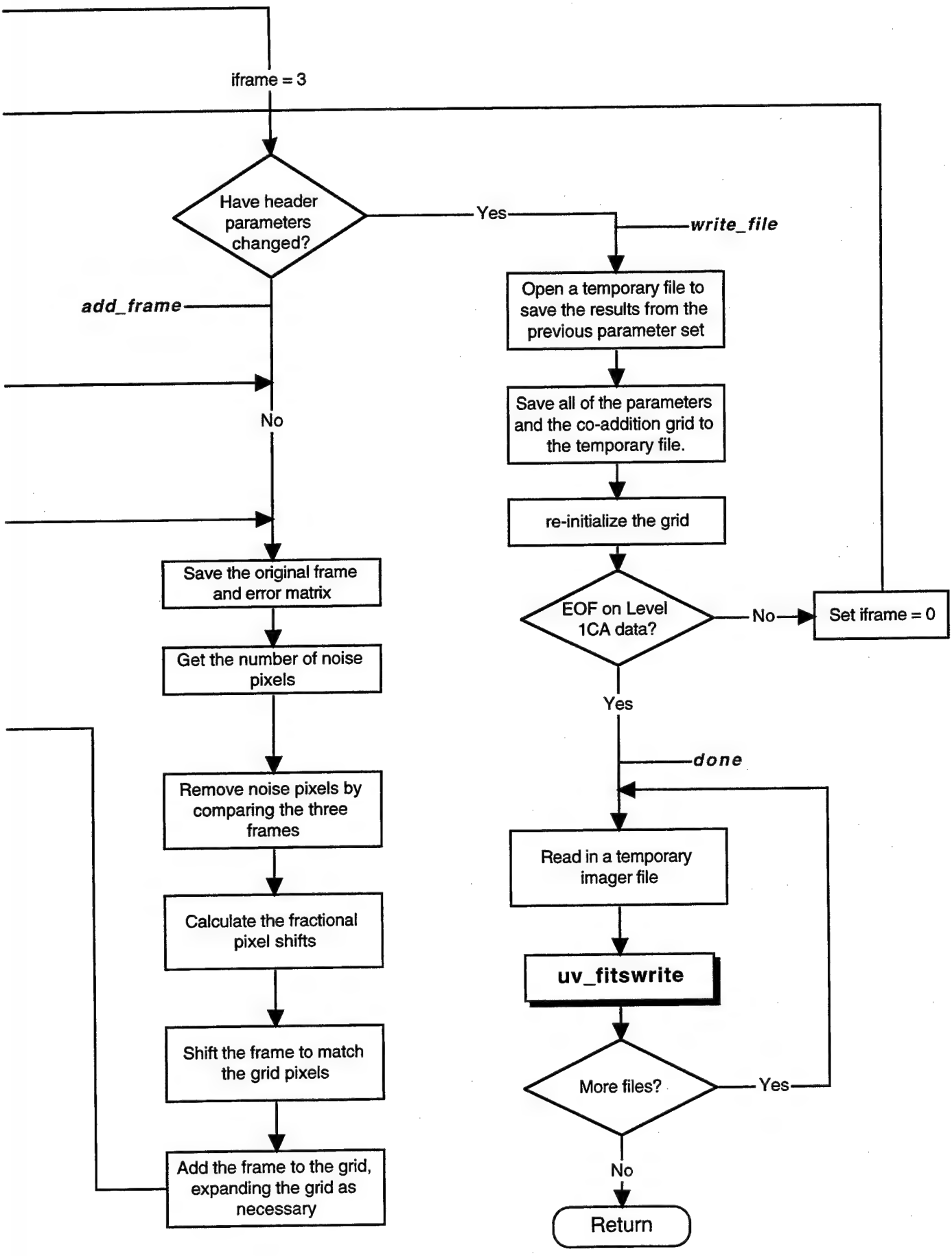
iframe = 3
Have header parameters changed?
Yes
write_file
Open a temporary file to save the results from the previous parameter set
Save all of the parameters and the co-addition grid to the temporary file.
re-initialize the grid
EOF on Level 1CA data?
No
Set iframe = 0
Yes
done
add_frame
No
Save the original frame and error matrix
Get the number of noise pixels
Remove noise pixels by comparing the three frames
Calculate the fractional pixel shifts
Shift the frame to match the grid pixels
Add the frame to the grid, expanding the grid as necessary
Read in a temporary imager file
uv_fitswrite
More files?
Yes
No
Return

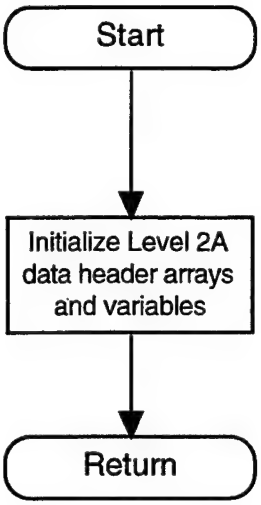
Start
Initialize Level 2A data header arrays and variables
Return

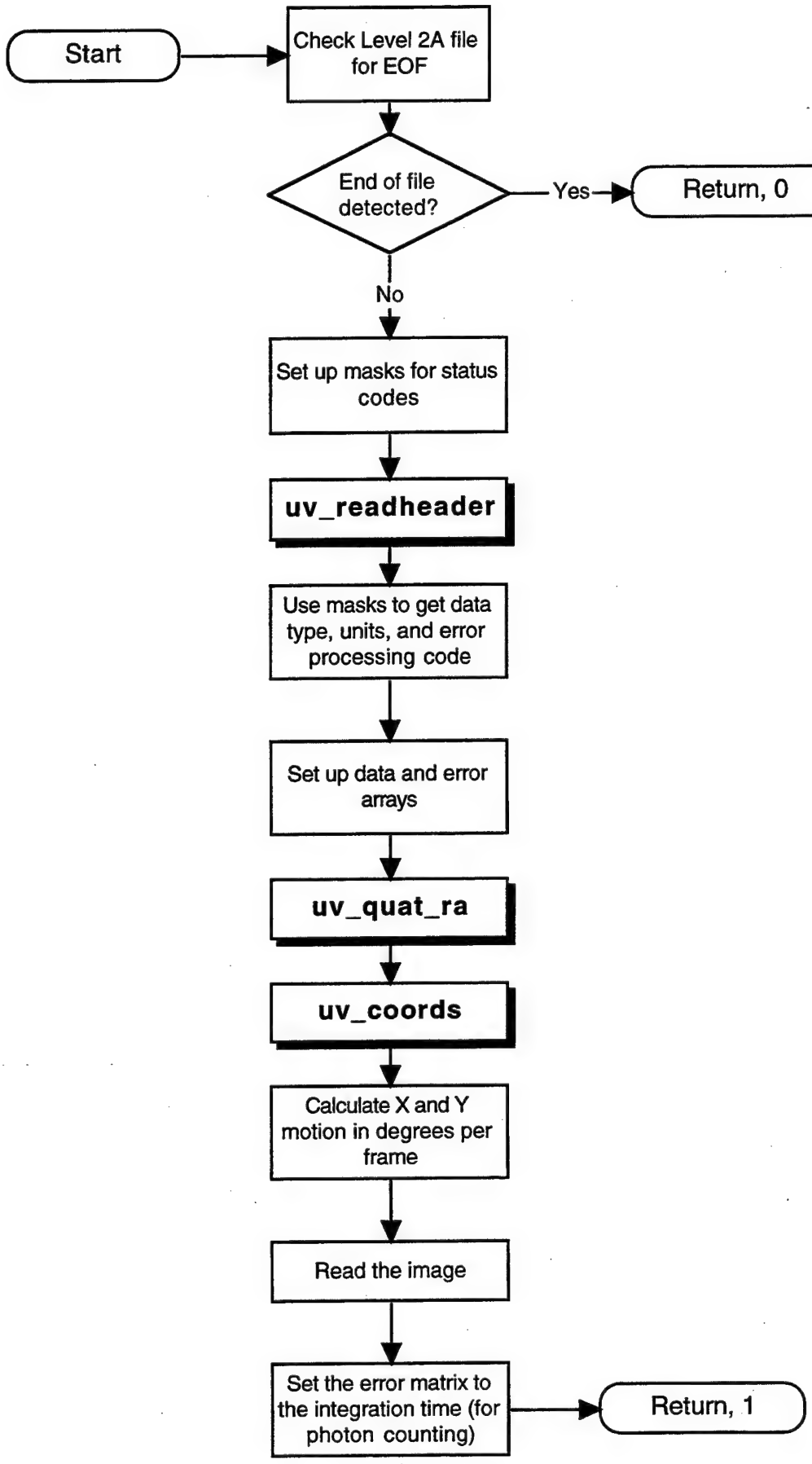
Start
Check Level 2A file for EOF
End of file detected?
Yes
Return, 0
No
Set up masks for status codes
uv_readheader
Use masks to get data type, units, and error processing code
Set up data and error arrays
uv_quat_ra
uv_coords
Calculate X and Y motion in degrees per frame
Read the image
Set the error matrix to the integration time (for photon counting)
Return, 1

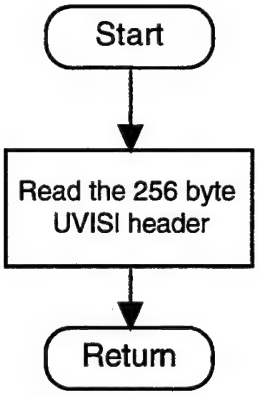
Start
Read the 256 byte UVISI header
Return

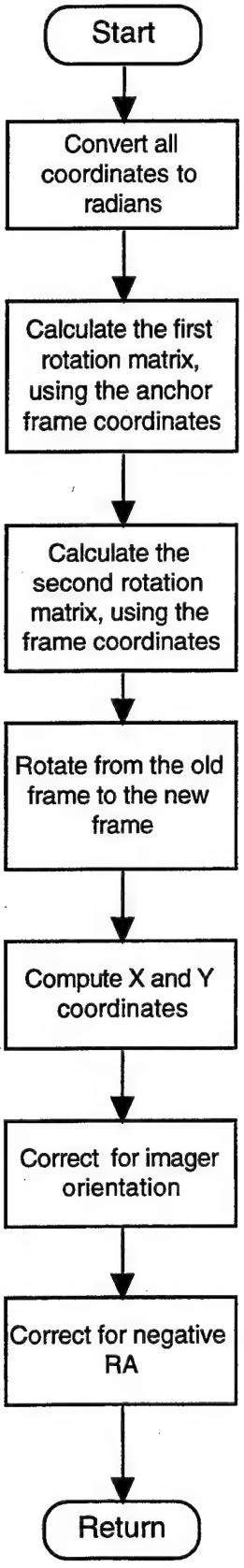
Start
Convert all coordinates to radians
Calculate the first rotation matrix, using the anchor frame coordinates
Calculate the second rotation matrix, using the frame coordinates
Rotate from the old frame to the new frame
Compute X and Y coordinates
Correct for imager orientation
Correct for negative RA
Return

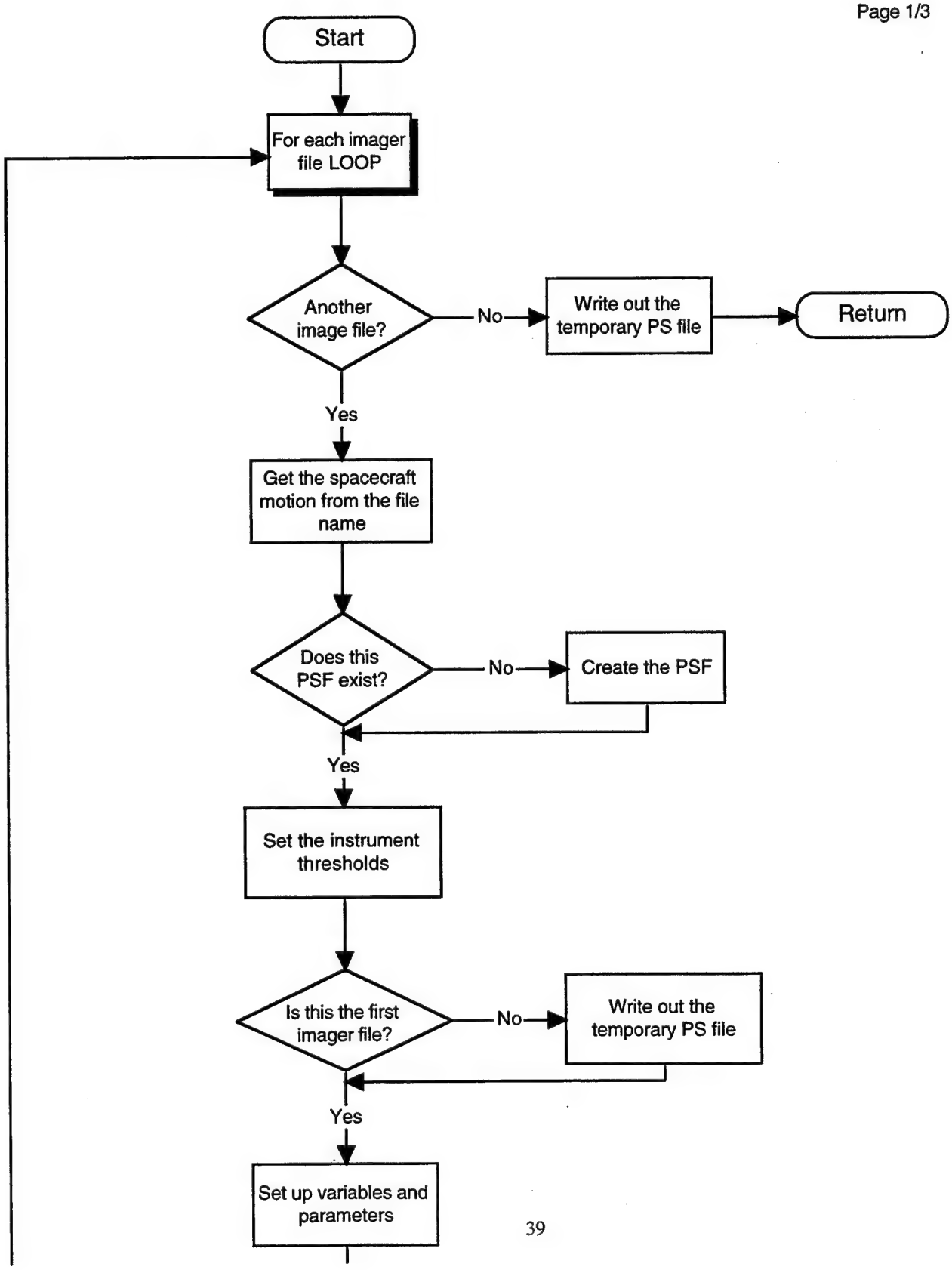
Start
For each imager file LOOP
Another image file?
No
Write out the temporary PS file
Return
Yes
Get the spacecraft motion from the file name
Does this PSF exist?
No
Create the PSF
Yes
Set the instrument thresholds
Is this the first imager file?
No
Write out the temporary PS file
Yes
Set up variables and parameters

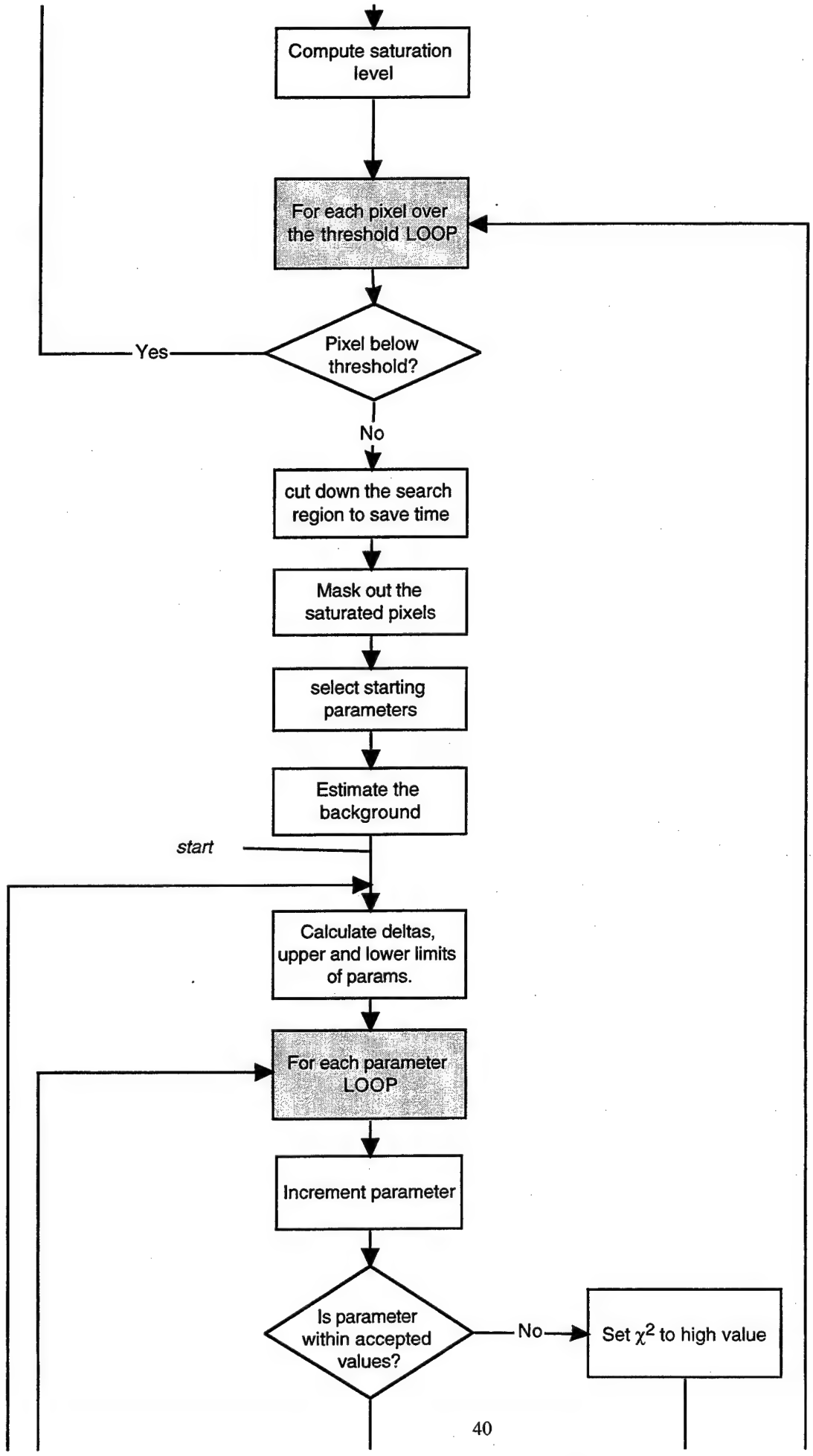
Compute saturation level
For each pixel over the threshold LOOP
Pixel below threshold?
Yes
No
cut down the search region to save time
Mask out the saturated pixels
select starting parameters
Estimate the background
start
Calculate deltas, upper and lower limits of params.
For each parameter LOOP
Increment parameter
Is parameter within accepted values?
No
Set χ^2 to high value

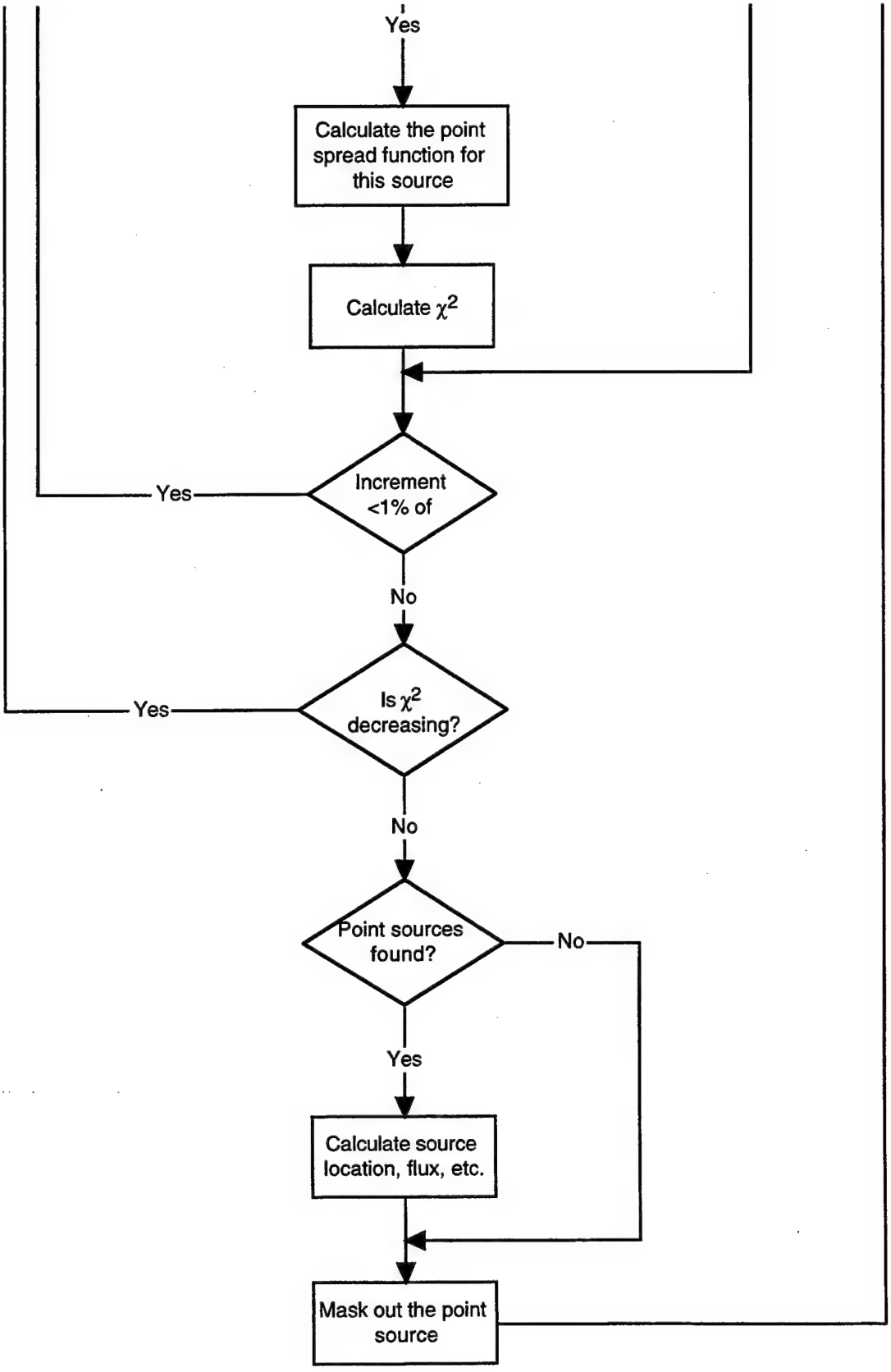
Yes
Calculate the point spread function for this source
Calculate χ^2
Increment <1% of
Yes
No
Is χ^2 decreasing?
Yes
No
Point sources found?
No
Yes
Calculate source location, flux, etc.
Mask out the point source

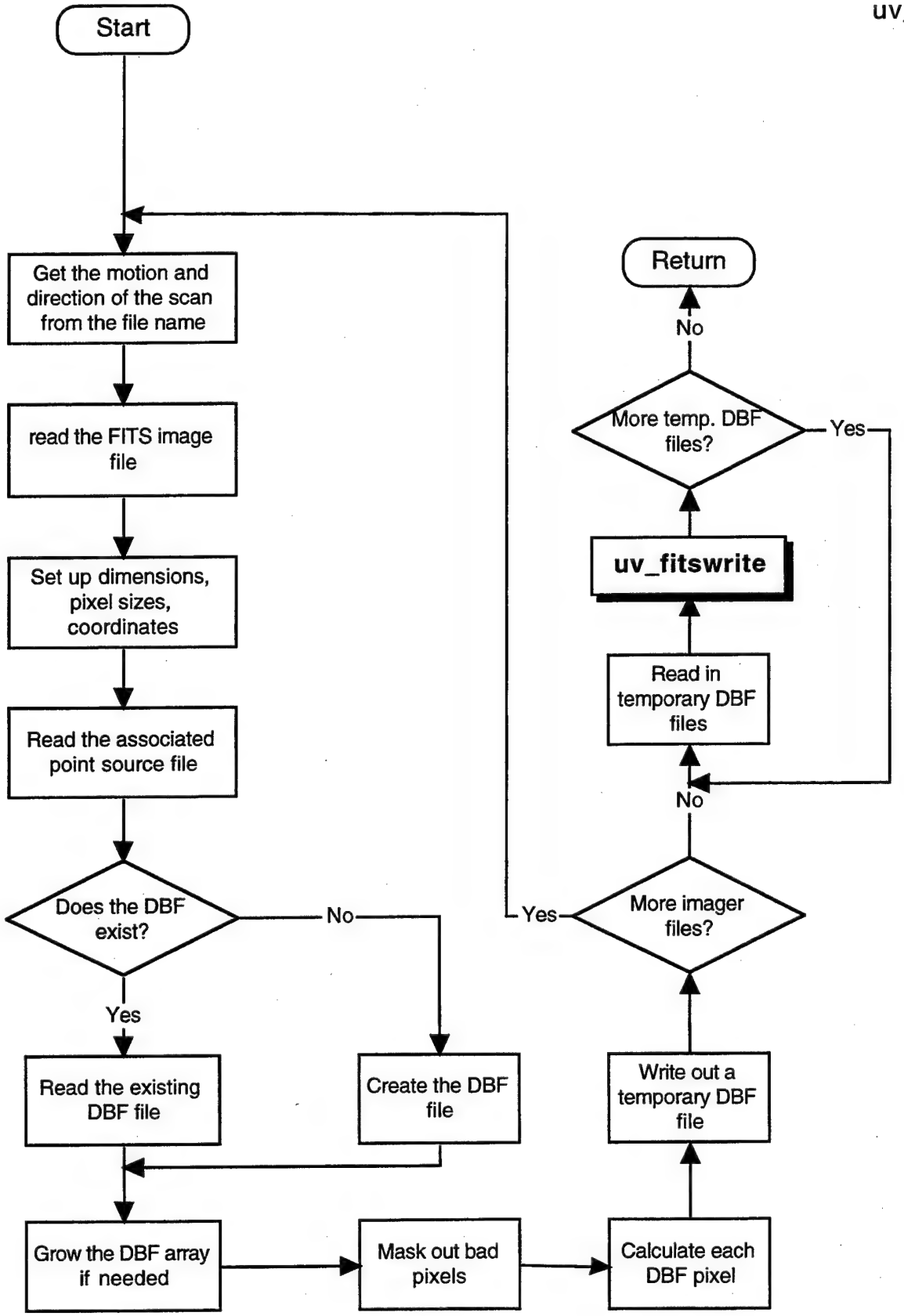
Start
Get the motion and direction of the scan from the file name
read the FITS image file
Set up dimensions, pixel sizes, coordinates
Read the associated point source file
Does the DBF exist?
No
Yes
Read the existing DBF file
Create the DBF file
Grow the DBF array if needed
Mask out bad pixels
Calculate each DBF pixel
Write out a temporary DBF file
More imager files?
Yes
No
Read in temporary DBF files
uv_fitswrite
More temp. DBF files?
Yes
No
Return

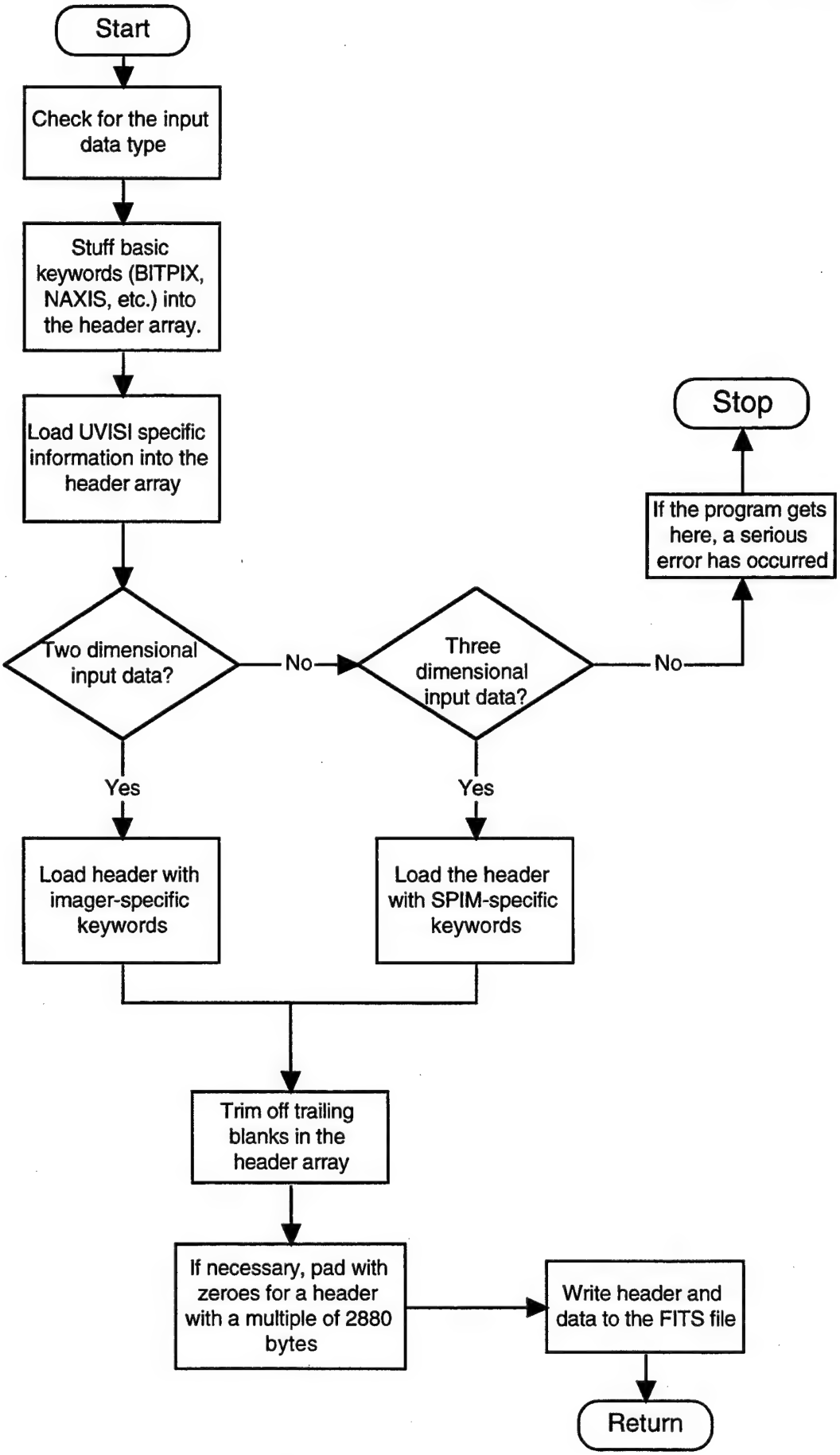
Start
Check for the input data type
Stuff basic keywords (BITPIX, NAXIS, etc.) into the header array.
Load UVISI specific information into the header array
Two dimensional input data?
No
Three dimensional input data?
No
Stop
If the program gets here, a serious error has occurred
Yes
Yes
Load header with imager-specific keywords
Load the header with SPIM-specific keywords
Trim off trailing blanks in the header array
If necessary, pad with zeroes for a header with a multiple of 2880 bytes
Write header and data to the FITS file
Return

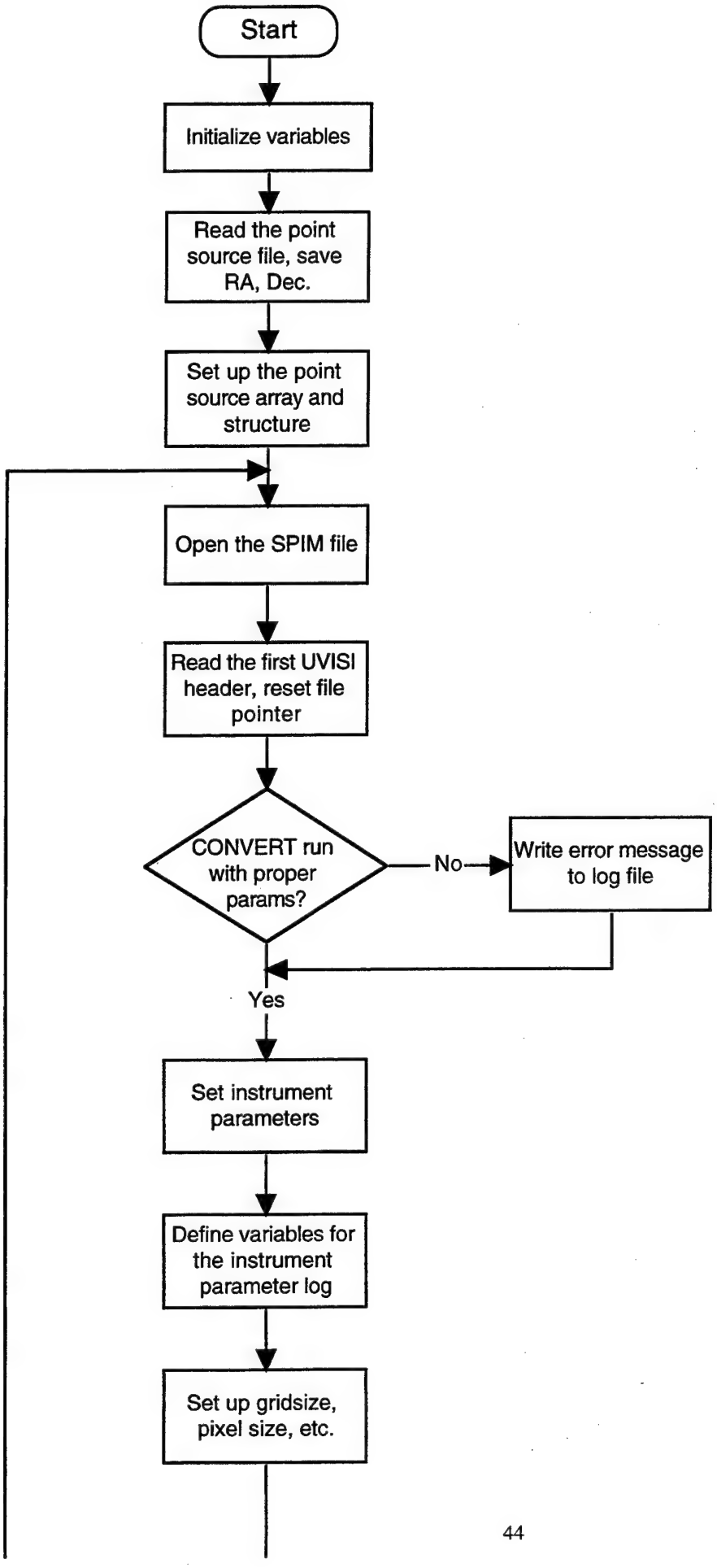
Start
Initialize variables
Read the point source file, save RA, Dec.
Set up the point source array and structure
Open the SPIM file
Read the first UVISI header, reset file pointer
CONVERT run with proper params?
No
Write error message to log file
Yes
Set instrument parameters
Define variables for the instrument parameter log
Set up gridsize, pixel size, etc.

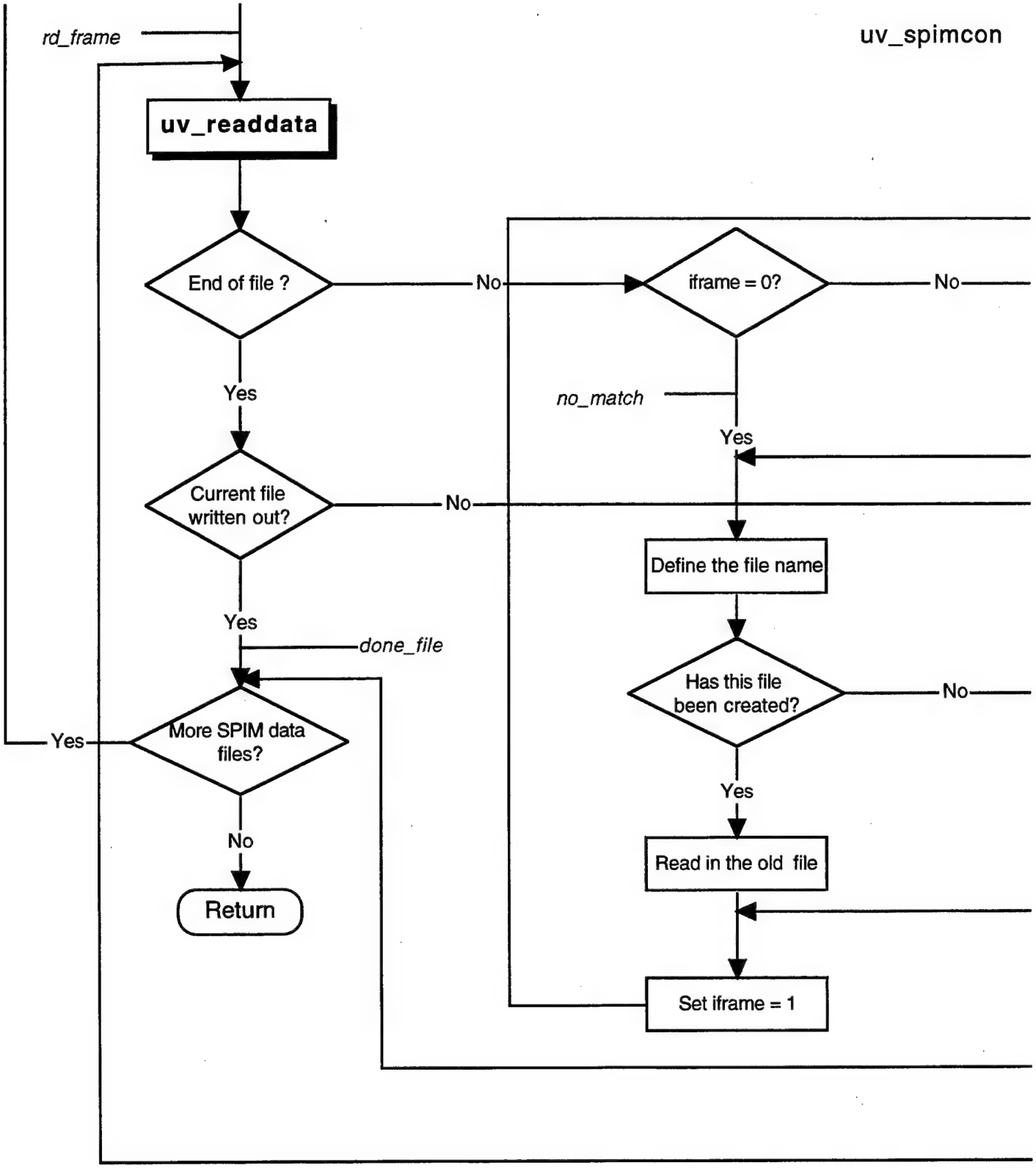
uv_spimcon
rd_frame
uv_readdata
End of file ?
No
iframe = 0?
No
Yes
no_match
Yes
Current file written out?
No
Define the file name
Yes
done_file
Has this file been created?
No
Yes
More SPIM data files?
Yes
Read in the old file
No
Return
Set iframe = 1

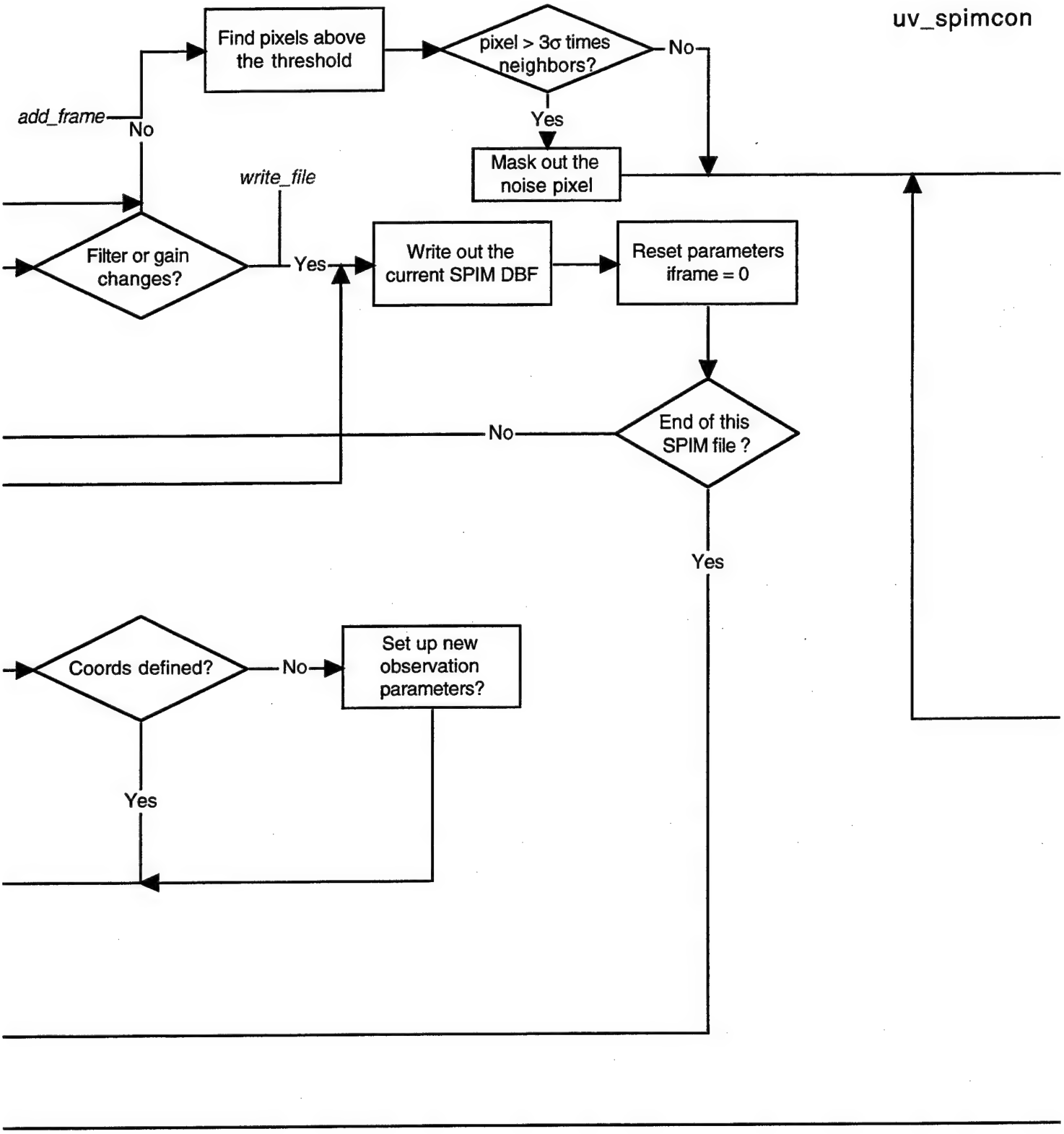
uv_spimcon
Find pixels above the threshold
pixel > 3σ times neighbors?
No
Yes
add_frame
No
Mask out the noise pixel
write_file
Filter or gain changes?
Yes
Write out the current SPIM DBF
Reset parameters iframe = 0
End of this SPIM file ?
No
Yes
Coords defined?
No
Set up new observation parameters?
Yes

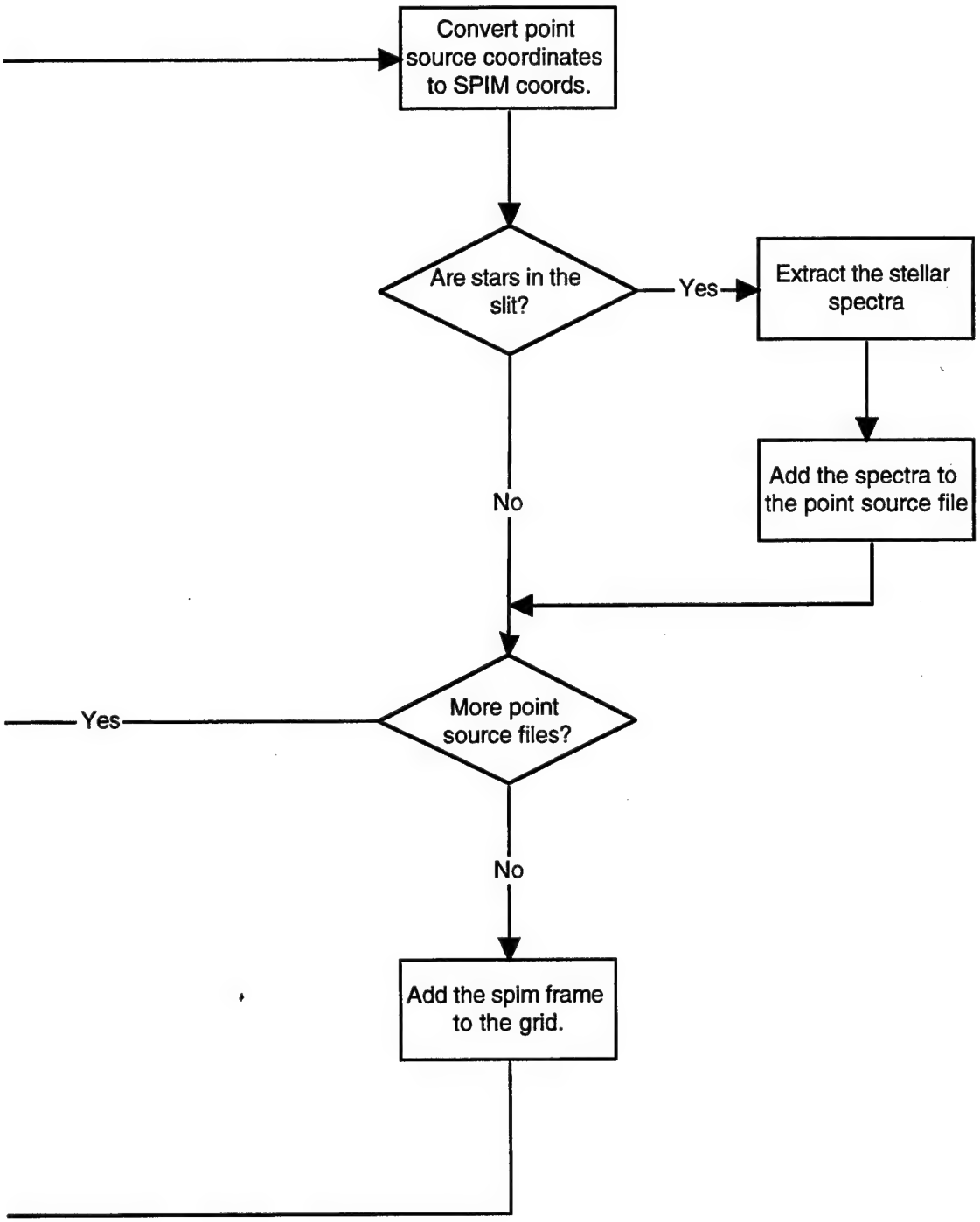
Convert point source coordinates to SPIM coords.
Are stars in the slit?
Yes
Extract the stellar spectra
Add the spectra to the point source file
No
More point source files?
Yes
No
Add the spim frame to the grid.

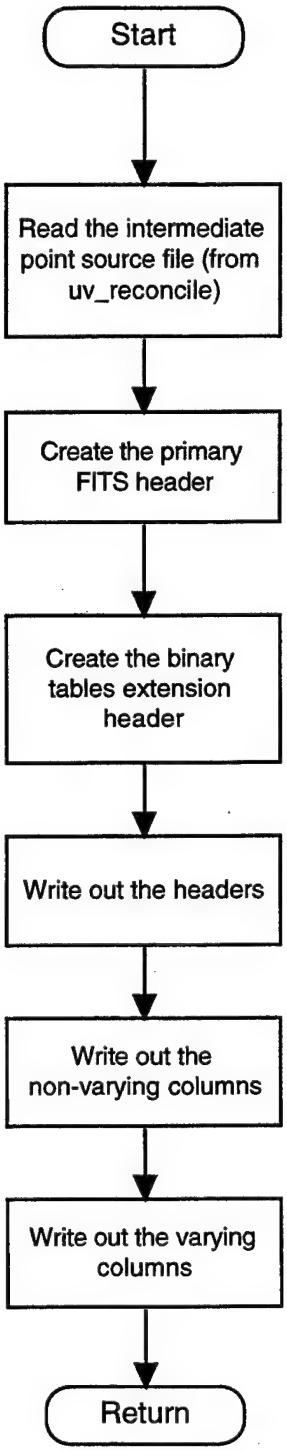
Start
Read the intermediate point source file (from uv_reconcile)
Create the primary FITS header
Create the binary tables extension header
Write out the headers
Write out the non-varying columns
Write out the varying columns
Return

7. SCIENCE SUMMARY

As part of our work under this contract, we have created a detailed summary of the kinds of science that were hoped for from the UVISI instruments, and we present that here. As mentioned above, background levels on the UVISI instruments proved higher than anticipated, precluding full implementation of these ideas, but the ideas themselves remain of value.

7.1 Sky Survey of UV Point Sources 600 Times Fainter Than Previous (TD-1) Survey

The major existing survey of the sky for point sources (stars, quasars, etc.) is the so-called TD-1 survey. TD-1 was a satellite of the European Space Research Organization (ESRO), and was launched from the U.S. Western Test Range, California, in March 1972. Among the experiments on board was an ultraviolet astronomy experiment called S2/68. The data from that experiment have been published in the form of paper catalogs and are also available on CD-ROM. In addition, the TD-1 S2/68 data were the basis for the ATLAS OF THE ULTRAVIOLET SKY, published in 1988 by the Johns Hopkins University press. The flux limit of the Atlas was 1.0×10^{-12} ergs cm^{-2} s^{-1} $Å^{-1}$, which is the flux to which the TD-1 data are believed to be complete over the sky. The Celestial Backgrounds Experiment on MSX includes an Experiment Plan, Experiment Plan 10, "Systematic Ultraviolet Sky Survey," which if carried to completion (about a two-year post-cryogen phase effort) will provide an all-sky catalog and atlas that is complete to approximately 1.0×10^{-15} ergs cm^{-2} s^{-1} $Å^{-1}$, which is to say a factor of one thousand better than TD-1. The factor 600 that appears in the bullet is conservative, and also allows for the fact that TD-1 did go fainter at the ecliptic poles than the flux limit to which it is complete.

The importance of such a sky-survey improvement is enormous. The overwhelming majority of the TD-1 objects are simply normal O and B type (that is, very hot) stars. These stars are of interest, but are not of extremely great scientific importance. In contrast, the MSX all-sky survey, by going much fainter, will for the first time bring in whole new populations of objects, that are almost entirely absent from TD-1. Examples include:

Quasars. MSX may go faint enough to detect the distant quasars that will allow us to probe the intergalactic medium, subsequently, using the Hubble Space Telescope and/or Lyman (an HST successor or adjunct mission that has been approved by NASA). The idea is to use the quasars as light sources, and see what absorption of those light sources is caused by the intergalactic medium. It is particularily important to find quasars that are distant enough, and

yet that have light that is not all absorbed by the intergalactic clouds, that can be used for the so-called Gunn-Peterson test for intergalactic helium. That test applied to hydrogen shows that there is no general neutral intergalactic medium, to extraordinarily low levels. Yet we know that among the various "missing masses" in the universe, there are large amounts of missing baryons. Could they be in the form of ionized intergalactic gas, hot enough that the hydrogen is ionized, but not so hot that the helium is ionized? Yes they could, and the key to detecting this missing mass is finding the necessary quasars: MSX is right at the edge of being capable of performing that task. What is needed for success is that the instruments perform as advertised, and that sufficient time be devoted to do a complete, or at least almost complete, deep all-sky survey.

X-ray emitters. Accretion of matter onto compact objects (white dwarf stars, neutron stars, and black holes) leads to copious emission of ultraviolet light. MSX could lead to large numbers of discoveries of such objects, and to better understanding of those already known.

Galaxies. The existing ultraviolet data on galaxies is very skimpy. MSX will result in a truly massive increase in our knowledge of the ultraviolet emission of galaxies other than our own. This is very important for improving our understanding of why galaxies occur in the variety they do; how galaxies evolve with time; and the nature of galaxies and their component parts.

Supernovae. These exploding stars are very useful as "standard candles" for trying to resolve the controversy concerning the size and age of the universe. In the course of an all-sky survey, MSX will detect many supernovae in other galaxies. Ultraviolet data should be very useful in resolving controversy concerning what kinds of stars eventually become supernovae, as well.

Faint, hot stars. There are many types of faint hot stars known: white dwarfs, OB subdwarfs, distant runaway OB stars, blue horizontal branch stars, post-asymptotic giant branch stars...most of which are too faint to appear at all in the TD-1 sample. Thus, MSX could make a major contribution to stellar astronomy.

7.2 Diffuse Galactic Light: Starlight Scattered from Dust at High Galactic Latitude

When we observe the milky way, that is, when we look out into our galaxy, we see a sample of the 100 billion stars of our galaxy, and we also see regions apparently lacking in stars. This lack is only apparent; the dark regions are caused by vast clouds of interstellar dust that are of not-well-determined composition.

If, instead of looking into our galaxy, we do our best to look out of our galaxy, that is, we look up out of the galactic plane into the depths of the universe, we are presented with a potential problem. We do know that above and below our location in the outskirts of the galaxy there is more of the interstellar dust that we see right in the galactic plane. We know this because of detection of thermal emission from such dust at 100 micrometers by IRAS, and also because the dust leads to the polarization of the light of stars that are observed at high galactic latitudes.

Why is that potentially a problem? Well, of course such dust will partially absorb the light of distant objects that we are interested in. But there is a much more serious potential problem. We know that there are very large numbers of extremely bright hot young stars in the galactic plane (many of them visible to the naked eye). The light of these hot stars will illuminate the dust clouds at high galactic latitudes and depending on the nature of the dust particles, could potentially reflect back, making the sky very bright in the ultraviolet. This would be very unfortunate indeed, for it would mean much greater difficulty in detecting potential sources of extragalactic light that are of the very greatest interest.

Where do matters stand? There are two parameters of the dust grains that affect the answer. The first is the albedo of the grains; that is to say, their reflectivity. Obviously, if the grains were to absorb all of the ultraviolet that strikes them, none would be available to reflect back and spoil our ultraviolet view of the universe. But suppose the grains do reflect very substantial amounts of light. That is not the end of the story, because the *way* the grains reflect is very important. There are many possibilites. The scattering properties of small grains are usually characterized by what is called the Henyey-Greenstein scattering function g (Astrophysical Journal, 1941, volume 93, page 70). A value of $g = 0$ signifies isotropic scattering (equal amounts of light scattered in all directions.) A positive value means that most of the light is forward scattered: $g = 1$ means that all of the reflected light continues in exactly the same direction it was going. A negative value means back-scattering; the light is reflected predominatly back in the direction from which it came. So what we would like to see, is either a very low albedo (not much reflected light), or failing that, at least a large positive g value, in which case the scattered light would proceed out of the galaxy and be lost in intergalactic space. What we would like *not* to see, is a high albedo and isotropic, or worse, back scattering.

Perhaps the best determination of the ultraviolet scattering properties of the interstellar grains is the recent paper by Witt, Petersohn, Bohlin, O'Connell, Roberts, Smith, and Stecher (Astrophysical Journal, 1992, volume 395, page L5), which involves analysis of light scattered in the nebula NGC 7023. They find a high albedo (~0.7) and a high g value (~0.7).

We are currently carrying out calculations to determine what background we can expect at high galactic latitudes, if these are the correct parameters of the grains. We also have preliminary data from our Voyager observation of the scattering of the light of very bright stars near the Coalsack nebula in our galaxy. Preliminary analysis yields albedo = 0.4, and g = 0.9. If these latter values are correct, we can be sure that there will be little or no scattered starlight at high galactic latitudes to trouble our MSX search for more interesting forms of radiation.

MSX can not only use the results of the above studies, it can also contribute very substantially to the resolution of the remaining controversy. Ideally, with an all-sky survey using MSX, we will be able to correlate the signal that we do observe at high galactic latitudes with indicators of the presence of interstellar dust, such as IRAS 100 micrometer emission. Deep pointings with MSX could clearly show back-scattered light, if such exists in significant amounts.

7.3 Optical Properties of Interstellar Grains

Why do we care about the optical properties of the interstellar grains? In fact, why to we care about the interstellar grains at all? Furthermore, as we shall see, the nature of interstellar grains is a problem where MSX will have only a tiny, incremental effect on the ultimate solution of the problem. If that is so, why do we bother with this bullet at all? The answer to these questions goes to the heart of the scientific process. The Greeks invented "science", in terms of the Questions: what is the nature of reality; what is the nature of matter; what is the nature of the universe? And the Greeks provided a huge piece of the fundamental tool for expressing the answers to these profound questions, namely, mathematics. What the Greeks did not provide was the successful technique for solving these deep problems. The techniques that work, are those that were developed by the scientists of the renaissance and their successors. The fundamental approach that has been found to work, is to try first to answer the small questions, not the big questions. The experience and insight that is gained by answering small, comparatively easy, questions, then leads to success in the case of the more and more deep and difficult questions that follow. In practice what this means is that a huge amount of scientific research is involved with questions that look, in isolation, perhaps not very interesting or important. But we have learned since the renaissance that if we want the big, deep, and interesting questions answered, we must patiently labor at the smaller, less intrinsically interesting questions.

How does this apply to our topic, "optical properties of interstellar grains?" Let's work backward from the MSX bottom line, which is simply that MSX, if it carries out a full sky survey in the post-cryogen phase, should utterly unambiguously determine the albedo and scattering pattern of the interstellar grains (see bullet 2). In turn, that will further constrict the possibilities as far as the question "what are the grains made of" is concerned. It will not answer that question. The all sky survey could also reveal that interstellar grains in different parts of the galaxy have different values for the albedo and scattering function, which would imply that their composition varies from place to place. Now, why we care about the interstellar grains (and their composition) is that they are a key element in determining the formation of the stars. The formation of the stars is a fundamental problem of astronomy, and of course human life exists only thanks to a locally formed star, the sun. Stars form from interstellar gas and dust by a complex process involving gravitational collapse of interstellar clouds. In order to collapse, the stars must radiate away large amounts of energy, and the grains play an important role in that process, directly and indirectly. Directly, the grains heat up, and emit themal radiation. Indirectly: the grains are the site of formation of molecular hydrogen (such homopolar molecules cannot form by direct radiative combination). The molecular hydrogen (and DH) can then be collisionally excited leading to infrared radiation, thus again acting to cool the cloud. Another coolant that is undoubtedly important is H_2O, water. Without grains, would there be stars? Probably there would, for the grains, whatever they are made of, are made of something other than hydrogen and helium, the products of the big bang. The heavier elements were essentially all made in supernova explosions of stars. Thus, the first stars must surely have formed in the absence of heavier elements, that is, in the absence of grains. Understanding grains is a key element in understanding the evolving process of star formation. And there are other related questions that are of great interest. For example, once a tiny grain has formed, it is fairly easy to see how it could grow, through atom-by-atom accretion of interstellar gas atoms. It is also fairly easy to see how grains could be destroyed: interstellar clouds move at velocities of kilometers per second, and when clouds collide, the collision of grains with each other (or even with gas atoms) could lead to their destruction. What is not so easy to see, is where those original tiny grains come from. It is unlikely in the extreme that gas-phase coagulation under interstellar conditions could lead to their formation on any reasonable time scale: the density is simply too low. This has led to the idea that the grain nuclei form in the thin outer atmosphere of cool giant stars; cool stars, so the grains are not destroyed; giant stars, so the grains are far enough out that they can conceivably escape from the gravitationl influence of the parent star.

MSX can make an important incremental improvement in our understanding of interstellar grains!

7.4 Fluorescence of Molecular Hydrogen in the Interstellar Medium

We have already seen, in the discussion of section 5.3, some indication of just how important molecular hydrogen is as a constituent of the interstellar medium. But interstellar molecular hydrogen is extremely difficult to detect! MSX will likely make an enormous contribution to our understanding of the distribution of molecular hydrogen in the galaxy, if a sensitive all-sky survey is carried out. To understand why this is so, let us briefly review the history of the discovery of interstellar matter in general, and of interstellar hydrogen in particular. In the discussion of bullet 2, we saw that interstellar dust was discovered as apparent voids in the galaxy. Interstellar gas was discovered through the fact that when the gas occurs near a hot star, the light of that hot star excites the atoms of the gas, which then re-radiate, revealing the location and physical state of the gas. The atoms that are revealed in this way are atoms of sodium, oxygen, etc.; that is to say, elements that were manufactured in stars and dispersed through supernovae, and also hydrogen and helium, the elements that were made in the big bang.

It was Cecelia Payne, of Harvard, who discovered just what the stars are made of. (Her son Mike Gaposhkin is an important MSX participant.) The stars are made of "90% hydrogen; 10% helium; and 1% everything else," so to speak! Thus, if we want to truly understand the interstellar gas, we must understand the distribution of hydrogen. Yet the technique described above only reveals the hydrogen if it is located near a hot star. This problem was considered during the Nazi occupation of Holland by the Dutch astronomer van de Hulst, who came to the remarkable conclusion that *cold* interstellar hydrogen should radiate in the radio spectrum, through the spin of its electron flipping. The probability of such a flip is astonishingly small, but what van de Hulst realized was that there should be astonishing amounts of interstellar hydrogen, thereby making up for the extremely low transition probability. Following the end of World War II, his technique was validated by the discovery of 21 cm emission and absorption by the interstellar medium, and a mapping of the distribution of cold atomic hydrogen throughout the galaxy was carried out. What is the result? Throughout the part of the galaxy where the sun is located, and in the regions farther out in the galaxy, and to some extent farther in toward the center of the galaxy, there is a vast, semi-uniform distribution of interstellar hydrogen gas, with condensations in the gas outlining and indeed defining the spiral arms of the galaxy. But if you go far enough in, suddenly the amount of atomic hydrogen is vastly reduced.

What is going on? That brings us (finally!) to the question of molecular hydrogen. Why is the interstellar hydrogen atomic, and not molecular? In a gas bottle, the hydrogen is all molecular, and there are no individual hydrogen atoms. The answer is, that the gas bottle has

walls, but the galaxy does not. As was mentioned in the discussion in section 5.3, molecular hydrogen cannot form by direct radiative recombination (well, actually it can, but the probability is excruciatingly low). Thus, in a gas bottle, if the gas were not already molecular, atoms would stick to the walls and there would join with each other to form hydrogen molecules. Similarily, in the interstellar medium the only way any significant quantity of molecular hydrogen could form, is on the surface of the interstellar grains. The supposition then is, that the hydrogen in the inner part of the galaxy is in the form of molecular hydrogen, not atomic hydrogen. So, where do we stand on the detection of interstellar molecular hydrogen? In the same place we stood for atomic hydrogen before van de Hulst's technique had been applied. Interstellar molecular hydrogen has been discovered in a few locations, but it has not yet been possible to map it generally. The detection of the molecular hydrogen in those few locations is a dramatic story of the space age. Professor Lyman Spitzer of Princeton, father of the Hubble Space Telescope, predicted absorption of the light of hot stars by molecular hydrogen, and initiated NASA construction of OAO-3, "Copernicus," to detect it. He was beaten out of the discovery by an African-American scientist, Dr. George Carruthers of the US Naval Research Laboratory. The next stage, where MSX can be the determinant, is the recent detection of molecular hydrogen fluorescence near an extremely bright star using IUE. That proves the technique; MSX can provide the all-sky map. The point is that the UVISI instruments are so sensitive, they should detect molecular hydrogen fluorescence anywhere, excited just by the general interstellar radiation field.

7.5 Line Emission from Hot Interstellar Medium and/or Hot Halo of Galaxy

Our galaxy is tens of thousands of light years across, but is only a few hundred light years thick. The interstellar matter in the galaxy is mostly confined to that thin plane, the Milky Way disk. It was long thought that the interstellar matter consisted only of cold gas, plus dust grains, except near hot stars, where the interstellar matter should be heated by the nearby hot star.

However, there are numbers of stars that are far up out of the plane of the galaxy, and when their spectra were examined, absorption lines of interstellar matter were seen. Very early the question was asked, why does that interstellar matter not fall down into the galactic plane? That was the first hint that there might be a hot component to the interstellar medium, and in particular that there might be a hot halo of the galaxy: the temperature needed to support the gas against gravity was estimated as hundreds of thousands or a few million degrees.

The next suggestion that there might be a hot component to the interstellar medium came from X-ray astronomy: it was discovered that at low galactic latitudes (and at high galactic latitudes as well) there is a general soft-X-ray glow to the galaxy. The idea was that this is due to emission from ~million degree gas.

This concept was made solid by observations with the satellite "Copernicus." The spectra of distant hot O and B type stars were found often to include strong broad interstellar absorption lines at 1031.9 Å and 1037.6 Å, the resonance wavelengths of OVI (Oxygen five times ionized). Now, the ionization potential of OV is 113.9 volts, so it was clear that the gas in question must be at a temperature of hundreds of thousands of degrees, to achieve the degree of ionization observed.

The OVI observations were essentially all of gas in the plane of the galaxy, because that is where the O and B type stars are located. However, there are also plenty of O and B type stars in the Magellanic Clouds, which are small nearby satellite galaxies to our own galaxy. Thus, observers using the International Ultraviolet Explorer satellite (IUE) were able to look for absorption lines due to highly ionized species in the direction of the Magellanic Clouds. Such lines were duly found, but the question remained (and still remains), exactly how far away is the hot gas that is observed? The only clue is the doppler shift of the wavelengths of the lines, which yields the velocity of the gas, not its distance. Modelling of the gas, which is very uncertain, is needed to try to estimate the distance.

A completely different approach, however, is not to look for absorption produced by the hot gas in the light of distant stars, but instead to look for direct emission of ultraviolet light from the gas itself. One can calculate how much emission should be produced by what quantity of gas at what temperature; the result is that for reasonable models of hot gas in the plane of the galaxy, and also for reasonable models of a hot halo of the galaxy, the UVISI imaging spectrometers should readily detect the emission, in such lines as 1549 Å (CIV). And with an all-sky survey, UVISI should map these emissions over the sky, delineating the structure of the hot halo of the galaxy for the first time. The various different emission lines that the UVISI spectrometers are capable of detecting each originate in gas of a somewhat different temperature, and so it should be possible to construct maps of the sky that in effect are maps of the distribution on the sky of gas of various temperatures. For example, 1663 Å emission of OIII corresponds to a temperature of ~80,000 degrees, while the CIV corresponds to ~100,000 degrees.

The only data on this topic that exist at the present time are fragmentary results from an Aries rocket flight and from the UVX experiment that was carried on the Space Shuttle in 1986. These data are of sufficient quality to strongly suggest that the MSX observations should be

extremely successful. Again, the recipe for excellent results will be deep (= long) pointings, and the surveying of as much of the sky as can be managed.

7.6 Integrated Light of Distant Galaxies in the Ultraviolet

The spiral galaxy within which the sun is located is made up, overwhelmingly, of stars: about 100 billion stars. Beyond stars, about ten percent of the mass of our galaxy is in the form of interstellar gas and dust; and, in addition, there may be a black hole (spent quasar?) of about a million solar masses located at the center of the galaxy.

Looking out from our own galaxy, there are about a dozen nearby galaxies. These galaxies appear to be related to each other; that is, they form a small cluster, or group, of galaxies. This cluster is imaginatively named "the Local Group." The Local Group is totally dominated by just two galaxies, our own and the Andromeda Galaxy. These two giant galaxies appear to be almost twins, and are among the largest galaxies known. The last statement is somewhat controversial, because judging the size of distant galaxies requires knowledge of their distance, and the distance scale for galaxies beyond the local region is uncertain to at least a factor of two. Nonetheless, our galaxy and Andromeda are large galaxies. The remaining members of the Local Group are dwarf galaxies.

What is the appearance of a Local Group galaxy in the ultraviolet? Remarkably, extremely little is known about this. The reason is that overwhelmingly, astronomical observations in the ultraviolet have been made with extremely small fields-of-view, of point objects. There have been few wide-field observations in the ultraviolet of anything, including galaxies. For example, the satellite OAO-2 looked in the ultraviolet in the very center of the Andromeda galaxy, and discovered a strong totally unexpected small ultraviolet-emitting source. The reason this was unexpected was that the central regions of spiral galaxies, including our own and Andromeda, are dominated by the light of red giant stars, which should emit essentially no ultraviolet radiation at all. The source of the ultraviolet radiation from the centers of galaxies is still not well understood, and observations with the ASTRO Space Shuttle mission and with the Hubble Space Telescope are continuing.

Rocket and Space Shuttle ultraviolet photos of a few galaxies from Goddard Space Flight Center astronomers have shown, in addition, what was naturally expected: the outer reaches of spiral galaxies, where large numbers of very hot young O and B type stars are being continually created, shine very brightly in the ultraviolet. That simple fact leads to the reason for the interest in the integrated light of distant galaxies in the ultraviolet. Once we look

beyond the Local Group, we find billions of galaxies in the more distant reaches of the universe. Many of these are spirals like Andromeda; many are elliptical galaxies, that are almost entirely free of ultraviolet-emitting O and B type stars.

What does one expect to see, then, in looking at a patch of sky at high galactic latitude? One is "looking to the end of the universe," so to speak; why does one not see an infinite amount of ultraviolet light from the infinite number of distant spiral galaxies? Two reasons! *First*, the light of more and more distant galaxies is more and more redshifted by the expansion of the universe: the light that was emitted as ultraviolet light from extremely distant galaxies is redshifted so much that it is received by us as visible light, not ultraviolet. (But would not still more energetic emission be redshifted into the ultraviolet? It would if it existed, but galaxies are expected to be much fainter short of 912 Å, the interstellar absorption edge of neutral hydrogen. So there is no emission to be shifted.) *Secondly*, by looking farther into the distance we are of course looking backward in time ..... to times before the galaxies formed! No galaxies; no light.

That is the clue to the interest in the integrated light of distant galaxies: it gives us a direct handle on the evolutionary history of the galaxies. The particular value will be in tracing the history of star formation in galaxies over the last few billion years. If star formation was much more active in the past, the sky will be brighter; if spiral arms just formed, the sky will be dimmer in the ultraviolet. Notice that all that is really needed is a typical spectrum of the darkest part of the sky in the ultraviolet. MSX should provide an excellent background spectrum for this research project.

7.7 Intergalactic Far-ultraviolet Radiation Field

What is our universe like? We tend to think that we know the answer to that question, because we live in this universe and because we have learned, through astronomical research, that the universe is homogeneous and isotropic, which is to say that if you've seen one spot in the universe, you've seen them all. However, we lose sight of the fact that we actually live in a very atypical location, namely a galaxy. Suppose you were to choose a location at random in the universe, and place yourself there. Looking around, you would see what our universe is *really* like, since you have now chosen a genuinely typical location. And of course what you would see is: next to nothing. Around you would be the intergalactic medium, if one exists (which is unknown). Not a single star would shine, since the chance is overwhelming that your random spot will be far outside any galaxy. In fact, the only thing you would see at all, would be the faint pale light of the few nearest distant galaxies.

Of course if you had a millimeter-wave radiation detector, you would also detect the famous 3-degree background radiation, which is the only component of the universe that is known to be present everywhere in the universe. So, we believe we know the microwave radiation field in which you would be bathed. We also are pretty sure we know the visible light radiation field in which you would be bathed, and of course that would be very faint indeed.

What about the ultraviolet radiation field in which you would be bathed; and why is it important?

We can predict a certain amount of ultraviolet radiation would be present, because we know the density of galaxies and we think we know roughly what their ultraviolet luminosity is. But that may not be all of the radiation field; there may be totally unknown sources, and there are additional known sources that are not so easy to model, such as ultraviolet emission from distant quasars.

The reason all of this is important goes to the early history of the universe. Following the big bang, the universe expanded and cooled. When the universe was about 100,000 years old, the hot ionized gas (the matter of the universe) recombined to form colder neutral gas. The radiation that had been emitted and reabsorbed by the ionized gas was now free, and could expand and redshift to become (today) the 3-degree background. What became of the matter? That is a burning question! Of course some of it became the galaxies and quasars, but how and why did that happen? What precipitated the gravitational collapse? For example, we do not even know if the clusters of galaxies formed first (and then the individual galaxies formed from the gas within the cluster), or if the galaxies formed first, and then were drawn together by gravitation to form the clusters.

Using large ground-based telescopes and the Hubble Space Telescope, there is much active investigation of these questions in progress. A powerful tool is the study of the most distant quasars. The quasars are believed to be black holes ingesting matter, which shines extemely brightly just before falling into the black hole. That bright light source reaches us across the universe, and across billions of years of time. Its light can be partially absorbed, in transit, by any intergalactic matter. And indeed, for the most distant quasars, hundreds of narrow absorption lines are seen. These are confidently believed to be Lyman alpha absorption lines produced by small intergalactic clouds of neutral hydrogen.

Now remarkably, there is a pronounced dearth of such clouds very close in redshift (and hence very close in space) to the quasar itself. This "proximity effect" as it is called is easily explained: if the quasar is emitting copious quantities of ionizing ultraviolet radiation, that

radiation could destroy the clouds. The radiation from the quasars is in addition to the general ambient radiation.

A redshifted record of these radiation fields is present today in the universe, and will be observed by MSX as a component of the general diffuse ultraviolet background radiation. Thus, observations by MSX at the present day can help to elucidate the process of destruction of the intergalactic medium in the very eary history of the universe.

7.8 Radiation from Recombining Intergalactic Medium

Is there an intergalactic medium? Between the stars in our own galaxy, there is of course an interstellar medium, composed of gas and dust. Is there a similar (or any) medium between the galaxies?

The astrophysical mechanisms for detecting such a medium are exactly the same as for detecting and studying the interstellar medium. Since there does not seem to be any intergalactic stars (this is a delicate idea not often discussed!) and the heavier elements, we believe, are all created in stars, we would expect any intergalactic medium to be composed almost exclusively of hydrogen and helium. Thus, intergalactic dust (which is made of the heavier elements) is not expected. Of course dust could blow out from galaxies in some quantity into intergalactic space, but certainly the first and strongest candidate for an intergalactic medium is hydrogen and helium.

Neutral hydrogen is easily detected by its emission and absorption of 21-cm radiation. Professor George Field very early used the techniques of radio astronomy to establish that no substantial intergalactic medium of cold neutral hydrogen exists. This was very important, because about 100,000 years after the big bang the universe recombined and the whole universe was "cold" (~3000 degrees) neutral hydrogen. In 1965 Gunn and Peterson invented another technique, much more powerful than 21-cm techniques, for sensing intergalactic neutral hydrogen. The quasars had just been discovered, and had been found to radiate a continuous spectrum far into the ultraviolet, even beyond 1216 Å, the resonance wavelength of the neutral hydrogen atom (and indeed, even beyond 912 Å, the wavelength short of which atomic hydrogen continuously absorbs.) Gunn and Peterson pointed out that a photon emitted by a quasar at 1000 Å, would redshift as it travelled, eventually spending some period of time at or near 1216 Å. During that period, if any neutral hydrogen was in the vicinity, the photon would be absorbed. Of course it would be re-emitted a small fraction of a second later, but in a random direction, and so it would never reach our observer on earth.

Different wavelengths would pass through 1216 Å at different positions along the line-of-sight, and as the emission spectrum of the quasar is continuous, every position along the line of sight would be "sampled" by 1216 Å radiation from the quasar. Any location on the line of sight that had any significant amount of neutral hydrogen would remove a chunk from the emitted spectrum of the quasar, and would be detected by the observer on earth as an absorption line in the spectrum of the quasar.

The Gunn-Peterson test turns out to be enormously sensitive, and turns out to show that intergalactic space is truly extraordinarily free of neutral hydrogen. How can this be? Could the process of galaxy formation be enormously efficient, trapping essentially all atoms? This seems highly unlikely, because the process of star formation (as we observe it in detail in our own galaxy) is very inefficient: the bright light of the hot young stars blows matter away from the region of star formation by means of light pressure.

Thus, a very strong case exists for an intergalactic medium; and it is not neutral, so it must be ionized. If it were ionized and very hot, it could be detected by its X-ray emission. Indeed, there is a strong X-ray background observed in the universe, and for a time many thought that some of the X-rays originated in emission from an intergalactic medium. However, for a variety of reasons, that idea is in disfavor: for example, where would the enormous energy come from, to heat the gas to so high a temperature? Instead, the remaining possibility is a "lukewarm" intergalactic medium, of ionized gas at say 200,000 or 300,000 degrees.

How might we detect such a medium? Well, any ionized plasma will tend to recombine. Radiative recombination of ionized hydrogen produces Lyman alpha radiation. MSX would observe this radiation as a redshifted ledge of emission longward of Lyman alpha. Thus, there is a possibility that MSX could reveal the baryonic dark matter of the universe.

7.9 Radiation from Re-heating of Intergalactic Medium Following Recombination

We have already seen (in bullet 8) the case that there might exist an ionized intergalactic medium. And we have seen that once created, such a medium must necessarily radiate (via recombination radiation), and that the UVISI instruments on MSX have some hope of detecting such radiation.

But now we will re-examine the process of creating such an ionized intergalactic medium. We will find another powerful emission process, one that offers additional hope both of

detecting an intergalactic medium, and even more interesting, of tracing the process of the creation of that medium. Recall that the universe began (10 to 20 billion years ago) in a big bang. We do not know for sure whether the universe is open (infinite) or closed (finite in volume, but without an edge). The best current ideas strongly suggest that the universe should be "just on the border" between being open and closed: which would mean a perfectly flat expanding universe of infinite volume. We naturally tend to think of the big bang as an explostion from a point, and indeed the portion of the universe that we see today surely originated in a volume of space smaller than a single proton. If the universe is infinite (as we believe it is), it was always infinite, and the big bang occurred everywhere at once in infinite space. The portion of that infinite big bang that became our present visible universe was just a proton-volume's worth. As we have seen, 100,000 years after the big bang the universe recombined, and continued expanding, the radiation field cooling to be the present-day 3-degree background radiation observed by COBE, and the matter expanding, and cooling even faster as a thin almost perfectly uniform gas. Then the gas collapsed under the influence of gravity to form quasars, and ultimately stars, galaxies, and clusters of galaxies in some order!

The process, we have emphasized, is not at all well understood, but a very reasonable case exists that the process was inefficient; that is, a great deal of the matter did not end up in objects, but remains as an ionized intergalactic medium. Highly in accord with this notion is the fact that we cannot account for most of the normal (called "baryonic") matter that we feel sure exists. Our certainty about how much baryonic matter there is, arises from "Copernicus" observations of deuterium in the interstellar medium and also from ground-based observations that have led to a determination of the helium abundance in the universe. It turns out that deuterium and helium were manufactured in the first three minutes of the big bang, and that the abundance of both is sensitively dependent on the density of matter. From the observed abundance, we can calculate what the density must have been. The result is that we believe we know how much baryonic matter must be out there, but we can only account for perhaps 10 percent of it in the form of stars and galaxies. Thus, the famous "missing matter" (baryonic component of; see bullet 10 for the rest!). Now the intergalactic medium of course started out neutral (the universe having recombined). But as quasars in particular form, they emit copious quantities of hard ionizing radiation, which will tend to re-ionize the intergalactic medium. This is what we believe happened.

So, now, look at the physics of that re-ionization process: first hydrogen is ionized, then helium (as the intergalactic medium becomes more and more transparent through being ionized.) The hydrogen tends to recombine again and again, but be re-ionized again and again. Each cycle produces a Lyman alpha photon: vast numbers of them. The first ionization of helium similarily produces vast numbers of 584 Å photons, but these are

efficiently destroyed by ionizing the residual hydrogen. However, by the time the second ionization of helium occurs, the universe is transparent to ionizing radiation, and the 304 Å photons survive just as did the 1216 Å Lyman alpha photons.

These vast numbers of photons would redshift, and might be detected today. The 1216 Å radiation is likely present now in the visible, and difficult or impossible to detect against strong zodiacal light. But the 304 Å radiation might form a broad bump in the far ultraviolet, potentially detectable by MSX.

7.10 Radiation from Radiative Decay of Dark Matter Candidates (neutrino, etc.)

The universe is believed, on the basis of the theory of inflation, to be just on the borderline between being open and closed.

The theory of inflation is a theory of the big bang's origin that is firmly rooted in modern theories of elementary particle physics. According to inflation, the universe expanded not linearly, but exponentially, for a tiny fraction of a second near the very beginning. During that tiny fraction of a second the universe expanded by an amount entirely inconceivable to the human mind. The universe then went over into the kind of normal linear expansion that we observe today.

That something like inflation did occur seems certain. The reason that we can have such confidence is because of what we observe of the big bang ourselves, namely the residual 3-degree background radiation. The fact is, that apart from doppler shifts due to the earth's motion through the universe, and tiny wrinkles that were recently discovered by COBE, we find the radiation temperature to be precisely the same over the sky, to a high degree of accuracy. Now, that this should be so, is truly remarkable. In particular, consider two points on the sky that are diametrically opposite to each other. In one direction, we are detecting 1-mm wavelength photons that were emitted off in that direction, 10 or 20 billion years ago; that is, that were emitted by gas that is 10 to 20 billion light years away in that direction. And the same occurred, in the opposite direction. Thus it appears that the two samples of emitting gas, located 20 to 40 billion light years apart, are of exactly the same temperature. How could this incredible coordination have occurred? The two gas samples, given the observed rate of expansion of the universe, could never have been in thermal contact with each other so as to achieve the observed perfect equilibrium! But according to inflation, they *were* in thermal contact at the big bang, and they are so distantly separated mostly because of the much faster exponential expansion that occurred during the inflation stage. Thus our observations almost certainly require that inflation (or something very much like it!) did

occur. There are also additional reasons for believing that inflation occurred. For example, the ordinary matter that we observe in the universe is about 2 percent of the amount needed to "close" the universe. The traditional old equations of cosmology then allow us to figure backward in time, toward the big bang, to see how close to being closed the universe was way back then. The answer is, incredibly close. It seems unnatural that the physical laws should not have made it right on the line exactly, as inflation predicts. Thus, many believe that the universe is indeed just on the border, and that the 2 percent of closure density that we have seen so far, is only a small fraction of the actual mass density of the universe. The rest is the "missing mass."

We have already discussed missing baryons. But baryons are apparently only about 10 percent of closure density. What is the non-baryonic missing matter, the 90 percent of the matter of the universe that did not participate, because of its nature, in the chemistry of the first three minutes?

No one knows; speculation abounds! Many exotic particles, theorized but not known to exist (the "etc's" of our bullet) are speculated upon. But one candidate is known to exist: neutrinos. These have been detected, and exist in three varieties, electron-neutrinos, muon-neutrinos, and tau-neutrinos. We are bathed in neutrinos left over from the big bang in exactly the same way that we are bathed in the 3-degree background radiation. Neutrinos were long believed to be of zero rest mass (in which case they would contribute no more to closure than does the 3-degree radiation field). But there are recent suggestions that this is not so, that they have a tiny rest mass. There are so many neutrinos that all it would take is about 30 eV or so of rest mass for the neutrinos to be successful as the missing non-baryonic dark matter! And 30 eV is a magic number, for if a heavier neutrino were to decay into a lighter neutrino with emission of a photon, that photon would thus be of energy of order 10 eV, which is to say ultraviolet, the range that will be meaured sensitively by UVISI on MSX.

7.11 Reflectivity of the Asteroids in the Ultraviolet

The Earth is a fragile haven for life in the solar system. NASA exploration of the Moon and the planets has not reveled life elswhere in the solar system, and evidence has accumulated that the solar system is a very violent place, hostile to life. The climate on Mars may vary drastically over the eons, with water present in the distant past. With Venus, perhaps there was a relentless loss of water followed by massive greenhouse heating. For our own Moon, there was a colossal bombardment by asteroids very early, leading to the mare or "sea" features we see on the Moon today.

The Earth itself underwent a similar bombardment at the same time, but the evidence has been largely buried by the extremely active geological processes at work on Earth. Nonetheless, the Meteor Crater in Arizona, and the record of such recent events as the Tungusku explosion in Siberia, remind us that we still exist "at the whim of the Gods". Most significantly, the evidence has increased massively in recent years for the theory that 65 million years ago the Earth was struck by an asteroid or a pair of asteroids leading to the extinction of the dinosaurs, and the succession of the mammals.

The fact that we are hostage to the asteroids suggests that we should make every effort to understand them well.

In all the history of the space program, only one image of an asteroid, Gaspra, has been obtained. All other data are remotely obtained data, but astronomers have long and excellent experience with making the most of remotely obtained data. In particular, spectral data measurements on the asteroids have led to the classification of asteroids on the basis of their nature, and in particular their composition. Observations may be compared with "ground truth," laboratory measurements of actual meteorite samples. The result is a great deal of knowledge concerning the orbits of the thousands of known asteroids, and also their composition. Special interest of course centers on the so-called "Earth-crossing asteroids," those asteroids having orbits that nearly intersect with the orbit of Earth. These are the candidate objects for being the next to wipe out the dominant life form on Earth!

As usual in any area of scientific investigation, knowledge grows most effectively by a multi-pronged approach, in which relevant data of all kinds are accumulated and checked against each other.

Very little data exist at present concerning the appearance of the asteroids in the ultraviolet. All we have to go on are a few IUE spectra, plus existing spectra of the Moon from Apollo 17, recently supplemented by measurements with Galileo on its fly-by of Earth. What we have realized from the work so far is that, compared with measurements in the visible, measurements in the ultraviolet have a significant advantage. The reason is that visible light penetrates significantly into the interior of rock before being reflected. The result is that very minor impurites in the rock can have a very big effect on the amount of light that is reflected, and hence on the observed brightness and spectrum of the asteroid. In comparison, ultraviolet light reflects directly from the surface of rock, and the reflectivity is determined by the bulk index of refraction of the material of which the rock is made. Thus, the ultraviolet brightness is determined by the bulk composition; the visible brightness by the amount and nature of unimportant contaminants. The case for carrying out classification of asteroids in the UVISI ultraviolet imager and spectrometer range appears compelling. In the

course of a systematic all sky survey, UVISI should detect hundreds if not thousands of asteroids. A great virtue of an all sky survey is that all of these asteroids would be observed with exactly the same instruments. Thus, a consistent and homogeneous database would exist for the first time for the classification of asteroids on a physical basis, complementing and supplementing the important infrared measurements that exist.

7.12 Zodiacal Light

In an age of city lights, few of us have experienced the "false dawn," light on the eastern horizon that turns out not to herald the sun, but to be a direct visual experience of a vast cloud of dust that pervades the inner part of the solar system. This light that is seen so easily and so brightly by the naked human eye is called zodiacal light. Its source does not have a name, unless it is called the zodiacal cloud.

The cloud is called zodiacal because the band of light follows the constellations of the zodiac in the sky, those constellations through which the planets of our solar system wander. That is the clue that the zodiacal cloud is indeed part of our own solar system. The variation of the brightness of the cloud as the Earth passes through it gives us an idea of its geometry. Many and difficult measurements are necessary, for except near the sun the zodiacal light is very faint, and must be disentangled from the light of stars, and from the glow of our atmosphere, which we tend to be unaware of, but which is as bright as the integrated light of the stars.

What is the origin of this vast cloud of dust? The thought that the cloud is an original part of the furniture of the solar system can be dismissed, for particles as small as those that make up the zodiacal cloud are subject to light pressure and the Poynting-Robertson effect, which remove them from the cloud on a time scale of only ten thousand years. There are two obvious candidates for producing a more or less continuous supply of dust in the inner solar system: asteroids, and comets. Comets are particularily obvious as a candidate, for comets enter the inner solar system frequently, and they clearly emit matter, as witnessed by their tails. The asteroids are less obvious candidates: for they are very solid objects. However, the asteroids exist in very large numbers, and if two asteroids were to collide, the violent collision would surely generate large amounts of rock dust. The analysis and study of the zodiacal light procedes according to the agenda of all astronomical investigations: observe the subject of interest in all possible ways at all possible wavelengths and try to construct physical models that have the observed properties. As has been mentioned, observation of zodiacal light in the visible is difficult because of the stars. In the infrared, the zodiacal light has been measured by IRAS, which made the remarkable discovery of bands of infrared zodiacal light, seemingly hovering like halos above and below the solar system. It turns out

that this is an optical illusion, and furthermore that the bands can be associated with the orbits of particular groups of asteroids!

In contrast, the ultraviolet is virtually terra incognita as far as observations of the zodiacal light are concerned. The only measurements that exist are rocket and space shuttle measurements by the Johns Hopkins group. Observation of zodiacal light in the ultraviolet is difficult for another reason: the zodiacal light is all reflected sunlight, and the sun is a cool star, emitting very little ultraviolet light. As a result, zodiacal light has never been detected shortward of about 2500 Å. The fragmentary near-ultraviolet measurements that exist are very interesting. First, the distribution of the zodiacal light on the sky appears to be very different in the ultraviolet, in comparison with the distribution in the visible. In the visible, the ecliptic plane (the zodiac) is about three times brighter than the ecliptic pole. Thus, the dust cloud seems to be rather flattened and confined to the plane. In contrast, there is much less variation over the sky of the ultraviolet zodiacal light. Yet there is no doubt that the light that is seen is true zodiacal light, for the spectrum of the light closely ressembles that of the sun. This would indicate that in the ultraviolet we are seeing a new component of the dust, presumably smaller particles than those responsible for the visible zodiacal light. Second, odd spectral features appear near 2800 Å that are completely unexplained.

UVISI on MSX can make the first complete spatial and spectral maps of zodiacal light in the ultraviolet, significantly increasing our knowledge of this interesting component of our own solar system.

8. SUMMARY AND CONCLUSION

We have successfully carried out a major modeling effort, resulting in publicly available descriptions of the expected ultraviolet sky. And, we have created working software for the acquisition and analysis of ultraviolet images and spectra of the sky. What has not been done is a comparison of such images and spectra with the models, due to the less than perfect quality of the data. Thus, verification and testing of the models remains a task for the future.

In connection with our effort, we created a proposal to NASA which would have allowed acquisition of a great deal more data from the MSX mission, the UVISI instruments in particular. It is unfortunate that NASA did not choose to fund our proposal, which would have resulted in a deep survey in the 2200 Å region of the spectrum (IUN) that would have been of great value.

For the future, NASA has selected and funded a project called GALEX, which is expected to map faint point sources on the sky. And the Principal Investigator on the present contract is submitting a proposal to NASA to carry out a spectroscopic examination of the diffuse ultraviolet background radiation: the radiation which has been modeled under the present contract.

9. REFERENCES

[1] Allen, M. M., Murthy, J., Daniels, J., Dring, A. R., Newcomer, R. E., Henry, R. C., Paxton, Tedesco, E., Price, S. D. 1997, *"UVISI Observations of The Pleiades,"* BAAS, **29**, 805, 1997

[2] Baggaley, W.J. 1977a, *"The Possibility of the Detection of Meteror Streams in Interplanetary Space,"* Observatory **97**, 123

[3] Baggaley, W.J. 1977b, *"The Meteoric Nightglow,"* Monthly Notices Roy. Astron. Soc. **181**, 203

[4] Bohlin, R.C., Savage, B. D., & Drake, J.F., *"A Survey of Interstellar H I from Lα Absorption Measurements. II,"* 1978, ApJ, **224**, 132

[5] Daniels, J., Murthy, J., Allen, M. M., Dring, A. R., Newcomer, R. E., Henry, R. C., Paxton, L., Tedesco, E., & Price, S. D. 1997, *"UVISI Observations of the Large Magellanic Cloud,"* BAAS, **29**, 805

[6] Dickey, J.M., & Lockman, F.J., 1990, *"HI In the Galaxy,"* ARA&A, **28**, 215

[7] Draine, B.T., & Lee, H.M., 1984, *"Optical Properties of Interstellar Graphite and Silicate Grains"*, ApJ, **285**, 89

[8] Dring, A. R. , Murthy, J., Allen, M. M., Daniels, J., Newcomer, R. E., Henry, R. C., Paxton, L., Tedesco, E., & Price, S. D. 1997, *"UVISI Observations of Orion Dust,"* BAAS, **29**, 785

[9] Dumont, R., Levasseur-Regourd, A.C. 1978, *"Zodiacal Light Photopolarimetry,"* Astron. Astrophys. **64**, 9

[10] Gottleib, D.M., 1978, *"Skymap : A New Catalog of Stellar Data,"* ApJS, **38**, 287

[11] Henry, R. C., J. Murthy, J., M. Allen, M., J. Daniels, J., A. R. Dring, A. R., L. J. Paxton, L. J., E. F. Tedesco, E. F., & S. D. Price, S. D. 1997, *"UVISI Observations of the Small Magellanic Cloud,"* BAAS, **28**, 1387

[12] Henry, R. C., Murthy, J., Allen, M., Corbin, M., and Paxton, L. J. 1992, *"Spectroscopy and Imaging of the Cosmic Diffuse UV Background Radiation,"* SPIE Conference Vol. 1764, "Ultraviolet Technology IV", ed. Robert E. Huffman, 61

[13] Henry, R.C., 1977, *"Far-Ultraviolet Studies. I. Predicted Far-Ultraviolet Interstellar Radiation Field,"* ApJ Suppl ApJS, **33**, 451

[14] Kurucz, R. 1979, *"Model Atmospheres for G, F, A, B, and O Stars,"* ApJS, **40**, 1

[15] Leinert, C., Pitz, E., Hanner, M., Link, H. 1977, *"Zodiacal Light,"* J. Geophys. **42**, 699

[16] Leinert, C., Hanner, M., Richter, I., Pitz, E. 1980, *"The Plane of Symmetry of Interplanetary Dust in the Inner Solar System,"* Astron. Astrophys. **82**, 328

[17] Leinert, C., Richter, I., Pitz, E., Hanner, M. 1982, *"Helios Zodiacal Light Measurements - A Tabulated Summary,"* Astron. Astrophys. **110**, 335-337

[18] Levasseur, A.C. 1976, *"Zodiacal Light,"* Thesis, Université de Paris

[19] Levasseur, A.C., Blamont, J.E. 1975, *"Study of Zodical Light,"* Space Res, **15**, 573

[20] Levasseur, A.C., Blamont, J.E. 1976, *"The Zodiacal Light,"* Lect. Notes Phys. **48**, 58

[21] Levasseur, A.C., Private Communication, 1994

[22] Levasseur-Regourd, A.C., Dumont, R. 1980, *"Absolute Photometry of Zodiacal Light,"* Astron. Astrophys. **84**, 277

[23] Lockman, F.J., Hobbs, L.M., & Shull, J.M., 1986, *"The Extent of the Local H I Halo,"* ApJ, **301**, 380 - 394

[24] McKee, C.F., 1990, in *The Evolution of the Interstellar Medium*, ed. L. Blitz (Astronomical Society of the Pacific: Conference Proceedings)

[25] Mercer, R.D., Dunkelman, L., Kinglesmith, D.A., Alvord, G.G. 1979, *"Dust at Libration Points,"* Space Res. **19**, 467

[26] Misconi, N.Y. 1977, *"On the Photometric Axis of the Zodiacal Light,"* Astron. Astrophys. **61**, 497

[27] Murthy, J., Allen, M. M., Daniels, J., Dring, A. R., Newcomer, R. E., Henry, R. C., Paxton, L., Tedesco, E. & Price, S. D. 1997 *"UVISI Observations of the Galactic Plane,"* BAAS, **29**, 838

[28] Murthy, J., Henry, R.C., Feldman, P.D., Tennyson, P.D. 1990, *"Observations of the Diffuse Near- UV Radiation Field,"* Astron. Astrophys. **231**, 187-198

[29] Murthy, J. and Henry, R.C., 1995, *"A Model of the Diffuse Ultraviolet Radiation Field,"* ApJ, **448**, 848

[30] Price, S. D., Tedesco, E. F., Cohen, M., Walker, R. G., Henry, R. C.,Moshir, M., Paxton, L. J., & Witteborn, F. C. 1997,*"Astronomy on the Midcourse Space Experiment,"* in Proceedings of IAU Symposium 179, *New Horizons from Multi-Wavelength Sky Surveys*, ed. B. J. McLean, D. A. Golombek, J. J. E. Hayes, and H. E. Payne, 115

[31] Price, S. D., Cohen, M., Walker, R. G., Henry, R. C., Moshir, M., Paxton, L. J., Witteborn, F. C., M. Egan, M. P., Shipman, R. F. 1997, *"Astronomy on the Midcourse Space Experiment,"* BAAS, **28**, 1341

[32] Spitzer, L., 1978, in Physical Processes in the Interstellar Medium (New York: John Wiley and Sons)

[33] Stark, A.A., Gammie, C.F., Wilson, R.W., Bally, J., Linke, R.A., Heiles, C., & Hurwitz, M., 1992, *"The Bell Laboratories H I survey,"* ApJS, **79**, 77-104

[34] Weinberg, J.L., Sparrow, J.G. 1978, Cosmic Dust, Wiley and Sons, New York, p. 75

Appendices

Appendix A, UVISI-MSX Sky Survey Targets *(showing targets completed)*

Appendix B, "A Model of the Diffuse Ultraviolet Radiation Field,"
by J. Murthy and R. C. Henry, Astrophysical Journal, 448, 848-857 (1995)

MSX - UVISI Sky Survey as partially completed

Black targets measured in 1280 Å - 1380 Å; Grey targets in 1450 Å - 1800 Å; Targets #356 and #357 in both

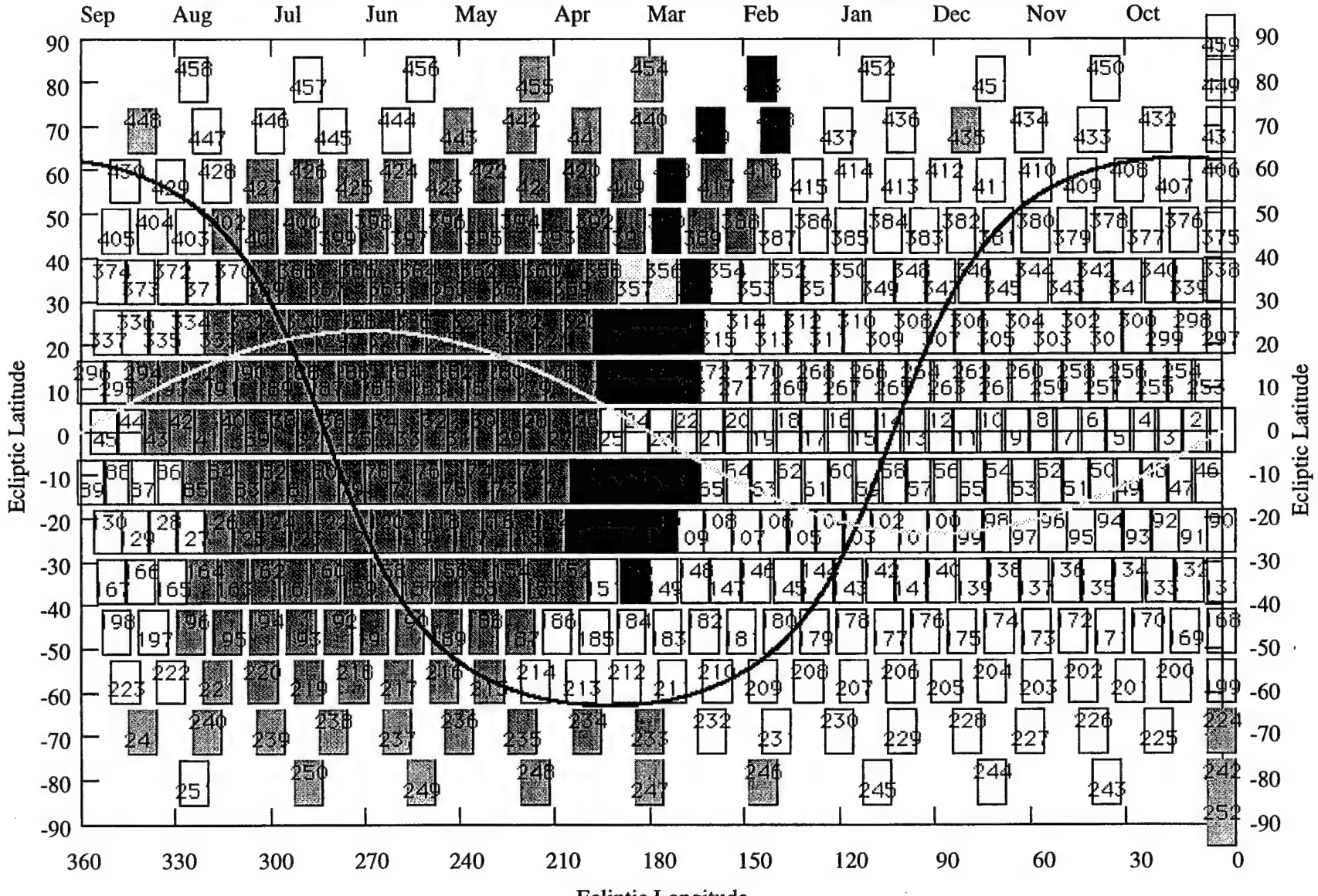

UVISI – MSX: Sky Survey Targets

Number	Ecliptic Longitude	Ecliptic Latitude	RA (hr)	RA (°)	Dec	Galactic Longitude	Galactic Latitude
UVS- 1	0.000	0.0	0	0.000	0.0	96.345	-60.184
UVS- 2	8.000	0.0	0	7.347	3.2	112.130	-59.230
UVS- 3	16.000	0.0	1	14.738	6.3	126.325	-56.523
UVS- 4	24.000	0.0	1	22.218	9.3	138.203	-52.444
UVS- 5	32.000	0.0	2	29.824	12.2	147.856	-47.390
UVS- 6	40.000	0.0	2	37.589	14.8	155.721	-41.672
UVS- 7	48.000	0.0	3	45.536	17.2	162.256	-35.508
UVS- 8	56.000	0.0	3	53.675	19.3	167.836	-29.043
UVS- 9	64.000	0.0	4	62.003	21.0	172.746	-22.374
UVS- 10	72.000	0.0	4	70.497	22.2	177.202	-15.572
UVS- 11	80.000	0.0	5	79.120	23.1	181.369	-8.685
UVS- 12	88.000	0.0	5	87.820	23.4	185.385	-1.755
UVS- 13	96.000	0.0	6	96.536	23.3	189.371	5.183
UVS- 14	104.000	0.0	6	105.204	22.7	193.446	12.096
UVS- 15	112.000	0.0	7	113.769	21.7	197.737	18.947
UVS- 16	120.000	0.0	8	122.183	20.2	202.394	25.690
UVS- 17	128.000	0.0	8	130.418	18.3	207.605	32.268
UVS- 18	136.000	0.0	9	138.461	16.0	213.616	38.599
UVS- 19	144.000	0.0	9	146.315	13.5	220.755	44.565
UVS- 20	152.000	0.0	10	153.997	10.8	229.444	49.987
UVS- 21	160.000	0.0	10	161.535	7.8	240.152	54.605
UVS- 22	168.000	0.0	11	168.966	4.7	253.204	58.059
UVS- 23	176.000	0.0	11	176.329	1.6	268.340	59.938
UVS- 24	184.000	0.0	12	183.671	-1.6	284.351	59.944
UVS- 25	192.000	0.0	12	191.034	-4.7	299.496	58.075
• UVS- 26	200.000	0.0	13	198.465	-7.8	312.561	54.629
• UVS- 27	208.000	0.0	13	206.003	-10.8	323.283	50.017
• UVS- 28	216.000	0.0	14	213.685	-13.5	331.982	44.598
• UVS- 29	224.000	0.0	14	221.539	-16.0	339.129	38.635
• UVS- 30	232.000	0.0	15	229.582	-18.3	345.146	32.306
• UVS- 31	240.000	0.0	16	237.817	-20.2	350.360	25.729
• UVS- 32	248.000	0.0	16	246.231	-21.7	355.020	18.986
• UVS- 33	256.000	0.0	17	254.796	-22.7	359.312	12.136
• UVS- 34	264.000	0.0	17	263.464	-23.3	3.388	5.224
• UVS- 35	272.000	0.0	18	272.180	-23.4	7.375	-1.715
• UVS- 36	280.000	0.0	18	280.880	-23.1	11.390	-8.645
• UVS- 37	288.000	0.0	19	289.503	-22.2	15.556	-15.532
• UVS- 38	296.000	0.0	19	297.997	-21.0	20.010	-22.335
• UVS- 39	304.000	0.0	20	306.325	-19.3	24.917	-29.004
• UVS- 40	312.000	0.0	20	314.464	-17.2	30.492	-35.471
• UVS- 41	320.000	0.0	21	322.411	-14.8	37.020	-41.637
• UVS- 42	328.000	0.0	21	330.176	-12.2	44.876	-47.358
• UVS- 43	336.000	0.0	22	337.782	-9.3	54.518	-52.417
UVS- 44	344.000	0.0	22	345.262	-6.3	66.382	-56.503
UVS- 45	352.000	0.0	23	352.653	-3.2	80.564	-59.219
UVS- 46	4.500	-11.5	0	8.722	-8.8	110.133	-71.217
UVS- 47	12.682	-11.5	0	16.142	-5.6	131.769	-68.229
UVS- 48	20.864	-11.5	1	23.572	-2.5	147.384	-63.343
UVS- 49	29.045	-11.5	1	31.052	0.4	158.363	-57.413
UVS- 50	37.227	-11.5	2	38.615	3.0	166.439	-50.924

• = 1450 Å – 1800 Å + = 1280 Å – 1380 Å + = Both

UVISI – MSX: Sky Survey Targets

Number	Ecliptic Longitude	Latitude	RA (hr)	RA (°)	Dec	Galactic Longitude	Latitude
UVS- 51	45.409	-11.5	3	46.286	5.4	172.755	-44.127
UVS- 52	53.591	-11.5	3	54.078	7.5	177.994	-37.160
UVS- 53	61.773	-11.5	4	61.993	9.2	182.571	-30.103
UVS- 54	69.955	-11.5	4	70.021	10.6	186.751	-23.009
UVS- 55	78.136	-11.5	5	78.138	11.5	190.722	-15.918
UVS- 56	86.318	-11.5	5	86.313	11.9	194.624	-8.863
UVS- 57	94.500	-11.5	6	94.506	11.9	198.579	-1.878
UVS- 58	102.682	-11.5	6	102.677	11.4	202.701	5.002
UVS- 59	110.864	-11.5	7	110.787	10.5	207.106	11.733
UVS- 60	119.045	-11.5	7	118.804	9.1	211.927	18.261
UVS- 61	127.227	-11.5	8	126.707	7.3	217.317	24.516
UVS- 62	135.409	-11.5	9	134.486	5.2	223.455	30.404
UVS- 63	143.591	-11.5	9	142.146	2.8	230.544	35.797
UVS- 64	151.773	-11.5	10	149.700	0.1	238.786	40.527
UVS- 65	159.955	-11.5	10	157.173	-2.8	248.324	44.383
+ UVS- 66	168.136	-11.5	11	164.600	-5.9	259.134	47.125
+ UVS- 67	176.318	-11.5	11	172.021	-9.1	270.904	48.530
+ UVS- 68	184.500	-11.5	12	179.484	-12.3	283.015	48.459
+ UVS- 69	192.682	-11.5	12	187.038	-15.6	294.716	46.921
+ UVS- 70	200.864	-11.5	13	194.736	-18.8	305.414	44.063
• UVS- 71	209.045	-11.5	13	202.630	-21.9	314.828	40.115
• UVS- 72	217.227	-11.5	14	210.768	-24.8	322.954	35.313
• UVS- 73	225.409	-11.5	15	219.190	-27.4	329.944	29.867
• UVS- 74	233.591	-11.5	15	227.921	-29.8	336.003	23.940
• UVS- 75	241.773	-11.5	16	236.965	-31.8	341.332	17.656
• UVS- 76	249.955	-11.5	16	246.301	-33.3	346.108	11.105
• UVS- 77	258.136	-11.5	17	255.873	-34.4	350.481	4.358
• UVS- 78	266.318	-11.5	17	265.600	-34.9	354.582	-2.533
• UVS- 79	274.500	-11.5	18	275.377	-34.9	358.527	-9.526
• UVS- 80	282.682	-11.5	18	285.092	-34.3	2.430	-16.585
• UVS- 81	290.864	-11.5	19	294.645	-33.2	6.414	-23.678
• UVS- 82	299.045	-11.5	19	303.953	-31.6	10.623	-30.771
• UVS- 83	307.227	-11.5	20	312.967	-29.6	15.249	-37.822
• UVS- 84	315.409	-11.5	21	321.666	-27.2	20.569	-44.777
• UVS- 85	323.591	-11.5	21	330.058	-24.5	27.017	-51.552
UVS- 86	331.773	-11.5	22	338.170	-21.6	35.308	-58.002
UVS- 87	339.955	-11.5	22	346.042	-18.5	46.643	-63.859
UVS- 88	348.136	-11.5	23	353.723	-15.3	62.792	-68.608
UVS- 89	356.318	-11.5	23	1.266	-12.0	84.963	-71.362
UVS- 90	0.000	-23.0	0	9.588	-21.0	96.211	-83.184
UVS- 91	8.780	-23.0	0	17.361	-17.6	147.425	-79.616
UVS- 92	17.561	-23.0	1	25.056	-14.4	167.041	-72.903
UVS- 93	26.341	-23.0	1	32.730	-11.3	176.489	-65.526
UVS- 94	35.122	-23.0	2	40.425	-8.5	182.559	-57.963
UVS- 95	43.902	-23.0	2	48.172	-6.0	187.209	-50.349
UVS- 96	52.683	-23.0	3	55.993	-3.8	191.187	-42.742
UVS- 97	61.463	-23.0	4	63.894	-2.1	194.847	-35.176
UVS- 98	70.244	-23.0	4	71.870	-0.8	198.392	-27.681
UVS- 99	79.024	-23.0	5	79.906	0.1	201.956	-20.283
UVS-100	87.805	-23.0	5	87.979	0.4	205.646	-13.014

• = 1450 Å – 1800 Å + = 1280 Å – 1380 Å + = Both

UVISI – MSX: Sky Survey Targets

Number	Ecliptic Longitude	Ecliptic Latitude	RA (hr)	RA (°)	Dec	Galactic Longitude	Galactic Latitude
UVS-101	96.585	-23.0	6	96.060	0.3	209.558	-5.912
UVS-102	105.366	-23.0	7	104.118	-0.3	213.790	0.976
UVS-103	114.146	-23.0	7	112.127	-1.4	218.445	7.593
UVS-104	122.927	-23.0	8	120.067	-2.9	223.639	13.861
UVS-105	131.707	-23.0	8	127.927	-4.9	229.495	19.685
UVS-106	140.488	-23.0	9	135.710	-7.2	236.135	24.940
UVS-107	149.268	-23.0	9	143.428	-9.9	243.660	29.476
UVS-108	158.049	-23.0	10	151.107	-12.8	252.108	33.117
UVS-109	166.829	-23.0	11	158.786	-16.0	261.401	35.682
+ UVS-110	175.610	-23.0	11	166.512	-19.3	271.302	37.014
+ UVS-111	184.390	-23.0	12	174.347	-22.7	281.428	37.017
+ UVS-112	193.171	-23.0	12	182.359	-26.2	291.331	35.693
+ UVS-113	201.951	-23.0	13	190.627	-29.7	300.628	33.134
• UVS-114	210.732	-23.0	14	199.233	-33.1	309.081	29.497
• UVS-115	219.512	-23.0	14	208.264	-36.3	316.610	24.966
• UVS-116	228.293	-23.0	15	217.794	-39.2	323.255	19.714
• UVS-117	237.073	-23.0	15	227.878	-41.8	329.114	13.893
• UVS-118	245.854	-23.0	16	238.526	-43.8	334.311	7.627
• UVS-119	254.634	-23.0	16	249.683	-45.4	338.970	1.012
• UVS-120	263.415	-23.0	17	261.219	-46.2	343.203	-5.875
• UVS-121	272.195	-23.0	18	272.932	-46.4	347.117	-12.976
• UVS-122	280.976	-23.0	18	284.585	-45.9	350.808	-20.244
• UVS-123	289.756	-23.0	19	295.953	-44.7	354.372	-27.641
• UVS-124	298.537	-23.0	19	306.867	-42.9	357.917	-35.137
• UVS-125	307.317	-23.0	20	317.235	-40.5	1.576	-42.702
• UVS-126	316.098	-23.0	21	327.038	-37.8	5.552	-50.309
UVS-127	324.878	-23.0	21	336.310	-34.7	10.197	-57.923
UVS-128	333.659	-23.0	22	345.118	-31.4	16.255	-65.486
UVS-129	342.439	-23.0	22	353.544	-28.0	25.675	-72.865
UVS-130	351.220	-23.0	23	1.674	-24.5	45.196	-79.584
UVS-131	0.000	-34.5	0	15.296	-31.3	276.626	-85.316
UVS-132	9.730	-34.5	0	23.499	-27.7	218.598	-80.548
UVS-133	19.459	-34.5	1	31.559	-24.2	207.344	-72.923
UVS-134	29.189	-34.5	1	39.549	-21.1	204.792	-64.959
UVS-135	38.919	-34.5	2	47.526	-18.3	204.828	-56.943
UVS-136	48.649	-34.5	3	55.525	-15.9	206.021	-48.960
UVS-137	58.378	-34.5	3	63.567	-13.9	207.897	-41.054
UVS-138	68.108	-34.5	4	71.660	-12.4	210.271	-33.264
UVS-139	77.838	-34.5	5	79.795	-11.5	213.079	-25.630
UVS-140	87.568	-34.5	5	87.958	-11.1	216.313	-18.196
UVS-141	97.297	-34.5	6	96.126	-11.2	220.000	-11.017
UVS-142	107.027	-34.5	7	104.277	-11.9	224.189	-4.159
UVS-143	116.757	-34.5	7	112.393	-13.1	228.947	2.294
UVS-144	126.486	-34.5	8	120.460	-14.8	234.347	8.240
UVS-145	136.216	-34.5	9	128.479	-17.0	240.459	13.556
UVS-146	145.946	-34.5	9	136.464	-19.6	247.327	18.097
UVS-147	155.676	-34.5	10	144.441	-22.6	254.941	21.704
UVS-148	165.405	-34.5	11	152.458	-25.9	263.208	24.221
UVS-149	175.135	-34.5	11	160.579	-29.5	271.928	25.519
+ UVS-150	184.865	-34.5	12	168.888	-33.2	280.812	25.522

• = 1450 Å – 1800 Å + = 1280 Å – 1380 Å + = Both

UVISI – MSX: Sky Survey Targets

Number	Ecliptic Longitude	Latitude	RA (hr)	RA (°)	Dec	Galactic Longitude	Latitude
UVS-151	194.595	-34.5	12	177.495	-37.0	289.534	24.230
• UVS-152	204.324	-34.5	13	186.535	-40.9	297.803	21.719
• UVS-153	214.054	-34.5	14	196.169	-44.7	305.421	18.116
• UVS-154	223.784	-34.5	14	206.585	-48.3	312.293	13.579
• UVS-155	233.514	-34.5	15	217.971	-51.6	318.408	8.267
• UVS-156	243.243	-34.5	16	230.476	-54.3	323.812	2.323
• UVS-157	252.973	-34.5	16	244.124	-56.4	328.573	-4.127
• UVS-158	262.703	-34.5	17	258.714	-57.7	332.764	-10.983
• UVS-159	272.432	-34.5	18	273.776	-57.9	336.453	-18.161
• UVS-160	282.162	-34.5	18	288.675	-57.2	339.689	-25.594
• UVS-161	291.892	-34.5	19	302.837	-55.5	342.499	-33.227
• UVS-162	301.622	-34.5	20	315.922	-53.0	344.876	-41.017
• UVS-163	311.351	-34.5	20	327.855	-50.0	346.754	-48.922
• UVS-164	321.081	-34.5	21	338.733	-46.5	347.951	-56.905
UVS-165	330.811	-34.5	22	348.734	-42.8	347.995	-64.920
UVS-166	340.541	-34.5	22	358.049	-39.0	345.463	-72.886
UVS-167	350.270	-34.5	23	6.853	-35.1	334.291	-80.514
UVS-168	0.000	-46.0	0	22.396	-41.3	276.449	-73.816
UVS-169	11.613	-46.0	0	31.351	-37.2	250.362	-71.457
UVS-170	23.226	-46.0	1	40.101	-33.4	234.643	-65.731
UVS-171	34.839	-46.0	2	48.758	-30.1	227.043	-58.483
UVS-172	46.452	-46.0	3	57.393	-27.4	223.881	-50.632
UVS-173	58.065	-46.0	3	66.046	-25.2	223.216	-42.585
UVS-174	69.677	-46.0	4	74.733	-23.6	224.126	-34.557
UVS-175	81.290	-46.0	5	83.450	-22.7	226.173	-26.691
UVS-176	92.903	-46.0	6	92.184	-22.6	229.148	-19.110
UVS-177	104.516	-46.0	6	100.912	-23.1	232.965	-11.937
UVS-178	116.129	-46.0	7	109.615	-24.3	237.601	-5.305
UVS-179	127.742	-46.0	8	118.284	-26.2	243.057	0.633
UVS-180	139.355	-46.0	9	126.925	-28.7	249.330	5.709
UVS-181	150.968	-46.0	10	135.564	-31.7	256.374	9.740
UVS-182	162.581	-46.0	10	144.256	-35.3	264.074	12.552
UVS-183	174.194	-46.0	11	153.092	-39.2	272.221	14.000
UVS-184	185.806	-46.0	12	162.207	-43.5	280.528	14.003
UVS-185	197.419	-46.0	13	171.803	-48.0	288.677	12.560
UVS-186	209.032	-46.0	13	182.170	-52.6	296.379	9.754
• UVS-187	220.645	-46.0	14	193.737	-57.1	303.427	5.727
• UVS-188	232.258	-46.0	15	207.111	-61.5	309.702	0.656
• UVS-189	243.871	-46.0	16	223.062	-65.2	315.162	-5.280
• UVS-190	255.484	-46.0	17	242.231	-68.1	319.801	-11.909
• UVS-191	267.097	-46.0	17	264.263	-69.4	323.621	-19.081
• UVS-192	278.710	-46.0	18	287.018	-68.9	326.600	-26.660
• UVS-193	290.323	-46.0	19	307.771	-66.8	328.651	-34.525
• UVS-194	301.935	-46.0	20	325.286	-63.4	329.566	-42.553
• UVS-195	313.548	-46.0	20	339.848	-59.3	328.908	-50.600
• UVS-196	325.161	-46.0	21	352.230	-54.9	325.760	-58.453
UVS-197	336.774	-46.0	22	3.133	-50.3	318.183	-65.704
UVS-198	348.387	-46.0	23	13.071	-45.7	302.506	-71.439
UVS-199	0.000	-57.5	0	31.991	-50.7	276.418	-62.316
UVS-200	14.400	-57.5	0	41.363	-46.1	260.639	-60.566

• = 1450 Å – 1800 Å + = 1280 Å – 1380 Å + = Both

UVISI – MSX: Sky Survey Targets

Number	Ecliptic Longitude	Ecliptic Latitude	RA (hr)	RA (°)	Dec	Galactic Longitude	Galactic Latitude
UVS-201	28.800	-57.5	1	50.594	-42.1	248.925	-55.889
UVS-202	43.200	-57.5	2	59.803	-38.9	241.991	-49.403
UVS-203	57.600	-57.5	3	69.046	-36.4	238.771	-42.013
UVS-204	72.000	-57.5	4	78.338	-34.8	238.183	-34.304
UVS-205	86.400	-57.5	5	87.666	-34.1	239.518	-26.667
UVS-206	100.800	-57.5	6	97.001	-34.3	242.363	-19.401
UVS-207	115.200	-57.5	7	106.314	-35.5	246.485	-12.770
UVS-208	129.600	-57.5	8	115.581	-37.5	251.729	-7.028
UVS-209	144.000	-57.5	9	124.803	-40.4	257.953	-2.425
UVS-210	158.400	-57.5	10	134.013	-44.0	264.970	0.803
UVS-211	172.800	-57.5	11	143.295	-48.3	272.514	2.472
UVS-212	187.200	-57.5	12	152.809	-53.2	280.244	2.474
UVS-213	201.600	-57.5	13	162.849	-58.5	287.789	0.811
UVS-214	216.000	-57.5	14	173.973	-64.1	294.808	-2.413
• UVS-215	230.400	-57.5	15	187.350	-69.8	301.035	-7.011
• UVS-216	244.800	-57.5	16	205.758	-75.3	306.283	-12.750
• UVS-217	259.200	-57.5	17	235.875	-79.7	310.408	-19.379
• UVS-218	273.600	-57.5	18	282.179	-80.8	313.258	-26.643
• UVS-219	288.000	-57.5	19	321.268	-77.7	314.598	-34.279
• UVS-220	302.400	-57.5	20	344.367	-72.6	314.017	-41.988
• UVS-221	316.800	-57.5	21	359.736	-66.9	310.808	-49.380
UVS-222	331.200	-57.5	22	11.776	-61.3	303.887	-55.870
UVS-223	345.600	-57.5	23	22.262	-55.8	292.190	-60.556
• UVS-224	0.000	-69.0	0	46.032	-58.9	276.405	-50.816
UVS-225	20.000	-69.0	1	55.169	-53.9	265.603	-49.149
UVS-226	40.000	-69.0	2	64.779	-49.9	257.517	-44.625
UVS-227	60.000	-69.0	4	74.728	-47.1	253.102	-38.299
UVS-228	80.000	-69.0	5	84.886	-45.7	252.020	-31.219
UVS-229	100.000	-69.0	6	95.114	-45.7	253.621	-24.225
UVS-230	120.000	-69.0	8	105.272	-47.1	257.342	-17.989
UVS-231	140.000	-69.0	9	115.221	-49.9	262.706	-13.067
UVS-232	160.000	-69.0	10	124.831	-53.9	269.236	-9.908
• UVS-233	180.000	-69.0	12	133.968	-58.9	276.383	-8.816
• UVS-234	200.000	-69.0	13	142.428	-64.9	283.531	-9.903
• UVS-235	220.000	-69.0	14	149.736	-71.5	290.063	-13.057
• UVS-236	240.000	-69.0	16	154.155	-78.5	295.430	-17.976
• UVS-237	260.000	-69.0	17	142.505	-85.5	299.155	-24.210
• UVS-238	280.000	-69.0	18	37.495	-85.5	300.762	-31.202
• UVS-239	300.000	-69.0	20	25.845	-78.5	299.687	-38.283
• UVS-240	320.000	-69.0	21	30.264	-71.5	295.281	-44.612
• UVS-241	340.000	-69.0	22	37.572	-64.9	287.202	-49.142
• UVS-242	0.000	-80.5	0	67.193	-64.8	276.396	-39.316
UVS-243	36.000	-80.5	2	74.500	-60.0	269.388	-37.321
UVS-244	72.000	-80.5	4	84.569	-57.4	265.688	-32.324
UVS-245	108.000	-80.5	7	95.431	-57.4	266.288	-26.500
• UVS-246	144.000	-80.5	9	105.500	-60.0	270.382	-21.999
• UVS-247	180.000	-80.5	12	112.807	-64.8	276.387	-20.316
• UVS-248	216.000	-80.5	14	113.748	-70.6	282.394	-21.994
• UVS-249	252.000	-80.5	16	101.599	-75.3	286.491	-26.493
• UVS-250	288.000	-80.5	19	78.401	-75.3	287.097	-32.317

• = 1450 Å – 1800 Å + = 1280 Å – 1380 Å + = Both

UVISI – MSX: Sky Survey Targets

	Number	Ecliptic Longitude	Latitude	RA (hr)	RA (°)	Dec	Galactic Longitude	Latitude
	UVS-251	324.000	-80.5	21	66.252	-70.6	283.402	-37.317
•	UVS-252	0.000	-90.0	0	90.000	-66.5	276.391	-29.816
	UVS-253	4.500	11.5	0	359.484	12.3	103.015	-48.459
	UVS-254	12.682	11.5	0	7.038	15.6	114.716	-46.921
	UVS-255	20.864	11.5	1	14.736	18.8	125.414	-44.063
	UVS-256	29.045	11.5	1	22.630	21.9	134.828	-40.115
	UVS-257	37.227	11.5	2	30.768	24.8	142.954	-35.313
	UVS-258	45.409	11.5	3	39.190	27.4	149.944	-29.867
	UVS-259	53.591	11.5	3	47.921	29.8	156.003	-23.940
	UVS-260	61.773	11.5	4	56.965	31.8	161.332	-17.656
	UVS-261	69.955	11.5	4	66.301	33.3	166.108	-11.105
	UVS-262	78.136	11.5	5	75.873	34.4	170.481	-4.358
	UVS-263	86.318	11.5	5	85.600	34.9	174.582	2.533
	UVS-264	94.500	11.5	6	95.377	34.9	178.527	9.526
	UVS-265	102.682	11.5	6	105.092	34.3	182.430	16.585
	UVS-266	110.864	11.5	7	114.645	33.2	186.414	23.679
	UVS-267	119.045	11.5	7	123.953	31.6	190.623	30.771
	UVS-268	127.227	11.5	8	132.967	29.6	195.249	37.822
	UVS-269	135.409	11.5	9	141.666	27.2	200.569	44.777
	UVS-270	143.591	11.5	9	150.058	24.5	207.017	51.552
	UVS-271	151.773	11.5	10	158.170	21.6	215.308	58.002
	UVS-272	159.955	11.5	10	166.042	18.5	226.643	63.859
+	UVS-273	168.136	11.5	11	173.723	15.3	242.792	68.608
+	UVS-274	176.318	11.5	11	181.266	12.0	264.963	71.362
+	UVS-275	184.500	11.5	12	188.722	8.8	290.133	71.217
+	UVS-276	192.682	11.5	12	196.142	5.6	311.769	68.229
•	UVS-277	200.864	11.5	13	203.572	2.5	327.384	63.343
•	UVS-278	209.045	11.5	13	211.052	-0.4	338.363	57.413
•	UVS-279	217.227	11.5	14	218.615	-3.0	346.439	50.924
•	UVS-280	225.409	11.5	15	226.286	-5.4	352.755	44.127
•	UVS-281	233.591	11.5	15	234.078	-7.5	357.994	37.160
•	UVS-282	241.773	11.5	16	241.993	-9.2	2.571	30.103
•	UVS-283	249.955	11.5	16	250.021	-10.6	6.751	23.009
•	UVS-284	258.136	11.5	17	258.138	-11.5	10.722	15.918
•	UVS-285	266.318	11.5	17	266.313	-11.9	14.624	8.863
•	UVS-286	274.500	11.5	18	274.506	-11.9	18.579	1.878
•	UVS-287	282.682	11.5	18	282.677	-11.4	22.701	-5.002
•	UVS-288	290.864	11.5	19	290.787	-10.5	27.106	-11.733
•	UVS-289	299.045	11.5	19	298.804	-9.1	31.927	-18.261
•	UVS-290	307.227	11.5	20	306.707	-7.3	37.317	-24.516
•	UVS-291	315.409	11.5	21	314.486	-5.2	43.455	-30.404
•	UVS-292	323.591	11.5	21	322.146	-2.8	50.544	-35.797
•	UVS-293	331.773	11.5	22	329.700	-0.1	58.786	-40.527
•	UVS-294	339.955	11.5	22	337.173	2.8	68.324	-44.383
	UVS-295	348.136	11.5	23	344.600	5.9	79.134	-47.125
	UVS-296	356.318	11.5	23	352.021	9.1	90.904	-48.530
	UVS-297	0.000	23.0	0	350.412	21.0	96.365	-37.184
	UVS-298	8.780	23.0	0	358.326	24.5	106.434	-36.517
	UVS-299	17.561	23.0	1	6.456	28.0	116.074	-34.559
	UVS-300	26.341	23.0	1	14.882	31.4	124.968	-31.439

• = 1450 Å – 1800 Å + = 1280 Å – 1380 Å + = Both

UVISI – MSX: Sky Survey Targets

Number	Ecliptic Longitude	Latitude	RA (hr)	RA (°)	Dec	Galactic Longitude	Latitude
UVS-301	35.122	23.0	2	23.690	34.7	132.961	-27.332
UVS-302	43.902	23.0	2	32.962	37.8	140.038	-22.420
UVS-303	52.683	23.0	3	42.765	40.5	146.275	-16.866
UVS-304	61.463	23.0	4	53.133	42.9	151.788	-10.809
UVS-305	70.244	23.0	4	64.047	44.7	156.700	-4.358
UVS-306	79.024	23.0	5	75.415	45.9	161.133	2.402
UVS-307	87.805	23.0	5	87.068	46.4	165.194	9.402
UVS-308	96.585	23.0	6	98.781	46.2	168.984	16.592
UVS-309	105.366	23.0	7	110.317	45.4	172.600	23.928
UVS-310	114.146	23.0	7	121.474	43.8	176.139	31.378
UVS-311	122.927	23.0	8	132.122	41.8	179.722	38.912
UVS-312	131.707	23.0	8	142.206	39.2	183.507	46.502
UVS-313	140.488	23.0	9	151.736	36.3	187.758	54.118
UVS-314	149.268	23.0	9	160.767	33.1	192.974	61.716
UVS-315	158.049	23.0	10	169.373	29.7	200.322	69.214
+ UVS-316	166.829	23.0	11	177.641	26.2	213.294	76.373
+ UVS-317	175.610	23.0	11	185.653	22.7	245.270	82.123
+ UVS-318	184.390	23.0	12	193.488	19.3	307.239	82.143
+ UVS-319	193.171	23.0	12	201.214	16.0	339.390	76.409
• UVS-320	201.951	23.0	13	208.893	12.8	352.412	69.253
• UVS-321	210.732	23.0	14	216.572	9.9	359.777	61.756
• UVS-322	219.512	23.0	14	224.290	7.2	5.000	54.158
• UVS-323	228.293	23.0	15	232.073	4.9	9.254	46.543
• UVS-324	237.073	23.0	15	239.933	2.9	13.042	38.952
• UVS-325	245.854	23.0	16	247.873	1.4	16.625	31.418
• UVS-326	254.634	23.0	16	255.882	0.3	20.164	23.968
• UVS-327	263.415	23.0	17	263.940	-0.3	23.779	16.630
• UVS-328	272.195	23.0	18	272.021	-0.4	27.568	9.440
• UVS-329	280.976	23.0	18	280.094	-0.1	31.628	2.438
• UVS-330	289.756	23.0	19	288.130	0.8	36.058	-4.323
• UVS-331	298.537	23.0	19	296.106	2.1	40.968	-10.776
• UVS-332	307.317	23.0	20	304.007	3.8	46.476	-16.836
• UVS-333	316.098	23.0	21	311.828	6.0	52.710	-22.392
UVS-334	324.878	23.0	21	319.575	8.5	59.782	-27.308
UVS-335	333.659	23.0	22	327.270	11.3	67.770	-31.420
UVS-336	342.439	23.0	22	334.944	14.4	76.659	-34.545
UVS-337	351.220	23.0	23	342.639	17.6	86.296	-36.510
UVS-338	0.000	34.5	0	344.704	31.3	96.370	-25.684
UVS-339	9.730	34.5	0	353.147	35.1	105.213	-25.035
UVS-340	19.459	34.5	1	1.951	39.0	113.740	-23.120
UVS-341	29.189	34.5	1	11.266	42.8	121.702	-20.044
UVS-342	38.919	34.5	2	21.267	46.5	128.953	-15.955
UVS-343	48.649	34.5	3	32.145	50.0	135.443	-11.011
UVS-344	58.378	34.5	3	44.078	53.0	141.195	-5.366
UVS-345	68.108	34.5	4	57.163	55.5	146.268	0.845
UVS-346	77.838	34.5	5	71.325	57.2	150.735	7.510
UVS-347	87.568	34.5	5	86.224	57.9	154.668	14.536
UVS-348	97.297	34.5	6	101.286	57.7	158.126	21.849
UVS-349	107.027	34.5	7	115.876	56.4	161.147	29.388
UVS-350	116.757	34.5	7	129.524	54.3	163.744	37.105

• = 1450 Å – 1800 Å + = 1280 Å – 1380 Å + = Both

UVISI – MSX: Sky Survey Targets

Number	Ecliptic Longitude	Latitude	RA (hr)	RA (°)	Dec	Galactic Longitude	Latitude
UVS-351	126.486	34.5	8	142.029	51.6	165.885	44.957
UVS-352	136.216	34.5	9	153.415	48.3	167.457	52.906
UVS-353	145.946	34.5	9	163.831	44.7	168.169	60.912
UVS-354	155.676	34.5	10	173.465	40.9	167.224	68.918
+ UVS-355	165.405	34.5	11	182.505	37.0	161.860	76.784
•+UVS-356	175.135	34.5	11	191.112	33.2	136.575	83.752
•+UVS-357	184.865	34.5	12	199.421	29.5	56.467	83.778
• UVS-358	194.595	34.5	12	207.542	25.9	30.971	76.821
• UVS-359	204.324	34.5	13	215.559	22.6	25.570	68.956
• UVS-360	214.054	34.5	14	223.536	19.6	24.613	60.951
• UVS-361	223.784	34.5	14	231.521	17.0	25.320	52.944
• UVS-362	233.514	34.5	15	239.540	14.8	26.889	44.995
• UVS-363	243.243	34.5	16	247.607	13.1	29.027	37.142
• UVS-364	252.973	34.5	16	255.723	11.9	31.622	29.425
• UVS-365	262.703	34.5	17	263.874	11.2	34.642	21.885
• UVS-366	272.432	34.5	18	272.042	11.1	38.097	14.571
• UVS-367	282.162	34.5	18	280.205	11.5	42.028	7.543
• UVS-368	291.892	34.5	19	288.340	12.4	46.492	0.876
• UVS-369	301.622	34.5	20	296.433	13.9	51.562	-5.337
UVS-370	311.351	34.5	20	304.475	15.9	57.310	-10.985
UVS-371	321.081	34.5	21	312.474	18.3	63.797	-15.933
UVS-372	330.811	34.5	22	320.451	21.1	71.044	-20.027
UVS-373	340.541	34.5	22	328.441	24.2	79.003	-23.108
UVS-374	350.270	34.5	23	336.501	27.7	87.528	-25.029
UVS-375	0.000	46.0	0	337.604	41.3	96.375	-14.184
UVS-376	11.613	46.0	0	346.929	45.7	104.642	-13.459
UVS-377	23.226	46.0	1	356.867	50.3	112.599	-11.320
UVS-378	34.839	46.0	2	7.770	54.9	119.994	-7.883
UVS-379	46.452	46.0	3	20.153	59.3	126.665	-3.311
UVS-380	58.065	46.0	3	34.714	63.4	132.535	2.215
UVS-381	69.677	46.0	4	52.229	66.8	137.583	8.518
UVS-382	81.290	46.0	5	72.982	68.9	141.814	15.436
UVS-383	92.903	46.0	6	95.737	69.4	145.219	22.827
UVS-384	104.516	46.0	6	117.769	68.1	147.751	30.564
UVS-385	116.129	46.0	7	136.938	65.2	149.270	38.527
UVS-386	127.742	46.0	8	152.889	61.5	149.476	46.585
UVS-387	139.355	46.0	9	166.263	57.1	147.733	54.569
• UVS-388	150.968	46.0	10	177.830	52.6	142.710	62.193
• UVS-389	162.581	46.0	10	188.197	48.0	131.644	68.853
+ UVS-390	174.194	46.0	11	197.793	43.5	110.511	73.187
• UVS-391	185.806	46.0	12	206.908	39.2	82.379	73.197
• UVS-392	197.419	46.0	13	215.744	35.3	61.201	68.876
• UVS-393	209.032	46.0	13	224.436	31.7	50.103	62.222
• UVS-394	220.645	46.0	14	233.075	28.7	45.062	54.601
• UVS-395	232.258	46.0	15	241.716	26.2	43.310	46.617
• UVS-396	243.871	46.0	16	250.385	24.3	43.509	38.559
• UVS-397	255.484	46.0	17	259.088	23.1	45.024	30.596
• UVS-398	267.097	46.0	17	267.816	22.6	47.552	22.858
• UVS-399	278.710	46.0	18	276.550	22.7	50.954	15.465
• UVS-400	290.323	46.0	19	285.267	23.6	55.181	8.544

• = 1450 Å – 1800 Å + = 1280 Å – 1380 Å + = Both

UVISI – MSX: Sky Survey Targets

	Number	Ecliptic Longitude	Latitude	RA (hr)	RA (°)	Dec	Galactic Longitude	Latitude
•	UVS-401	301.935	46.0	20	293.954	25.2	60.226	2.239
•	UVS-402	313.548	46.0	20	302.607	27.4	66.093	-3.290
	UVS-403	325.161	46.0	21	311.242	30.1	72.761	-7.867
	UVS-404	336.774	46.0	22	319.899	33.4	80.153	-11.309
	UVS-405	348.387	46.0	23	328.649	37.2	88.108	-13.453
	UVS-406	0.000	57.5	0	328.009	50.7	96.379	-2.684
	UVS-407	14.400	57.5	0	337.738	55.8	104.062	-1.847
	UVS-408	28.800	57.5	1	348.224	61.3	111.383	0.616
	UVS-409	43.200	57.5	2	0.264	66.9	118.034	4.554
	UVS-410	57.600	57.5	3	15.633	72.6	123.791	9.753
	UVS-411	72.000	57.5	4	38.732	77.7	128.494	15.969
	UVS-412	86.400	57.5	5	77.821	80.8	132.005	22.948
	UVS-413	100.800	57.5	6	124.125	79.7	134.137	30.432
	UVS-414	115.200	57.5	7	154.242	75.3	134.584	38.146
	UVS-415	129.600	57.5	8	172.650	69.8	132.800	45.754
•	UVS-416	144.000	57.5	9	186.027	64.1	127.890	52.786
•	UVS-417	158.400	57.5	10	197.151	58.5	118.665	58.509
+	UVS-418	172.800	57.5	11	207.191	53.2	104.628	61.863
•	UVS-419	187.200	57.5	12	216.705	48.3	88.206	61.869
•	UVS-420	201.600	57.5	13	225.987	44.0	74.155	58.524
•	UVS-421	216.000	57.5	14	235.197	40.4	64.915	52.807
•	UVS-422	230.400	57.5	15	244.419	37.5	59.993	45.778
•	UVS-423	244.800	57.5	16	253.686	35.5	58.201	38.171
•	UVS-424	259.200	57.5	17	262.999	34.3	58.641	30.457
•	UVS-425	273.600	57.5	18	272.334	34.1	60.769	22.971
•	UVS-426	288.000	57.5	19	281.662	34.8	64.275	15.990
•	UVS-427	302.400	57.5	20	290.954	36.4	68.975	9.772
	UVS-428	316.800	57.5	21	300.197	38.9	74.729	4.569
	UVS-429	331.200	57.5	22	309.406	42.1	81.378	0.626
	UVS-430	345.600	57.5	23	318.637	46.1	88.696	-1.841
	UVS-431	0.000	69.0	0	313.968	58.9	96.383	8.816
	UVS-432	20.000	69.0	1	322.428	64.9	103.531	9.903
	UVS-433	40.000	69.0	2	329.736	71.5	110.063	13.057
	UVS-434	60.000	69.0	4	334.155	78.5	115.430	17.976
•	UVS-435	80.000	69.0	5	322.505	85.5	119.155	24.210
	UVS-436	100.000	69.0	6	217.495	85.5	120.762	31.202
	UVS-437	120.000	69.0	8	205.845	78.5	119.687	38.283
+	UVS-438	140.000	69.0	9	210.264	71.5	115.281	44.612
+	UVS-439	160.000	69.0	10	217.572	64.9	107.202	49.142
•	UVS-440	180.000	69.0	12	226.032	58.9	96.405	50.816
•	UVS-441	200.000	69.0	13	235.169	53.9	85.603	49.149
•	UVS-442	220.000	69.0	14	244.779	49.9	77.517	44.625
•	UVS-443	240.000	69.0	16	254.728	47.1	73.102	38.299
	UVS-444	260.000	69.0	17	264.886	45.7	72.020	31.219
	UVS-445	280.000	69.0	18	275.114	45.7	73.621	24.225
	UVS-446	300.000	69.0	20	285.272	47.1	77.342	17.989
	UVS-447	320.000	69.0	21	295.221	49.9	82.706	13.067
•	UVS-448	340.000	69.0	22	304.831	53.9	89.236	9.908
	UVS-449	0.000	80.5	0	292.807	64.8	96.387	20.316
	UVS-450	36.000	80.5	2	293.748	70.6	102.394	21.994

• = 1450 Å – 1800 Å + = 1280 Å – 1380 Å + = Both

UVISI – MSX: Sky Survey Targets

	Number	Ecliptic Longitude	Latitude	RA (hr)	RA (°)	Dec	Galactic Longitude	Latitude
	UVS-451	72.000	80.5	4	281.599	75.3	106.491	26.493
	UVS-452	108.000	80.5	7	258.401	75.3	107.097	32.317
+	UVS-453	144.000	80.5	9	246.252	70.6	103.402	37.317
•	UVS-454	180.000	80.5	12	247.193	64.8	96.396	39.316
•	UVS-455	216.000	80.5	14	254.500	60.0	89.388	37.321
	UVS-456	252.000	80.5	16	264.569	57.4	85.688	32.324
	UVS-457	288.000	80.5	19	275.431	57.4	86.288	26.500
	UVS-458	324.000	80.5	21	285.500	60.0	90.382	21.999
	UVS-459	0.000	90.0	0	-90.000	66.5	96.391	29.816

• = 1450 Å – 1800 Å + = 1280 Å – 1380 Å + = Both

THE ASTROPHYSICAL JOURNAL, 448:848–857, 1995 August 1

A MODEL OF THE DIFFUSE ULTRAVIOLET RADIATION FIELD

JAYANT MURTHY AND R. C. HENRY
Department of Physics and Astronomy, Johns Hopkins University, Baltimore, MD 21218
Received 1994 September 1; accepted 1995 February 6

ABSTRACT

We have developed a model to predict the intensity of the diffuse ultraviolet radiation field from any direction in the sky as a function of the scattering parameters of interstellar dust—the albedo and the phase function—and the intensity of a possible extragalactic component. We have applied this model to a restricted set of archival data between 1250 and 2000 Å, placing limits of 0.3–0.6 on the albedo of the dust grains and 100–400 photons cm^{-2} s^{-1} sr^{-1} $Å^{-1}$ on the intensity of an extragalactic background.

Subject headings: diffuse radiation — dust, extinction — scattering — ultraviolet: general

1. INTRODUCTION

Initial interest in the diffuse ultraviolet background was sparked by the hope of discovering emission from a hot intergalactic medium (Weymann 1967), and thus the first observations were selected specifically to be at high Galactic latitudes where both the star density and the total extinction are low. Indeed, a uniform and isotropic background of about 300 photons cm^{-2} s^{-1} sr^{-1} $Å^{-1}$ (units)[1] was detected and identified as extragalactic emission (Anderson et al. 1979, and references therein). Further observations revealed a significant Galactic component of the diffuse radiation field, due to starlight scattered by interstellar dust (Holberg 1990; see also Bowyer 1991; Henry 1991). Such scattered light is of considerable interest in its own right, providing one of the best probes into the scattering properties of the dust grains in the UV, where most of the grain heating that powers the cirrus emission so prominent in the *IRAS* sky occurs. Unfortunately, many of the data have been of dubious quality, as eloquently described in the reviews by Bowyer (1991) and Henry (1991), and some controversy developed concerning both the level and relative importance of the Galactic and extragalactic components.

Advances in techniques and instrumentation have obviated many of the difficulties which afflicted early observations of the diffuse radiation, and recent measurements have tended to yield much more consistent results. In this work, we take a critical look at observations of the diffuse radiation field between Lyα (1216 Å) and the onset of the zodiacal light at 2000 Å. Except for a few atypical locations, in which emission from highly excited species or molecular hydrogen fluorescence may have been observed (Martin, Hurwitz, & Bowyer 1990; Martin & Bowyer 1990), virtually the only contributors to the diffuse radiation in this spectral region are dust-scattered starlight and extragalactic radiation; hence observations here offer an unmatched opportunity to differentiate and model the two components. We have developed a model to predict the level of emission expected from dust scattering which we have applied to the observations in order to place strong constraints both on the scattering parameters of the interstellar dust and the brightness of the extragalactic component.

[1] At 1500 Å, one unit is equal to 1.32×10^{-11} ergs cm^{-2} s^{-1} sr^{-1} $Å^{-1}$ or 1.32×10^{-13} W m^{-2} sr^{-1} nm^{-1}. Equivalently, multiplying the surface brightness in units by a constant factor of 2×10^{-8} will yield an energy density (νI_ν) in units of ergs cm^{-2} s^{-1} sr^{-1}.

2. MODEL

We first described our model for the diffuse Galactic emission in Murthy, Henry, & Holberg (1991), but as we have made several modifications since, we will again describe the model and its predictions here. The primary component of the diffuse radiation field in most directions is starlight scattered by interstellar dust along the line of sight, with a level dependent both on the number and distribution of the scatterers—interstellar dust—and on the strength and location of the sources—stars. Until recently, a lack of computational resources has forced the use of analytical expressions for the dust-scattered radiation; the most commonly used was Jura's (1979), in which starlight from a plane-parallel Galactic disk is back-scattered by high-latitude, optically thin dust clouds. Unfortunately, the limitations Jura placed on his model have often been ignored, and it has been used in many inappropriate situations (see the discussion in Witt 1989) with concomitant effects on the derived properties of the grains. As part of our program to map the diffuse UV radiation field, we have attempted to create a more sophisticated model which can predict the amount of scattered light at any point in the sky as a function of the total H I column density and the optical constants of the dust grains—the single-scattering albedo (a) and the phase function asymmetry factor (g)—at any specified wavelength between 912 and 2000 Å. In the rest of this section, we will discuss our model and the assumptions that enter into it, followed by a comparison with other recent published models.

The interstellar radiation field (ISRF) in the UV is dominated by emission from a relatively small number of O and B stars, with some contribution from hot A stars in the near-UV, and a catalog integration will yield a reasonable estimate of the sky brightness (Henry 1977). We have used the SKYMAP star catalog (Ver. 3.3; Gottlieb 1978) as our source of stars, and from the information tabulated therein—the location, brightness, spectral type, and distance of each star—we can calculate the vector ISRF at any point in space (with the spectral emission of each star modeled by a Kurucz 1979 spectrum of the appropriate temperature). As an example of this procedure, and to test its fidelity, we have compared our prediction for the sky brightness at the Earth of direct (extincted) starlight at 1600 Å (Fig. 1*a*) with that observed by the *TD-1* satellite (Gondhalekhar 1990) at 1565 Å (Fig. 1*b*). The strongly anisotropic nature of the stellar radiation field is apparent, with Gould's Belt (the projection of the local spiral arm on the sky) containing virtually all of the brightest sources. The UV sky is

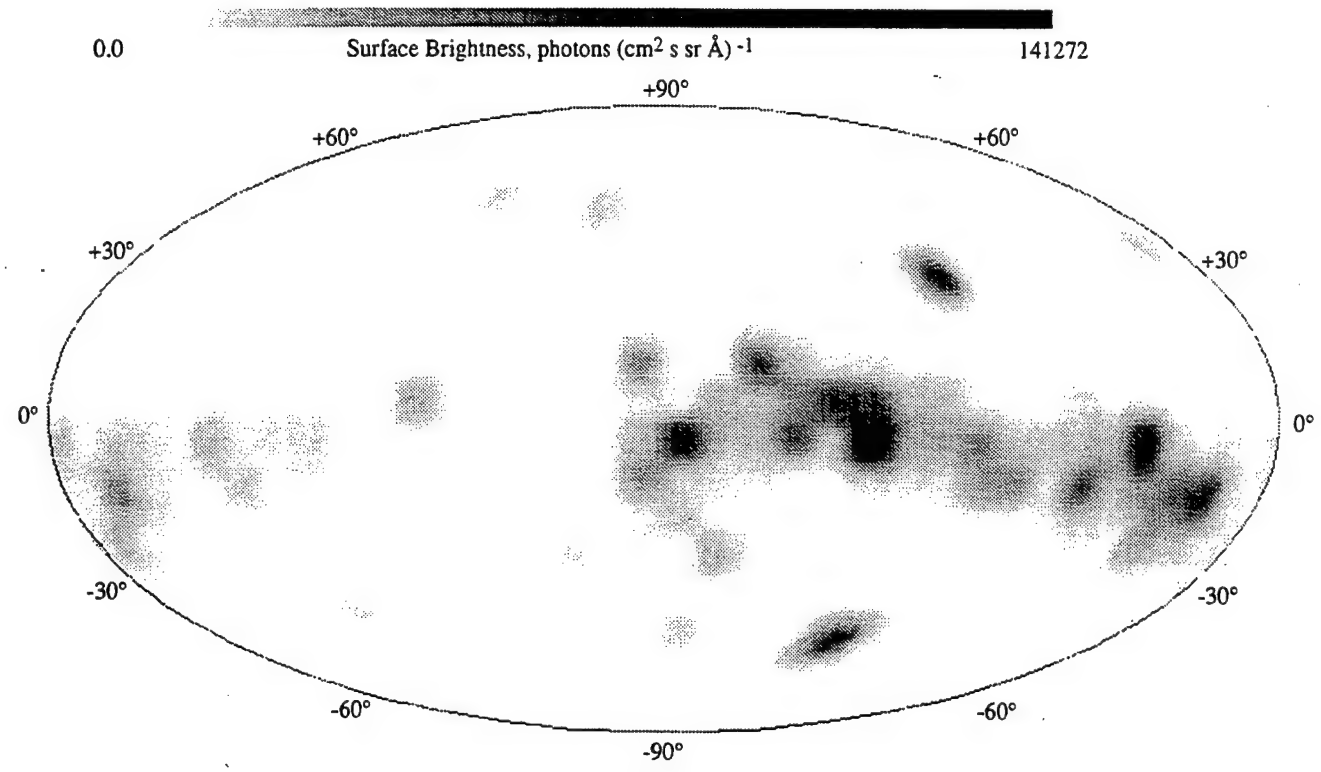

FIG. 1*a*

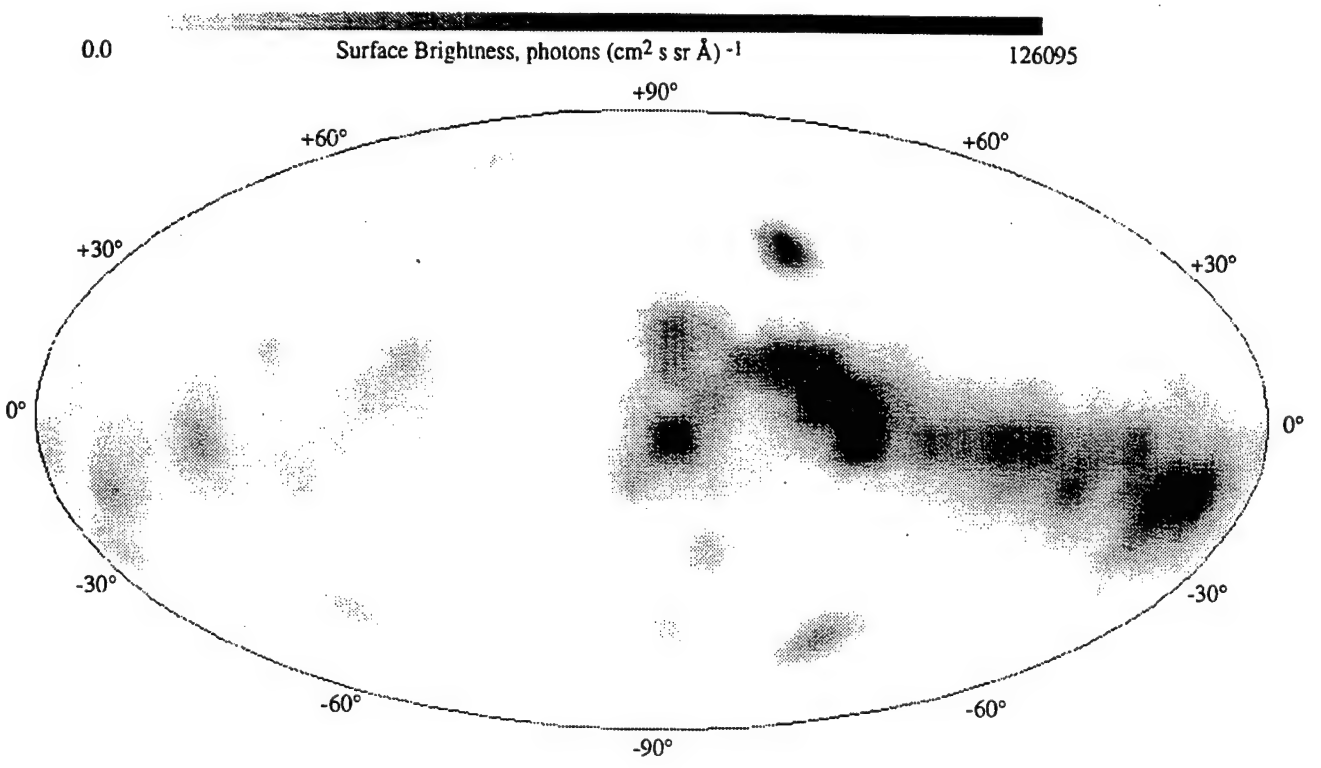

FIG. 1*b*

FIG. 1.—Aitoff projection of our predicted sky brightness at the Earth from direct stellar illumination at 1600 Å is shown in (*a*). We have integrated the stars in the SKYMAP catalog (Gottlieb 1978) attenuated by an interstellar attenuation corresponding to a gas density of 1 cm^{-3}. The radiation field at 1565 Å observed by the *TD-1* satellite (Gondhalekhar 1990) is shown in (*b*). Our model reproduces the observed sky quite well, both in distribution and intensity.

surprisingly patchy, with dark regions even in the Galactic plane, and no model which assumes a symmetrical source function can yield realistic predictions for the ISRF.

In order to calculate the radiation field at an arbitrary point in space, we have to make an assumption about the interstellar extinction from each star to that point. The integrated stellar radiation field from the *TD-1* stellar observations is plotted at two wavelengths in Figure 2 (*asterisks*) along with our predicted radiation field for two different values of the average interstellar hydrogen density: $n_H = 0.6$ cm^{-3} (*thin solid line*), corresponding to an extinction A_V of 1 mag kpc^{-1}, and $n_{H\,I} = 1.2$ cm^{-3} (*thick solid line*), the canonical interstellar gas density (Spitzer 1978). The n_H of 1.2 cm^{-3} provides the best fit to the *TD-1* observations, but we have derived the optical constants for both values of the interstellar absorption as a measure of the uncertainties in the modeling.

With the source function (the ISRF) defined, we have to determine the distribution of the scatterers—the interstellar dust. We have used the Bell Laboratories H I Survey (Stark et al. 1992) to estimate the total H I column density N(H I) along the line of sight, which we then converted into a dust optical depth (τ) using the cross sections of Draine & Lee (1984). These cross sections implicitly assume a uniform gas-to-dust ratio of $N(H)/E(B-V) = 5.8 \times 10^{21}$ cm^{-2} (Bohlin, Savage, & Drake 1978). The distribution of the gas, and therefore of the dust, is not well constrained and may vary considerably in different directions (see Dickey & Lockman 1990; McKee 1990). We used two models for the gas distribution in this work: one with an exponential scale height of 200 pc and the other with a scale height of 500 pc, representing upper and lower limits on the distribution of the dust. The exponential scale height of 200 pc is very close to the two-component model of Lockman, Hobbs, & Shull (1986), consisting of a Gaussian of scale height 135 pc and an exponential of scale height 500 pc, each containing half of the total amount of gas. It is to be hoped that a combination of UV, IR, and radio observations of interstellar gas and dust will soon lead to a three-dimensional model for the interstellar absorption, but that is beyond the scope of this work.

In order to perform the actual calculation of the scattered starlight from an arbitrary line of sight, we divided the line of sight into a number of cells, calculated the amount of scattered radiation from each of the cells using a Henyey-Greenstein scattering function (Henyey & Greenstein 1941), as is standard in the literature, and summed the contribution from each of the cells along the line of sight, reddening the emission from each cell by the total amount of dust between that cell and the observer. The resultant background can be expressed as a function of the albedo (a) and the phase function asymmetry factor ($g = \langle \cos\theta \rangle$). To this purely Galactic component we added an isotropic extragalactic component (E) which was reddened by an amount of dust given by the total H I column along the line of sight using the gas-to-dust ratio of Bohlin et al. (1978). Finally, we used a χ^2 analysis to place limits on the three parameters a, g, and E.

As data accumulated, it became apparent that Jura's (1979) model could not adequately represent the observed back-

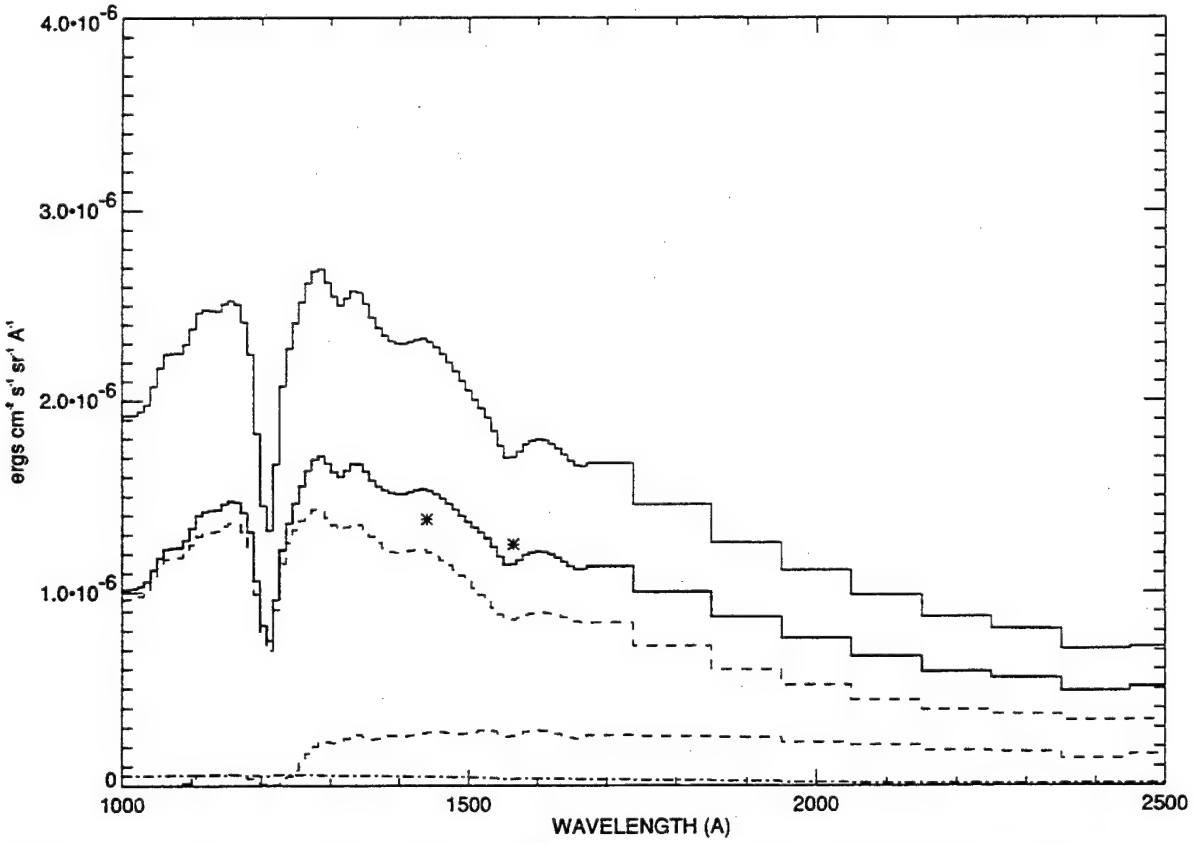

FIG. 2.—Predictions from our model for the integrated (over the entire sky) radiation field at the Earth for interstellar gas densities of 0.6 and 1.2 cm^{-3} are plotted as the thin and thick lines, respectively. The two asterisks represent the integrated *TD-1* brightness at 1440 and 1560 Å. The three dashed lines represent the contributions (assuming $n_{H\,I} = 1.2$ cm^{-3}) by O stars (*dot-dashed line*), B stars, and A stars separately, with B stars being by far the most important. The contribution from A and later stars is negligible below 1100 Å.

TABLE 1

MODELS OF THE DIFFUSE RADIATION FIELD

Reference	Applied To	Sources	Scattering Medium	Special Comments
Jura 1979	High-latitude clouds	Plane-parallel galaxy	Optically thin clouds	
Anderson, Henry, & Fastie 1982	High-latitude clouds	Plane-parallel galaxy	Optically thin clouds	
Onaka & Kodaira 1991	Near Virgo Cluster	*TD-1* catalog	Optically thin clouds	Same as Jura except for an anisotropic ISRF
Hurwitz et al. 1991	UVX observations of the diffuse galactic light (DGL)	Plane-parallel Galactic plane	Exponential distribution	Isotropic radiation field but did include self-extinction
Witt & Petersohn 1994	DE-1 observations of the DGL	*TD-1* catalog	Three-cloud spectrum	Includes multiple scattering; nonisotropic radiation field
Hurwitz 1994	Taurus molecular cloud	*TD-1* catalog	2D slab	Includes multiple scattering; main uncertainty is the local radiation field
Gordon et al. 1994	Sco OB2 association	32 nearby stars with 3D positions	Spherical nebula	Monte Carlo modeling, includes multiple scattering
This work	UVX observations	3D distribution from SKYMAP	Exponential distribution	No multiple scattering, but accurate representation of radiation field

grounds, and a number of models have arisen (Table 1), each with its own strengths and weaknesses. The primary advantage of our model is that we calculate the radiation field *at the point of scattering* and we believe that we do so more accurately than any other model to date. However, we do not include multiple scattering. While this is almost certainly not important at low column densities, it may become significant at optical depths near 1 (see Hurwitz 1994).

3. RESULTS

For the purposes of this work, we are interested only in those observations of the diffuse UV radiation field in the wavelength regime between 1250 and 2000 Å, avoiding Lyα contamination at the short-wavelength side and the beginning of the zodiacal light on the other side. While there are a surprisingly large number of such observations (see Bowyer 1991 and Henry 1991 for references), we can use only those observations in which the look direction is explicitly specified, because the amount of scattered light depends not only on the H I column density but also on the direction observed. We have listed these observations in Table 2 and plotted them as a function of H I column density in Figure 3. The errors are those in the original publication if given; otherwise they were arbitrarily taken to be the square root of the background flux.

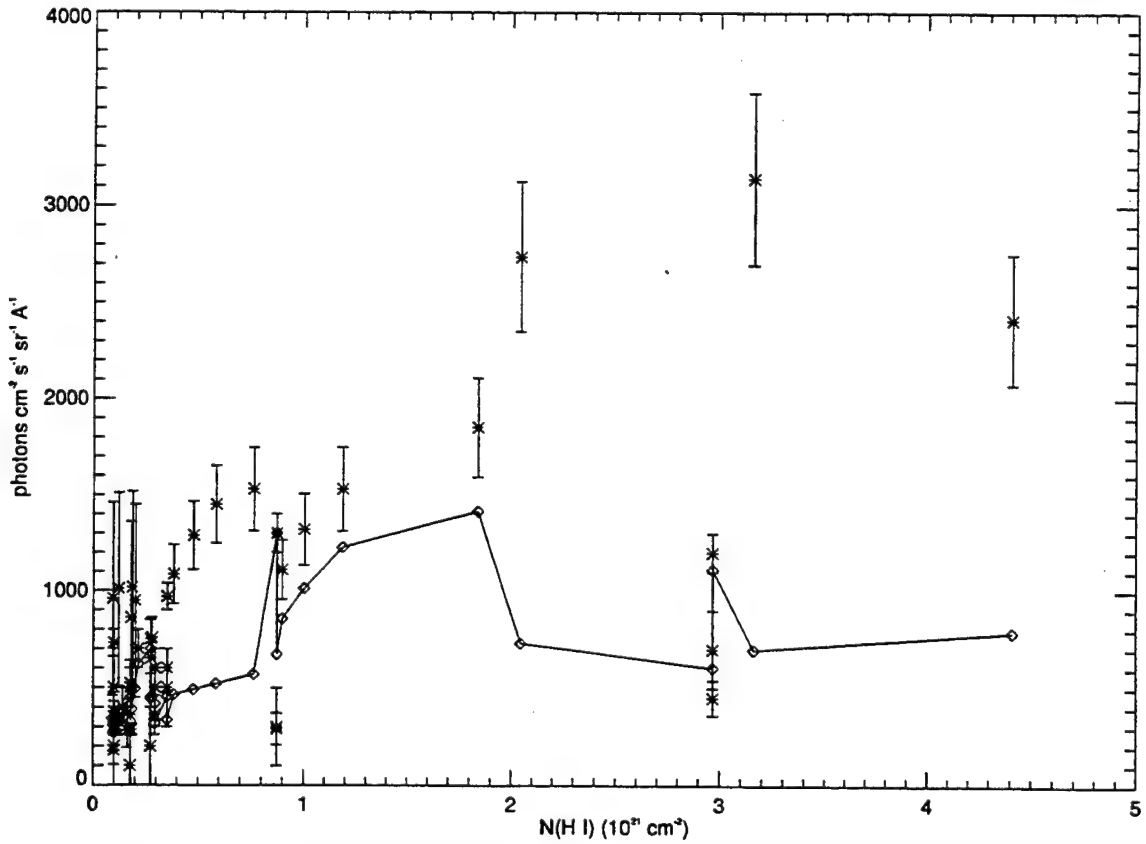

FIG. 3.—All observations of the diffuse UV radiation field which include pointing information are plotted as diamonds with error bars as quoted in the original publication. Our best-fit model to the data is shown as the asterisks connected by a solid line. Although the fit is exceptionally poor, most of the discrepancies are due to the low quality of the data and not of the model.

TABLE 2

BACKGROUND DATA

l	b	Wavelength (Å)	Background (photons cm^{-2} s^{-1} sr^{-1} $Å^{-1}$)	N(H I) (10^{19} cm^{-2})	Reference
155°	58°.....	2500	730 ± 70	9.8	1
132	40.....	2500	970 ± 70	35.3	1
0	90.....	2500	350 ± 80	10.0	1
168	−16.....	2500	290 ± 80	87.5	1
135	10.....	2500	450 ± 90	297.0	1
141	38.....	2500	360 ± 100	29.5	1
216	−39.....	2500	650 ± 80	27.5	1
335	78.....	2500	520 ± 120	17.8	1
155	58.....	1500	500 ± 200	9.8	2
132	40.....	1500	500 ± 200	35.3	2
0	90.....	1500	200 ± 200	10.0	2
168	−16.....	1500	300 ± 200	87.5	2
135	10.....	1500	700 ± 200	297.0	2
141	38.....	1500	500 ± 200	29.5	2
216	−39.....	1500	200 ± 200	27.5	2
335	78.....	1500	100 ± 200	17.8	2
155	58.....	1500	300 ± 100	9.8	3*
132	40.....	1500	600 ± 100	35.3	3*
0	90.....	1500	375 ± 100	10.0	3*
168	−16.....	1500	1300 ± 100	87.5	3*
135	10.....	1500	1200 ± 100	297.0	3*
141	38.....	1500	600 ± 100	29.5	3*
216	−39.....	1500	750 ± 100	27.5	3*
335	78.....	1500	500 ± 100	17.8	3*
335	78.....	1500	285 ± 32	17.8	4*
245	87.....	1500	285 ± 32	11.2	4*
179	65.....	1500	285 ± 32	18.6	4*
0	90.....	1400	180 ± 75	10.0	5*
0	−90.....	1400	280 ± 88	16.4	5*
242	87.....	1440	1010 ± 500	12.1	6
67	87.....	1440	960 ± 500	9.3	6
323	75.....	1440	1017 ± 500	18.6	6
333	77.....	1440	859 ± 500	18.1	6
341	80.....	1440	949 ± 500	20.1	6
115	−58.....	1600	757 ± 105	28.1	7
155	−43.....	1600	1110 ± 153	90.0	7
163	−35.....	1600	1320 ± 185	100.4	7
169	−29.....	1600	1529 ± 217	118.8	7
176	−18.....	1600	1851 ± 258	184.1	7
188	3.....	1600	2415 ± 338	441.1	7
191	6.....	1600	3139 ± 443	316.3	7
192	9.....	1600	2737 ± 386	204.6	7
196	15.....	1600	1529 ± 217	76.4	7
198	18.....	1600	1449 ± 201	58.5	7
200	21.....	1600	1288 ± 177	47.8	7
205	27.....	1600	1087 ± 153	38.5	7
130	57.....	2000	400 ± 100	13.9	8*
318	60.....	1500	700 ± 100	21.6	9

NOTE.—Targets marked by asterisks are those in which there was both spectroscopy and a firm measure of the dark noise.

REFERENCES.—(1) Murthy et al. 1990; (2) Murthy et al. 1989; (3) Hurwitz et al. 1991; (4) Anderson et al. 1979; (5) Weller 1983; (6) Paresce, McKee, & Bowyer 1980; (7) Zvereva et al. 1982; (8) Tennyson et al. 1988; (9) Onaka & Kodaira 1991.

We have used our model to predict the amount of dust-scattered emission for each of the 75 directions listed in Table 2 and have added an isotropic extragalactic background attenuated by the dust along that line of sight. Assuming that the optical constants of the grains and the level of the extragalactic background are the same everywhere in the sky, we can find the combination of a, g, and E which best fits the data for a given H I distribution. We have plotted the best-fit model for an average interstellar gas density of 1.2 cm^{-3} and a dust distribution falling off with an exponential scale height of 200 pc as asterisks in Figure 3. Note that the scattered radiation saturates at an H I column density of about 10^{20} cm^{-2}, although there can be significant deviations due to variations in the local interstellar radiation field. The fit is atrocious and, if we were to take the data at face value, would result in our being forced to consider other sources for the diffuse radiation field. However, the history of diffuse UV measurements has been filled with poorly designed or ill-starred experiments (see the comprehensive discussion in Henry 1991), and it is likely that many of the data points are wrong. Henry has pointed out that when working at such low light levels, it is important to have both a measured dark current and spectral information—to distinguish other sources such as instrument noise, zodiacal light, and airglow from the cosmic background—and so, for our second pass, we further restrict our data set to only those observations which satisfy both conditions. This cuts our

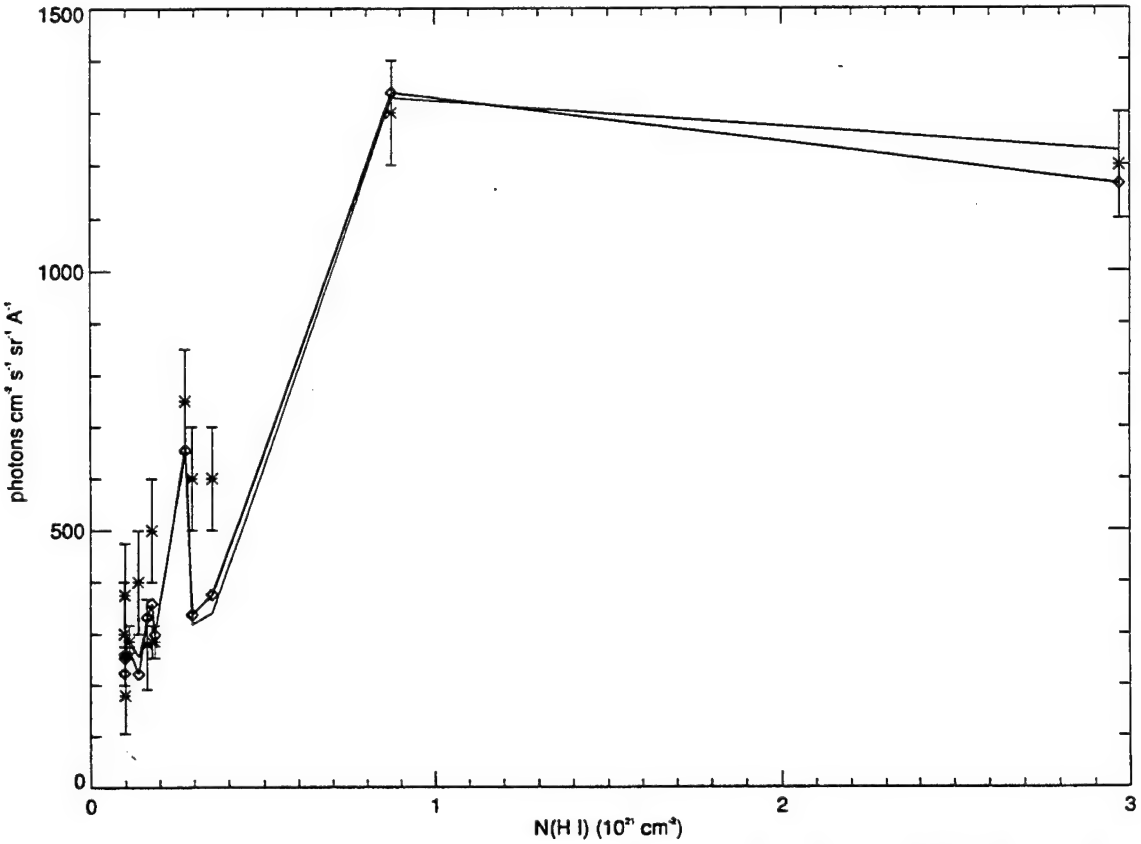

FIG. 4.—We have selected a small subset of data with well measured dark currents and with spectral information (*asterisks*). Although some of the excluded points may actually be of high quality, the present criteria ensure an unambiguous measurement and interpretation of the diffuse radiation field. Our model (diamonds connected by a thick line is for a scale height of 200, by a thin line for a scale height of 500 pc) fits this restricted data set quite well.

sample size to 14 data points, marked in Table 2 and plotted in Figure 4.

Our model (thick line in Fig. 4) yields a much better fit for this more restricted data set, although there are still some differences between the predictions and the observations, whether due to residual deficiencies in the data or in the model. We have tabulated the 90% confidence limits on the three parameters in our model in Table 3 for different assumptions on the interstellar dust distribution and average interstellar density (which affects the value of the local radiation field). The "extragalactic" background, under which umbrella we have collected all isotropic emissions, has its largest contribution at low H I columns, where the dust-scattered starlight is at a minimum, and so is relatively independent of the model assumptions with limits of about 100 to 400 photon units, in accord with most other determinations (Henry & Murthy 1993, and references therein). It is probably due largely, but not entirely, to the integrated light of other galaxies (Armand, Milliard, & Deharveng 1994). Other suggestions have been scattering from dust in the Galactic halo (Hurwitz, Bowyer, & Martin 1991) and recombination radiation from Lyα clouds in the intergalactic medium (Henry 1991).

The optical constants of the grains, especially the albedo, depend on the assumptions in our model, and we have plotted the allowed parameter space for several different cases in Figures 5 and 6. If we assume an interstellar H I density of 0.6 cm^{-3} (corresponding to an interstellar extinction of 1 mag kpc^{-1}) and a scale height of 200 pc for the dust distribution, we can place stringent limits of 0.24–0.30 on the albedo; however, at the other extreme of an interstellar H I density of 1.2 cm^{-3}

TABLE 3

LIMITS ON PARAMETERS

	SCALE HEIGHT OF 200 pc		SCALE HEIGHT OF 500 pc	
PARAMETER	$n(H) = 0.6$ cm^{-3}	$n(H) = 1.2$ cm^{-3}	$n(H) = 0.6$ cm^{-3}	$n(H) = 1.2$ cm^{-3}
a	0.17–0.22	0.32–0.42	0.24–0.37	0.46–0.62
g	<0.7	<0.4	<0.8	<0.6
E	110–340	70–240	140–370	160–320

NOTES.—The 14 targets marked by asterisks in Table 1 have been used in deriving the albedo (a), phase function (g), and extragalactic background (E in units of photons cm^{-2} s^{-1} sr^{-1} $Å^{-1}$). The limits have been calculated for two different values for the scale height of the interstellar dust and for two values of the average interstellar absorption from each star to the point of scattering.

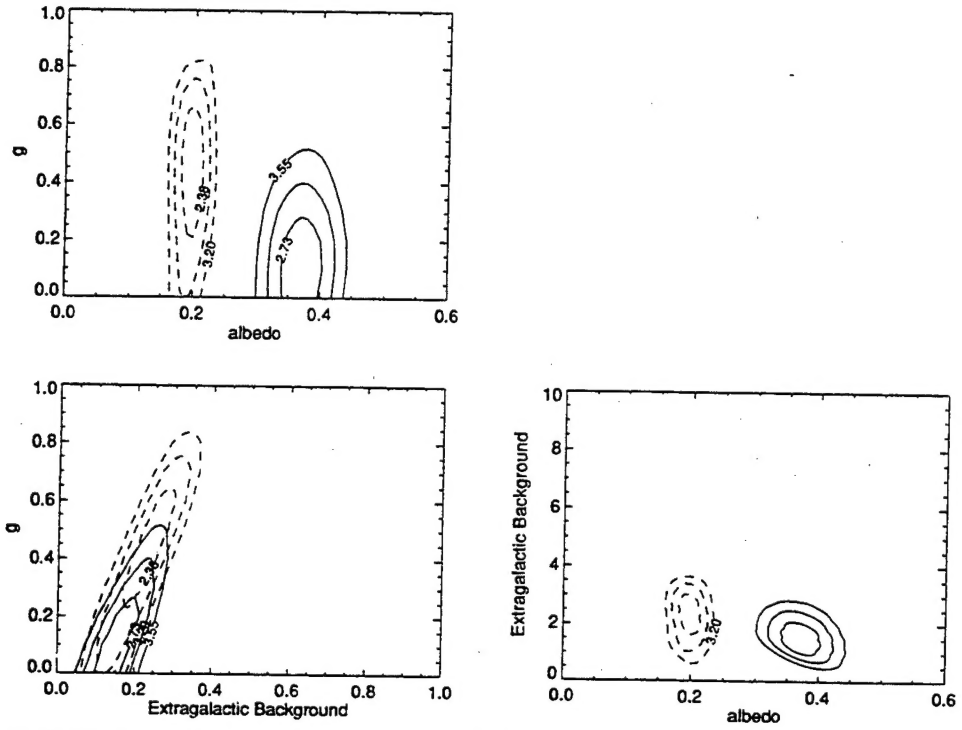

FIG. 5.—Parameter space allowed by our model for the three parameters—albedo (a), phase function (g), and extragalactic background (E)—is shown as 50%, 90%, and 99% confidence contours. We have assumed a scale height for the interstellar dust of 200 pc. The dashed contours represent the case where the average interstellar gas density is 0.6 cm^{-3}, while the solid contours represent the case where the interstellar gas density is 1.2 cm^{-3}. The local radiation field is lower if the interstellar gas density is 1.2 cm^{-3}, resulting in a higher derived albedo. The extragalactic background (E) is determined by the high-latitude points, where the amount of scattering is low and is independent of the interstellar absorption.

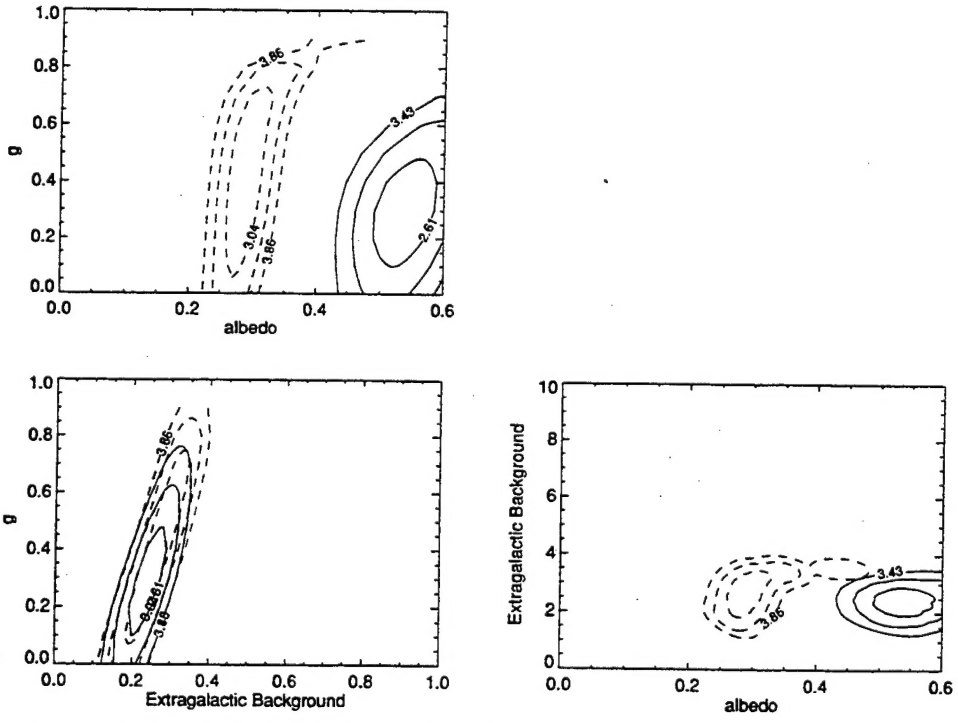

FIG. 6.—Contours identical to those in Fig. 5, but for the case where the scale height of the dust is 500 pc. While the "preferred" parameters may be a scale height of 200 pc for the gas with an average interstellar density of 1.2 cm^{-3}, leading to limits of 0.32–0.42 for the albedo, the uncertainties are such that we should consider any value between about 0.3 and 0.6 acceptable.

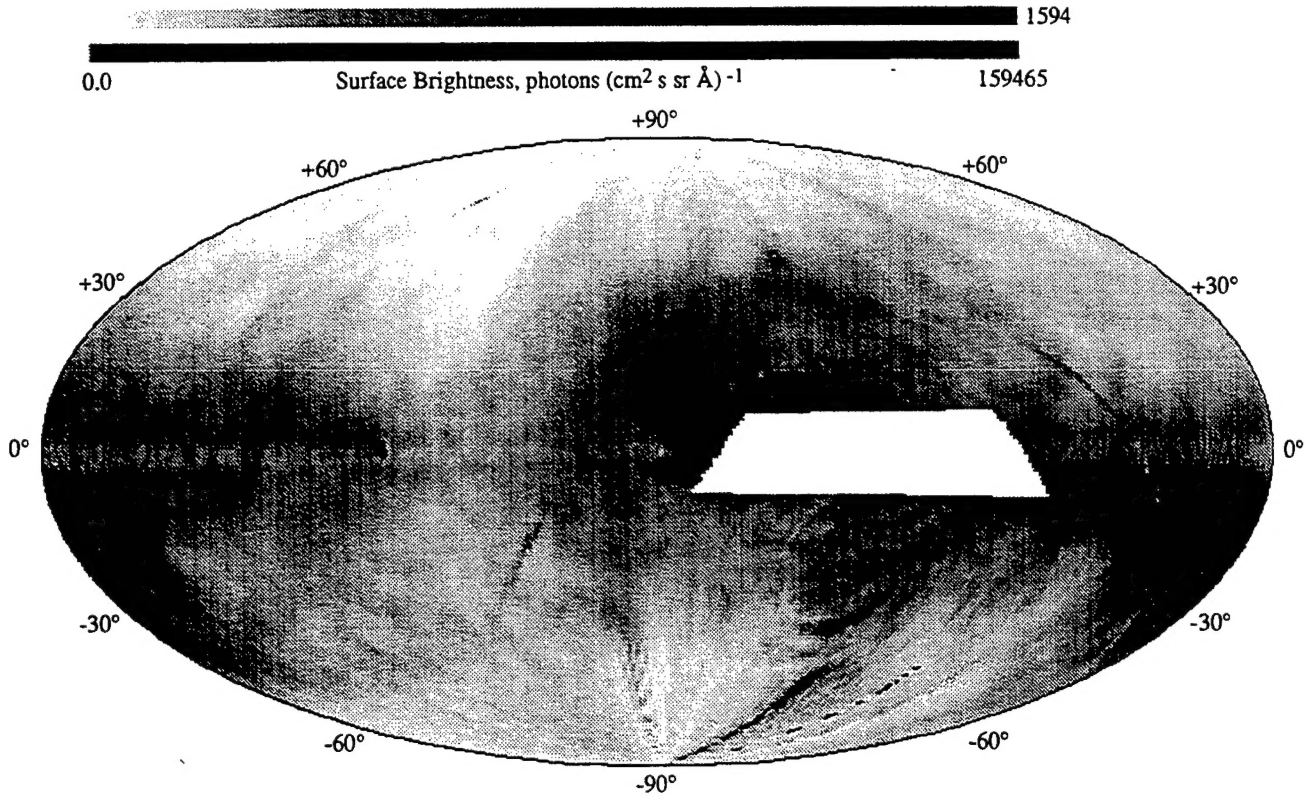

FIG. 7a

FIG. 7.—Aitoff projections of the diffuse radiation field over the entire sky (*a*) for $g = 0.1$, (*b*) for $g = 0.5$, and (*c*) for $g = 0.9$ are shown. We have assumed a scale height of 200 pc for the interstellar dust with a gas density of 1 cm^{-3} and an albedo of 0.1. As we assume only single scattering in our model, the level of emission is directly proportional to the assumed albedo. There are several locations which are obviously artifacts of our model—because of the coarse sampling used to produce these plots, it sometimes happened that the line of sight passed very near a star which would then yield an anomolously high value for the scattered flux—or the plotting procedure. The blank region near the center of the plots is due to a lack of H I 21 cm data. Note also the nonlinear scale; the radiation field is saturated at a value of about 1600 photons $cm^{-2}\ s^{-1}\ sr^{-1}\ Å^{-1}$. While there are considerable variations over the sky for all three values of g, the diffuse radiation field becomes much more patchy and concentrated toward the bright stars as the phase function becomes more highly forward scattering.

(which provides the best fit to the ISRF observed by *TD-1* at the Earth) and a scale height of 500 pc, the albedo is constrained to lie between 0.46 and 0.62. The "preferred" values for the interstellar gas seem to be an n_H of 1.2 cm^{-3} and a scale height of 200 pc (e.g., McKee 1990), in which case we obtain an albedo of 0.31–0.40 with g constrained to lie below 0.4.

A crucial assumption of our model is that the optical constants of the grains are constant over the entire sky. However, we note that there are significant variations in the extinction curve over the sky which are quite probably reflected in the optical properties of the grains. We have explored the effects of leaving out the two lowest latitude UVX targets (Targets 5 and 6 of Hurwitz et al. 1991), which include some molecular clouds in their fields of view. Leaving out Target 6 has little effect on our derived parameters; however, there is not a wide enough range in N(H I) to significantly constrain the albedo without Target 5. Both g and E are determined largely by the observations at high Galactic latitudes and hence are relatively unaffected. With the limited amount of data we have, there is no compelling evidence that the optical constants change from one location to another; hence we will not pursue this thread any further at this time.

4. DISCUSSION

There are still significant differences in both theoretical and observational determinations of the optical constants of interstellar grains, and these have been summarized in several recent papers (Bowyer 1991; Mathis 1993; Kim, Martin, & Hendry 1994) to which the reader is referred for further information (also see Hurwitz 1994 and Gordon et al. 1994 for still more recent determinations of the optical constants of the grains). We will discuss here explicitly the work of Hurwitz et al. (1991), Henry & Murthy (1993), and Hurwitz (1994). as they all deal with the UVX data and are most directly comparable to this work. Hurwitz et al. (1991), the source of the Berkeley UVX data, derived a low albedo (~ 0.2) and an isotropic scattering function ($g \sim 0$), entirely consistent with our present derivation. Hurwitz (1994) has reanalyzed one of the UVX targets (Target 5, an observation in the Taurus molecular clouds) and derived a much higher albedo of 0.6 ± 0.1 with $g = 0.5 \pm 0.15$, which are marginally inconsistent with our values. While his new model is quite sophisticated and accounts for multiple scattering and self-shielding, it should be recognized that there are uncertainties in all of the assumptions, most notably in the local radiation field (as pointed out by Hurwitz), and thus that the "true" uncertainty is probably much larger than that quoted: a comment applying to all derivations of the optical constants, including those here.

Finally, Henry & Murthy (1993) have used the high-latitude UVX targets with the model of Onaka & Kodaira (1991)—which is basically that of Jura (1979) with an inhomogeneous radiation field—to set limits on the optical constants of the

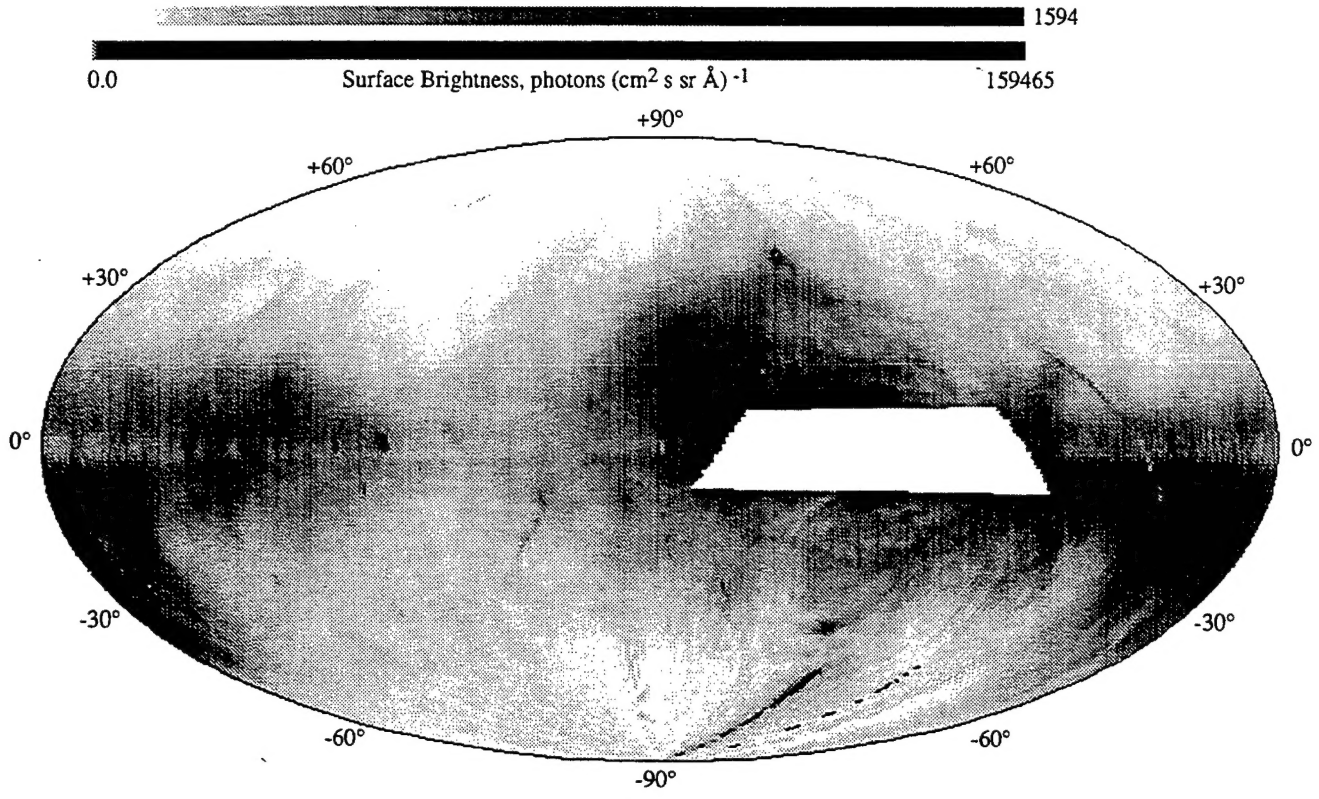
1594
0.0
Surface Brightness, photons (cm2 s sr Å) -1
159465
+90°
+60°
+60°
+30°
+30°
0°
0°
-30°
-30°
-60°
-60°
-90°

FIG. 7*b*

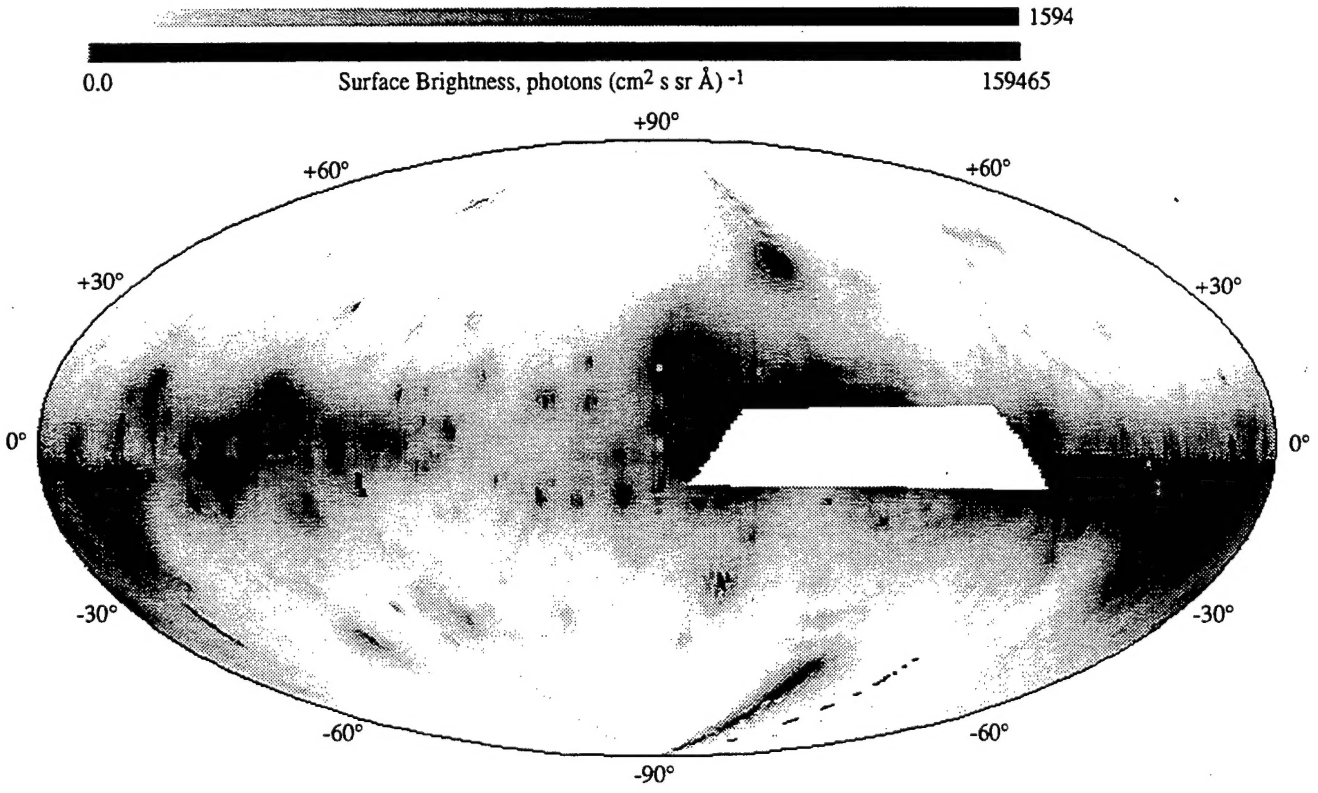
1594
0.0
Surface Brightness, photons (cm2 s sr Å) -1
159465
+90°
+60°
+60°
+30°
+30°
0°
0°
-30°
-30°
-60°
-60°
-90°

FIG. 7*c*

grains and the extragalactic background. Although this model does not include self-shielding by the dust, this should not be important at the low column densities of the UVX targets used. Our results fall within the parameter range allowed by Henry & Murthy but are much more restrictive. However, one of the main conclusions in that work was that the UVX results could be reconciled with the high albedo ($a = 0.65$) and g of 0.75 obtained by Witt et al. (1992) from an analysis of the Ultraviolet Imaging Telescope (UIT) observation of the bright reflection nebula NGC 7023. This conclusion is only consistent with the present analysis if we use an exponential scale height of 500 pc with an average interstellar absorption of 1.2 cm^{-3}. It should be reiterated that there is no particular reason that the dust in a dense reflection nebula should be the same as that in the diffuse interstellar medium.

5. FURTHER WORK

This work is the first stage of a comprehensive effort to understand and predict the diffuse UV radiation field and its different components over the entire sky. We have used our model to predict the gross characteristics of the scattered component of the diffuse radiation field over the entire sky as a function of the optical constants of the interstellar dust. Three cases, for g of 0.1 (near isotropic scattering), 0.5, and 0.9 (highly forward scattering grains), are shown in Figure 7. We have assumed an albedo of 0.1 in making these plots—as we assume single scattering, the plots can simply be scaled for other values of a—and an exponential scale height of 200 pc for the dust distribution. There are significant differences in the predictions for the different phase functions. As might be expected, the scattered radiation is heavily concentrated near the bright stars which are the ultimate source for highly forward scattering grains (Fig. 7*c*) while being much more spread out (but still very patchy) for isotropically scattering grains. Unfortunately, there are no additional reliable (in our estimation) published data at wavelengths above Lyα, and we anxiously await new results with which to confront our model. In the meantime, we are in the midst of a project to use the *Voyager* UV spectrometers to map the diffuse radiation field at wavelengths below Lyα. There are several hundred *Voyager* observations of the diffuse sky, and we hope that these will finally allow us to use observations of interstellar scattering to significantly constrain grain models.

This work was supported by US Air Force contract F19628-93-K-0004 and by NASA grant NAG 1890. We thank the referee, Mark Hurwitz, for useful suggestions, in particular for Table 1, and we thank Stephan Price for his support.

REFERENCES

Anderson, R. C., Henry, R. C., Brune, W. H., Feldman, P. D., & Fastie, W. G. 1979, ApJ, 234, 415
Anderson, R. C., Henry, R. C., & Fastie, W. G. 1982, ApJ, 259, 573
Armand, C., Milliard, B., & Deharveng, J. M. 1994, A&A, 284, 12
Bohlin, R. C., Savage, B. D., & Drake, J. F. 1978, ApJ, 224, 132
Bowyer, S. 1991, ARA&A, 29, 59
Dickey, J. M., & Lockman, F. J. 1990, ARA&A, 28, 215
Draine, B. T., & Lee, H. M. 1984, ApJ, 285, 89
Gondhalekhar, P. M. 1990, in IAU Symp. 139, Galactic and Extragalactic Background Radiation Optical, Ultraviolet, and Infrared Components, ed. S. Bowyer & C. Leinert (Dordrecht: Kluwer), 49
Gordon, K. D., Witt, A. N., Carruthers, G. R., Christensen, S. A., & Dohne, B. C. 1994, ApJ, 432, 641
Gottlieb, D. M. 1978, ApJS, 38, 287
Henry, R. C. 1977, ApJS, 33, 451
———. 1991, ARA&A, 29, 89
Henry, R. C., & Murthy, J. 1993, ApJ, 418, L17
Henyey, L. G., & Greenstein, J. L. 1941, ApJ, 93, 70
Holberg, J. B. 1990, in Proc. IAU Symp. 139, Galactic and Extragalactic Background Radiation Optical, Ultraviolet, and Infrared Components, ed. S. Bowyer & C. Leinert (Dordrecht: Kluwer), 220
Hurwitz, M. 1994, ApJ, 433, 149
Hurwitz, M., Bowyer, S., & Martin, C. 1991, ApJ, 372, 167
Jura, M. 1979, ApJ, 227, 798
Kim, S. H., Martin, P. G., & Hendry, P. D. 1994, ApJ, 422, 164
Kurucz, R. 1979, ApJS, 40, 1
Lockman, F. J., Hobbs, L. M., & Shull, J. M. 1986, ApJ, 301, 380
Martin, C., & Bowyer, S. 1990, ApJ, 350, 242
Martin, C., Hurwitz, M., & Bowyer, S. 1990, ApJ, 354, 220
Mathis, J. S. 1993, Prog. Phys., 56, 605
McKee, C. F. 1990, ASP Conf. Ser., 12, The Evolution of the Interstellar Medium, ed. L. Blitz (San Francisco: ASP), 3
Murthy, J., Henry, R. C., Feldman, P. D., & Tennyson, P. D. 1989, ApJ, 336, 954
———. 1990, A&A, 35, 361
Murthy, J., Henry, R. C., & Holberg, J. B. 1991, ApJ, 383, 198
Onaka, T., & Kodaira, K. 1991, ApJ, 379, 532
Paresce, F., McKee, C. F., & Bowyer, C. S. 1980, ApJ, 240, 387
Spitzer, L. 1978, in Physical Processes in the Interstellar Medium (New York: Wiley)
Stark, A. A., Gammie, C. F., Wilson, R. W., Bally, J., Linke, R. A., Heiles, C., & Hurwitz, M. 1992, ApJS, 79, 77
Tennyson, P. D., Henry, R. C., Feldman, P. D., & Hartig, G. F. 1988, ApJ, 330, 435
Weller, C. S. 1983, ApJ, 268, 899
Weymann, R. 1967, ApJ, 147, 887
Witt, A. N. 1989, in IAU Symp. 135, Interstellar Dust, ed. L. J. Allamandola & A. G. G. M. Tielens (Dordrecht: Kluwer), 87
Witt, A. N., & Petersohn, J. K. 1994, in ASP Conf. Ser., 58, The First Symposium on the Infrared Cirrus and Diffuse Interstellar Clouds, ed. R. M. Cutri & W. B. Latter (San Francisco: ASP), 91
Witt, A. N., Petersohn, J. K., Bohlin, R. C., O'Connell, R. W., Roberts, M. S., Smith, A. M., & Stecher, R. P. 1992, ApJ, 395, L5
Zvereva, A. M., Severny, A. B., Granitzky, L. V., Hua, C. T., Cruvellier, P., & Courtes, G. 1982, A&A, 116, 312